1968

The magnetic properties of single crystals of erbium and some yttrium-erbium and lutetium-erbium alloys between 1.2 and 300°K

Walter James Gray
Iowa State University

68-10,462

GRAY, Walter James, 1938-
THE MAGNETIC PROPERTIES OF SINGLE CRYSTALS OF ERBIUM AND SOME YTTRIUM-ERBIUM AND LUTETIUM-ERBIUM ALLOYS BETWEEN 1.2 AND 300° K.

Iowa State University, Ph.D., 1968
Physics, solid state

University Microfilms, Inc., Ann Arbor, Michigan

THE MAGNETIC PROPERTIES OF SINGLE CRYSTALS OF ERBIUM AND SOME YTTRIUM-ERBIUM AND LUTETIUM-ERBIUM ALLOYS BETWEEN 1.2 AND 300°K

by

Walter James Gray

A Dissertation Submitted to the
Graduate Faculty in Partial Fulfillment of
The Requirements for the Degree of
DOCTOR OF PHILOSOPHY

Major Subject: Physical Chemistry

Approved:

Signature was redacted for privacy.

In Charge of Major Work

Signature was redacted for privacy.

Head of Major Department

Signature was redacted for privacy.

Dean of Graduate College

Iowa State University
Ames, Iowa

1968

TABLE OF CONTENTS

ABSTRACT

Carefully analyzed spherical single crystal samples were prepared of erbium and of alloys whose approximate compositions were: $Y_{25}Er_{75}$, $Y_{50}Er_{50}$, $Y_{75}Er_{25}$, $Lu_{25}Er_{75}$, $Lu_{50}Er_{50}$, and $Lu_{75}Er_{25}$. Magnetic measurements were made on each of these samples along the three principle crystallographic axes in the range 1.2 to 300°K and applied fields up to 27.9 K-Oe.

For pure erbium, the saturation moment along the c-axis was found to be 276.0 ±2.0 emu/g. by fitting the data to a T^2 plot and extrapolating to 0°K. This is to be compared with a theoretical value of 300.5 emu/g. The discrepancy between experiment and theory is apparently the result of a ferromagnetic spiral arrangement of spins where the spins are cocked at an angle to the c-axis rather than being aligned parallel to it. Curie and Néel temperatures were found at 18.2 ±0.5 and 86.5 ±0.5°K respectively. Peaks in the c-axis moment vs. temperature curves were also observed which extrapolated to zero-field temperatures of 28.0 ±0.5 and 50.5 ±0.5°K. The latter corresponds to the transition from one antiferromagnetic structure to another while the significance of the former is unknown. Peaks occurred in both the a- and b-axis moment vs. temperature curves below about 18.5 K-Oe. Below about 10 K-Oe., the temperature of the peaks was field independent and occurred at about 18.2°K. In both the a- and b-axis moment vs. field curves, there were discontinuous increases in moment at about 18.5 K-Oe. near 4.2°K. These apparently correspond to a sudden transition to a nearly parallel alignment of spins at an angle of about 23° to the c-axis. Some very small basal-plane anisotropy was observed below 40°K. At 4.2°K, the b-axis moment was about 2% larger at high

fields.

None of the alloys studied were ferromagnetic in zero field. The Néel temperatures of the alloys were proportional to the 2/3 power of the average de Gennes factor, $T_N = A\bar{G}^{\frac{2}{3}}$. The constant, A, was found to be 49.0 for the yttrium-erbium alloys and 53.5 for the lutetium-erbium alloys. An anomalous peak was observed in the c-axis moment vs. temperature curves for two alloys, $Lu_{25}Er_{75}$ and $Y_{50}Er_{50}$. In both alloys, the peak was not observed at fields less than about 6 K-Oe. However, by extrapolating to zero field, the temperatures of the peaks were determined to be 27.5 ±1.0 and 17.5 ±1.0°K respectively for the two alloys. In addition to these anomalies, a peak was observed at 29.0 ±0.5°K for a polycrystalline $Y_{25}Er_{75}$ alloy by a zero-field mutual-inductance bridge technique. These peaks are evidently due to a transition between two different magnetic structures, but whether they correspond to the structure change observed by Child et al.[1] in yttrium-erbium alloys is not known. Peaks occurred in both the a- and b-axis moment vs. temperature curves for the $Y_{25}Er_{75}$, $Lu_{25}Er_{75}$, $Y_{50}Er_{50}$, and $Lu_{50}Er_{50}$ alloys at 16.4, 16.1, 12.5, and about 9.0°K respectively. These peaks are apparently related to the 18.0°K basal-plane peak in pure erbium. This peak corresponds to the ferromagnetic-antiferromagnetic transition in pure erbium. The small basal-plane anisotropy observed in the alloys at low temperatures (b-axis moment larger) was found to decrease with increasing temperature and with decreasing erbium concentration.

---

[1] H. R. Child, W. C. Koehler, E. O. Wollan, and J. W. Cable, Phys. Rev. 138, 1655 (1965).

From the paramagnetic data, the magnetic moments, in terms of the effective number of Bohr magnetons per erbium ion, were found to be within experimental error of 9.97 ±0.1 for erbium as well as for all the alloys.

I. INTRODUCTION

The study of the magnetic properties of the rare-earth metals and alloys has commanded a great deal of interest ever since they became available in macro quantities about 1947. This interest has been sparked because most of the rare-earths have at least one unpaired 4f electron, and these electrons give rise to large dipole moments and even ferro- and antiferromagnetism. Even before the ion exchange process for separating the elements (1) and the methods for reduction of macro quantities of the halides to metals (2) were developed, some work was done on mixtures of the rare-earth metal and some salt such as an alkali chloride. In fact, gadolinium was discovered to be ferromagnetic below about 16°C in 1935 (3). In 1937 (4) and 1939 (5), Klemm and Bommer studied the paramagnetic susceptibility of gadolinium, terbium, dysprosium, holmium, and erbium and found that the susceptibility was large in all cases and that they all had paramagnetic Curie temperatures between 0°K and room temperature.

Although the large dipole moments of some of the rare-earths are of the same order of magnitude (actually nearly twice as large in the case of dysprosium and holmium) as those of the classic iron group magnetic elements, the early work demonstrated that there is a basic difference between these two groups of metals. In the rare-earths, the 4f electrons responsible for the large dipole moments lie deep inside the electron cloud, shielded from the effect of the field of neighboring ions by the 5s and 5p electrons. Thus the orbital and spin angular momentum of the 4f electrons couple to give a total angular momentum quantum number, J, which is found by combining L and S according to Hund's rules. In the

iron group elements, on the other hand, the 3d electrons which are responsible for the magnetic properties are exposed to the field of the neighboring ions. This field, the effect of which is one or two orders of magnitude larger than in the rare-earths, tends to decouple the orbital and spin angular momentum so that J is not a good quantum number.

For the rare-earths, therefore, quantum theory of paramagnetism shows that the magnetization of N atoms in a magnetic field, H, is given by

$$M = NgJ\mu_B B_J(x) \tag{1-1}$$

where g is the spectroscopic splitting factor given by

$$g = 1 + \frac{J(J+1) + S(S+1) - L(L+1)}{2J(J+1)} . \tag{1-2}$$

μ_B is the Bohr magneton given by

$$\mu_B = \frac{eh}{4\pi mc} = 9.27 \times 10^{-21} \text{ ergs/oersted} \tag{1-3}$$

and $B_J(x)$ is the Brillouin function given by

$$B_J(x) = \frac{2J+1}{2J} \coth \frac{(2J+1)x}{2J} - \frac{1}{2J} \coth \frac{x}{2J} \tag{1-4}$$

where

$$x = \frac{gJ\mu_B H}{kT} . \tag{1-5}$$

For the case where $x < 1$ (i.e., at sufficiently high temperatures so that the system is well within the paramagnetic region), $B_J(x)$ becomes $\frac{(J+1)x}{3J}$ and so the susceptibility is given by

$$\chi = \frac{M}{H} = \frac{Ng^2 J(J+1)\mu_B^2}{3kT} . \tag{1-6}$$

This is just the Curie law. The moment per atom, μ, is seen to be proportional to $g\mu_B [J(J+1)]^{\frac{1}{2}}$ and the effective number of Bohr magnetons is given by

$$\mu_{eff} = \frac{\mu}{\mu_B} = g[J(J+1)]^{\frac{1}{2}} \qquad (1\text{-}7)$$

For very low temperatures and large fields such that $x \to \infty$, $B_J(x) \to 1$ so that the saturation magnetization, according to Equation 1-1 is given by

$$M = NgJ\mu_B \ . \qquad (1\text{-}8)$$

Here, the effective number of Bohr magnetons is

$$\mu_{eff} = gJ \ . \qquad (1\text{-}9)$$

This corresponds to the situation where the spins of all the ions are parallel and in this regard is equivalent to the ferromagnetic case.

From the beginning, as the state of the art of preparation of the rare-earth metals has progressed, so has the understanding of their properties. As already stated, most of the earliest work was carried out on mixtures of the rare-earth metal and some salt. When the pure metals became available, the magnetic properties of pure polycrystalline samples were investigated. Information about the magnetic properties was obtained not only by bulk magnetization methods but also from heat capacity and resistivity measurements.

The work on polycrystalline metals, done mostly in the late 1950's, has been focused primarily on the so-called heavy rare-earths (those elements from gadolinium, atomic number 64, to lutetium, atomic number 71, and also yttrium). One reason for this is that the heavy rare-earth metals, with the exception of ytterbium, are isostructural. Each crystallizes in the hexagonal closest packing arrangement with an AB, AB stacking sequence. In addition, the heavy rare-earths exist in a wide variety of magnetic states. In particular, terbium, dysprosium, holmium, and erbium

each transform first to an antiferromagnet and then to a ferromagnet as the temperature is lowered. Gadolinium transforms directly to a ferromagnet. Thulium transforms first to an antiferromagnet and then to a ferrimagnet. The other heavy metals, ytterbium, lutetium, and yttrium, have no unpaired 4f electrons and are therefore only weak paramagnets. Thus, although the heavy rare-earth metals have a wide variety of magnetic properties, they are otherwise quite similar. This makes them ideal for comparison with theory.

When it was found that the rare-earths exhibit antiferromagnetism in some temperature ranges, there was some speculation on the type of magnetic ordering responsible for this behavior. It remained for neutron diffraction experiments done mainly by Koehler and others at Oak Ridge National Laboratory, however, to elucidate the interesting variety of magnetic structures, not only among the rare-earths in general, but also within any one particular metal. These structures are represented schematically in Figure 1. In Figure 1a, the ferromagnetic state is represented where all the spins are parallel and lie entirely in the basal plane. Figure 1b represents one type of antiferromagnetism where all the spins within any given basal plane lie entirely in the plane and are parallel, but the spin direction from one plane to the next differs by what is called the interlayer turn angle. Figure 1c is similar to 1b except that there is a spin component parallel to the c-axis. This is called a ferromagnetic spiral since there is a net moment parallel to the c-axis. Figure 1d represents another type of antiferromagnetism. This structure is similar to 1c except that there is an antiphase domain with equal numbers of spins parallel and antiparallel to the c-axis. In Figure 1e, no long-range order in the basal

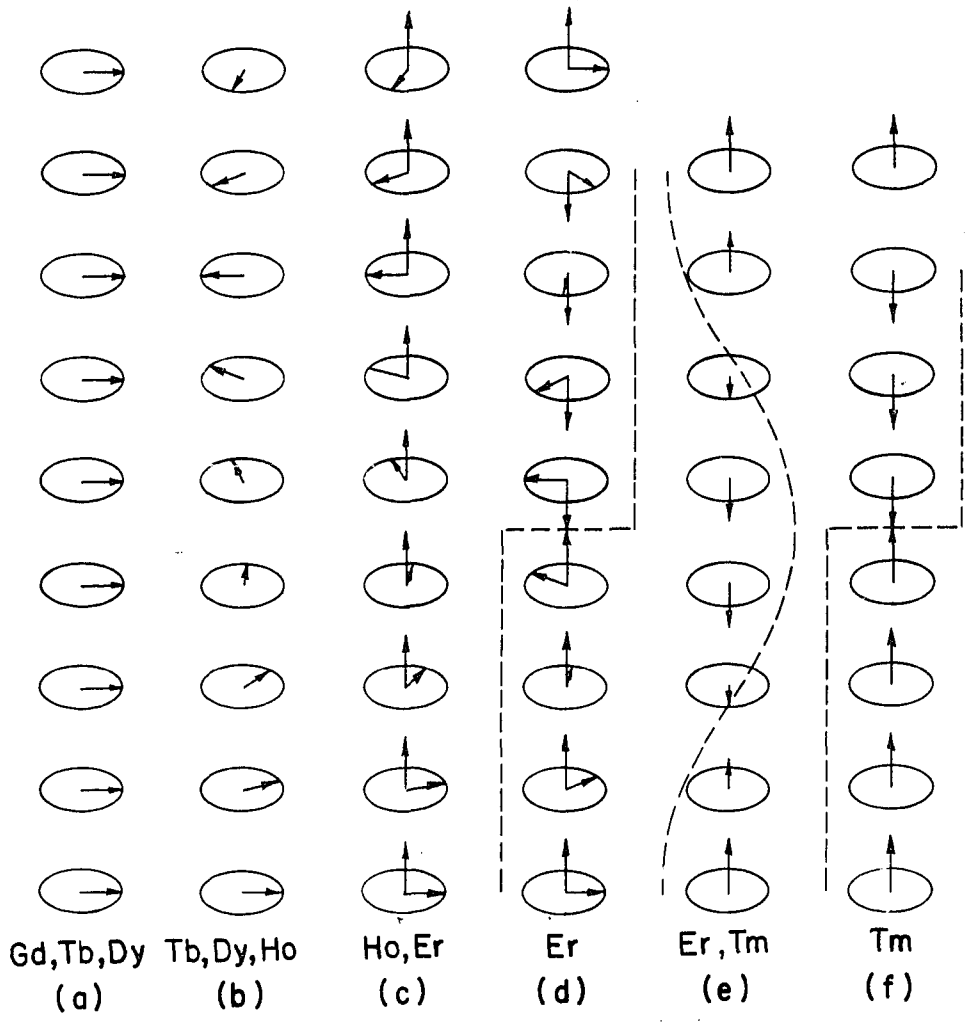

Figure 1. Schematic representations of the magnetic structures observed in the heavy rare-earth metals

plane is observed. Along the c-axis, the spins vary according to a sinusoidal relationship. Figure 1f is somewhat like 1d except that there is no long-range order in the basal plane and there is an unequal number of spins parallel and antiparallel to the c-axis. Thus thulium is actually ferrimagnetic.

The next refinement in the magnetic measurements came with the availability of single crystals whose preparation is described by Nigh (6). Single crystal data was particularly desirable for the rare-earths because of their extremely large anisotropies and their interesting magnetic structures. Bulk magnetic measurements have been made on most of the heavy rare-earth single crystals and neutron diffraction measurements have been made on some. These results have provided a much better understanding of the various zero field magnetic structures and of the magnetization processes (i.e., the magnetic structures as a function of field).

A theory which applies to the magnetic properties of the rare-earth metals was developed in the 1950's and is briefly discussed here. In 1951, Zener (7) proposed a mechanism of polarizing the conduction electrons by the exchange interaction with the d-electrons of transition metal paramagnetic ions. Since then, a number of authors have revised and modified this model into what has come to be known as the Ruderman-Kittell-Kasuya-Yosida (RKKY) theory (8, 9, 10). This theory, along with crystalline anisotropy arguments (11, 12), qualitatively predicts the various magnetic structures observed in the rare-earth metals. In some cases, there is even reasonable quantitative agreement although it is not certain at this time but what this may be fortuitous.

The essential feature of the RKKY theory is that there is an exchange interaction between localized moments via the indirect exchange with the conduction electrons. This interaction is of the form

$$E_{ex} = -\sum_{i,j} J(\vec{r}_j - \vec{r}_i)\vec{S}_i \cdot \vec{S}_j \qquad (1\text{-}10)$$

where $J(\vec{r}_j - \vec{r}_i)$ represents the exchange integral between spins $\vec{S}_i$ and $\vec{S}_j$ on the i'th and j'th lattice sites. Under a number of simplifying assumptions, one obtains an isotropic interaction whose radial dependence is given by $\frac{X\cos X - \sin X}{X^4}$ where $X = 2k_F|\vec{r}_j - \vec{r}_i|$ and k_F is the Fermi wave vector. This function has the necessary property of being long range and oscillatory and therefore allows one to visualize how antiferromagnetism can exist in a pure metal.

The oscillatory spin structures of the rare-earth metals can be understood in terms of the following simple calculation. For spin structures represented by Figures 1b, 1c, and 1d, the interaction described above can be summed over planes and it takes the form

$$\frac{E}{N} = S^2(J_o + 2J_1 \cos\theta + 2J_2 \cos 2\theta + \cdots) \qquad (1\text{-}11)$$

where J_o is the total in-plane interaction, J_1 the interaction between nearest neighbor planes, J_2 the interaction between next nearest neighbor planes, and θ the interlayer turn angle. One now looks for an energy minimum by setting $\frac{\partial E}{\partial \theta} = 0$. If only the first two terms are considered, a minimum occurs at $\theta = 0$, the ferromagnetic case, and at $\theta = \pi$, the classic antiferromagnetic case. When the third term is included, a minimum is also found for $\cos\theta = -\frac{J_1}{4J_2}$ which corresponds to the helical structure.

This solution requires the exchange interaction to be long-range (at least 3 terms are required) and oscillatory (J_1 and J_2 should have opposite signs to minimize the energy). These are just the properties possessed by the indirect exchange described above.

As a better understanding of the properties and theory of the pure metals was being acquired, people began to wonder what would happen to these properties if an alloy of two of the heavy rare-earths was prepared. Two basic types of alloys can be considered; one combining a magnetic rare-earth with a non-magnetic rare-earth such as lutetium, yttrium, or even scandium, and the other an alloy of two of the magnetic rare-earths.

Bozorth and Gambino (13) and Bozorth (14) have studied a large number of alloys of both types but have reported only Néel and Curie temperatures for the most part. Several alloys have been studied by Child and others (15, 16) at Oak Ridge National Laboratory and this work includes investigations into the actual magnetic structures. In general, the properties of the alloys seem to be related to those of the pure metals in a fairly straightforward manner and are qualitatively described by the theory developed for the pure metals. Also, Bozorth reported that when the Néel temperatures of all the metals and alloys, except alloys containing scandium, are plotted vs. the 2/3 power of the average de Gennes factor (17), they all lie roughly on a straight line, the slope of which is given by a "universal" constant, A = 46.7.

$$T_N = A\bar{G}^{\frac{2}{3}} \qquad (1\text{-}12)$$

where $G = J(J + 1)(g - 1)^2$

$\bar{G} = c_1 G_1 + c_2 G_2$

where c_1 and c_2 refer to the atomic fractions of the two components. The Curie temperatures, on the other hand, were found to be characteristic of the alloy system. In addition to the work cited above by Bozorth, the magnetic properties of the rare-earth metals and alloys have been summarized in a review article by Koehler (18).

To date, the study of alloys has involved very little work on single crystals. Much of the work on polycrystalline materials, even, has been somewhat cursory and there would seem to be a need, now, for a thorough study of at least some of the alloys using single crystal specimens. A particular case in point has to do with alloys containing one of the magnetic rare-earths and either yttrium or lutetium. The assumption, supported by available data, has been that there is very little difference in the magnetic properties of these two groups of alloys. It was felt that this assumption should be further investigated by a thorough study of these two systems.

Having decided to undertake a study of the magnetic properties of two systems of alloys, one with yttrium and the other with lutetium, the question of which of the magnetic rare-earths to use remained. There seemed to be no reason to choose one over any of the others. As it turned out, erbium was chosen for the following reasons.

About the time this study was started, another project was just getting underway at Iowa State to try to gain at least a factor of ten in purity of the rare-earth metals, particularly with respect to oxygen. Since both yttrium and lutetium were to be used in the magnetic study, special emphasis, with some success, was placed upon getting these metals in purer form. One of the first of the magnetic rare-earths to yield to

better purification was erbium. Since erbium also has the interesting property of at least two different antiferromagnetic structures, it was the one chosen for use in this investigation.

So far, the magnetic properties of the rare-earths in general have been discussed. The next few paragraphs will be devoted to previous work on the magnetic properties of erbium and yttrium-erbium and lutetium-erbium alloys in particular.

The work on erbium metal up to about 1960 was done on polycrystalline samples. Resistivity measurements by Legvold et al. (19) and Colvin et al. (20) gave anomalies at about 20, 55, and 80°K. Heat capacity measurements by Skochdopole et al. (21) gave anomalies at 19.9, 53.5, and 84°K. Magnetization measurements by Elliott et al. (22) showed an anomaly at 78°K and the authors concluded that the sample was probably ferromagnetic below 20°K. Koehler and Wollan (23) made neutron diffraction measurements on erbium and concluded that it is ferromagnetic at 4.2°K and possibly antiferromagnetic below 80°K.

In 1961, Green et al. (24) reported the results of magnetization and resistivity measurements on erbium single crystals. The c-axis resistivity data showed anomalies at about 20, 53, and 85°K. The magnetic data showed that the c-axis was the easy direction of magnetization but that the observed saturation magnetization of 8 Bohr magnetons was somewhat less than the theoretical value of 9 Bohr magnetons. This was attributed to a spin arrangement where the spins are not parallel to the c-axis but have a component in the basal plane. A peak in the moment vs. temperature data occurred at 85°K which was taken to be a Néel peak. The Curie temperature was found to be 19.6°K. Green et al. did not report any

anomalous behavior in the neighborhood of 52°K for the magnetic data.

In 1965, the results of a neutron diffraction study on an erbium single crystal were reported by Cable (25). Three distinct regions of long-range magnetic order were observed. These are shown schematically in Figure 1. In the high temperature region (52 - 80°K) shown in Figure 1e, no order was observed in the basal plane, while the c-axis component was found to obey a sinusoidal relationship. In the intermediate region (20 - 52°K), the sinusoidal c-axis component begins to square up as the temperature is lowered from 52°K and the basal-plane component orders into a spiral. The details of the structure in this region are somewhat obscure and Figure 1d is only an approximate representation of the structure. In the low-temperature region (4.2 - 20°K), a ferromagnetic spiral represented by Figure 1c is found. The c-axis component of the moment was reported to be 7.9 μ_B and the basal-plane component 4.3 μ_B per ion so that the total moment is 9.0 μ_B which is the ground state free ion value.

Bozorth and Gambino (13) reported the results of magnetic studies on several alloys and pure metals, mostly polycrystalline, in 1966. They reported 19 and 84°K for the Curie and Néel temperatures respectively for pure erbium. They also observed a peak in the moment vs. temperature curves at 54°K which corresponds to the transition from one antiferromagnetic structure to another. They also reported a peak in the moment vs. temperature curves at 28°K. To the author's knowledge, this anomaly had not been reported previously.

Bozorth and Gambino (13) have also reported magnetic measurements on polycrystalline lutetium-erbium alloys containing 98, 95, 90, and 75

atomic percent erbium. These alloys all showed magnetic hysteresis at 4.2°K, and the data indicated the existence of two magnetic structures at 4.2°K in the alloy containing 75% erbium. It was not clear from their paper whether the other alloys also showed evidence for two magnetic structures.

Child et al. (15) have carried out a neutron diffraction study on polycrystalline yttrium-erbium alloys. Alloys containing 90, 70, 50, and 30 atomic percent erbium were studied. None of the alloys became ferromagnetic down to 4.2°K. The Néel temperatures of all alloys were given roughly by Equation 1-12 when the universal constant, A = 46.7, was used. All alloys were also found to transform from one antiferromagnetic structure to another at low temperatures. The temperatures of the transitions were found to vary in a manner similar to Néel temperatures of these alloys. Since polycrystalline samples were used, the authors were unable to determine the details of the two antiferromagnetic structures, but they seem to be similar to those in pure erbium.

The purpose of the present study is to carry out an investigation of the magnetic properties of single crystals of erbium and its alloys with yttrium and lutetium. It was felt that a comparison between the two alloy systems should be made and also that a more complete study of each system for its own sake was needed. The proper approach seemed to be to limit the study by looking at a few alloys encompassing the entire range of compositions and to let the results of this study be a guide for additional future work on these same alloy systems.

The choice of apparatus to be used for measuring the magnetic properties was governed primarily by the fact that large moments were to

be measured. Many of the force methods of measuring magnetic properties are not particularly well suited to measurement of large moments. Any of the three types of magnetometers which take advantage of the voltage induced in a coil when either the coil or a sample is moved in the vicinity of the other is very well suited to the measurement of large moments. Of the three, a vibrating-sample magnetometer similar to one described by Foner (26) seemed to offer the most advantages.

The following sections describe the preparation of single crystals of yttrium-erbium and lutetium-erbium alloys containing 75, 50, and 25 atomic percent erbium, as well as pure erbium, and the results of magnetic measurements along the a, b, and c (i.e., $[2\bar{1}\bar{1}0]$, $[10\bar{1}0]$, and [0001]) crystallographic axes. The measurements were made in the range 1.2 to 300°K and in magnetic fields up to 27.9 K-Oe. The vibrating-sample magnetometer used for this study is also briefly described.

II. APPARATUS

A. Vibrating-Sample Magnetometer

1. Theory

The theory of the vibrating-sample magnetometer (VSM) must be capable of establishing the flux pattern at any point in space due to an oscillating magnetic dipole. Gauss' law provides a convenient starting point. This law gives a relation for the electric field, E, outside any closed surface, S, containing a total charge, q. In vector notation, it is written

$$\int_S \vec{E} \cdot d\vec{S} = 4\pi q \ . \tag{2-1}$$

See Scott (27), for example, for a discussion of Gauss' law. If the surface is taken to be a sphere and we let its radius go to zero, it can be shown that the electric field at the origin due to a point charge located at r is given by

$$\vec{E} = \frac{q}{r^3} \vec{r} \ . \tag{2-2}$$

The potential, ϕ, is defined by

$$\vec{E} = -\vec{\nabla}\phi \tag{2-3}$$

and therefore

$$\phi = \frac{q}{r} \ . \tag{2-4}$$

Now if we consider two point charges, +q located at r and -q located at r + dr, the potential at the origin is given by

$$\phi = -\frac{q}{r + dr} + \frac{q}{r} \simeq \frac{q\,dr}{r^2} \tag{2-5}$$

if dr is small. If we let dr vanish, we have a dipole, $\vec{m}$, such that $\vec{m} = q\vec{dr}$. If the dipole is located at r, then the potential due to the dipole is given by

$$\phi = \frac{\vec{m} \cdot \vec{r}}{r^3} . \tag{2-6}$$

This is true for either electric or magnetic dipoles. One can also derive Equation 2-6 by starting with the law of Biot and Savart.

It is now convenient to turn the problem around and consider the dipole, $\vec{m}$, to be located at the origin of a Cartesian coordinate system. The potential at the point $\vec{r}$ is still given by Equation 2-6, of course. If the dipole is assumed to be oriented along the X-axis, the scalar potential can be written as

$$\phi = \frac{mx}{r^3} . \tag{2-7}$$

If the dipole is now vibrated in the Z direction with a small amplitude, b, the time varying portion of the scalar potential can be taken to be

$$\phi(z,t) = \phi(z)\exp(i\omega t) , \tag{2-8}$$

where

$$\phi(z) = -b\frac{\partial \phi}{\partial Z} = -b\frac{\partial(\frac{mx}{r^3})}{\partial Z} . \tag{2-9}$$

Substituting $r^2 = x^2 + y^2 + z^2$ into the above equation and performing the indicated differentiation, we get

$$\phi(z) = \frac{3bmxz}{r^5} . \tag{2-10}$$

The flux pattern established by the time varying part of the field is given by $\vec{E} = -\vec{\nabla}\phi(z)$. The configuration of the flux pattern in the X-Z plane is shown in Figure 2 (26).

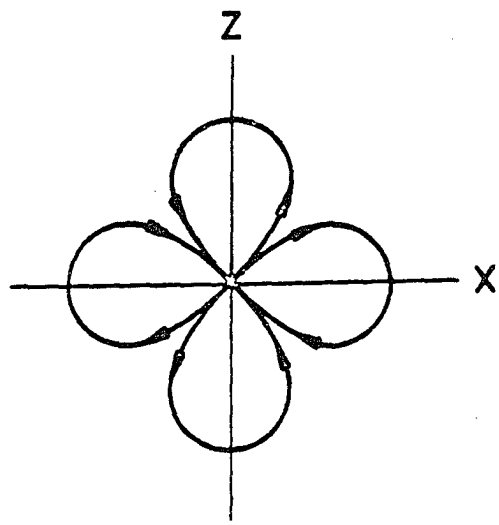

Figure 2. Time-varying portion of the dipole field in the X-Z plane for oscillation parallel to Z and dipole moment parallel to X

Now a magnetic dipole moment is, of course, induced in any material which is placed in a magnetic field. The problem of measuring the magnetic moment of that material then becomes one of choosing the most advantageous coil arrangement to sense the dipole field and of measuring the voltage induced in the coils. Various pick-up coil arrangements are discussed by Foner (26) and Mallinson (28).

2. Apparatus

The vibrating-sample magnetometer which was used in this investigation was a modified version of the one described by Miller in his Ph.D. thesis (29), and was similar to the magnetometer described by Foner (26). The modified version was also described in detail by Miller in a paper to be published (30). In this paper, Miller also included a discussion on the use of several different types of materials as calibration standards for this type of magnetometer. Therefore, the discussion in this thesis will be limited to just the basic characteristics and operation of the apparatus.

A schematic diagram of the apparatus used in this study is shown in Figure 3. An audio oscillator was used to drive a loudspeaker transducer system at about 90 cycles per second. The reference signal was fed to a phase shifting network and then to a precision potentiometer voltage divider. A portion of the reference signal from the voltage divider was then mixed with the sample signal from the two pick-up coils which sensed the time-varying portion of the oscillating magnetic dipole moment of the sample. The resultant signal was put into a 90 cycle narrow band amplifier where it was amplified by a factor of 10^6. The amplified signal was

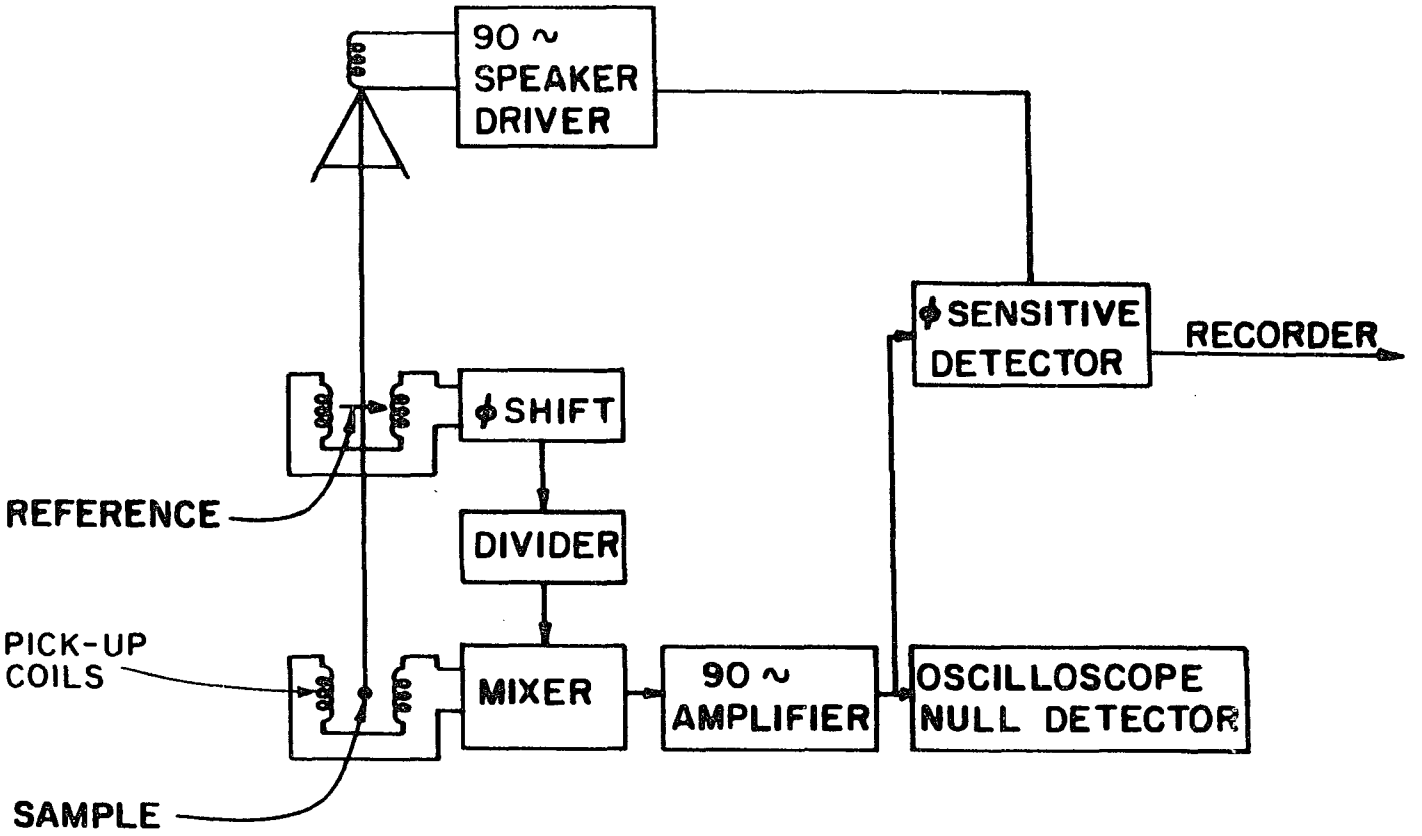

Figure 3. Schematic diagram of the vibrating-sample magnetometer

applied to the Y input of an oscilloscope that was synced at 90 cycles per second. When the magnitudes of the two signals were not equal or when the signals were not 180° out of phase or when both of these conditions existed simultaneously, the trace observed on the oscilloscope was a sine wave. By watching for a minimum in the trace as the phase of the reference signal was adjusted, it was possible to get the two signals 180° out of phase. A balanced condition, i.e., a horizontal trace, was then obtained by adjusting the precision potentiometer.

The transducer assembly and mounting system is shown in Figure 4. The 90 cycle oscillator described above was used to drive the 20 watt loudspeaker coil at a peak-to-peak amplitude of about 1 mm. This transducer coil was rigidly fastened to a connecting rod which was mounted, in turn, to two phosphor bronze springs. Phosphor bronze springs were used rather than the regular speaker cone assembly for reasons of physical strength. At the top of the connecting rod was mounted a second coil which, when oscillated in the reference magnet, provided the reference signal. The lower end of the connecting rod was fastened, by means of a collet type connector, to the sample rod shown in Figure 5. By taking the reference signal from the same oscillating shaft to which the sample was mounted, the net signal was made insensitive to small changes in amplitude. This would not be true if the reference signal were taken directly from the oscillator.

The sample chamber and sample rod assembly is shown in Figure 5. The sample rod, which provided a link between the sample and the transducer, was made of fiberglass sleeving impregnated with Araldite epoxy resin. The heater and thermocouples were passed up through the center of the

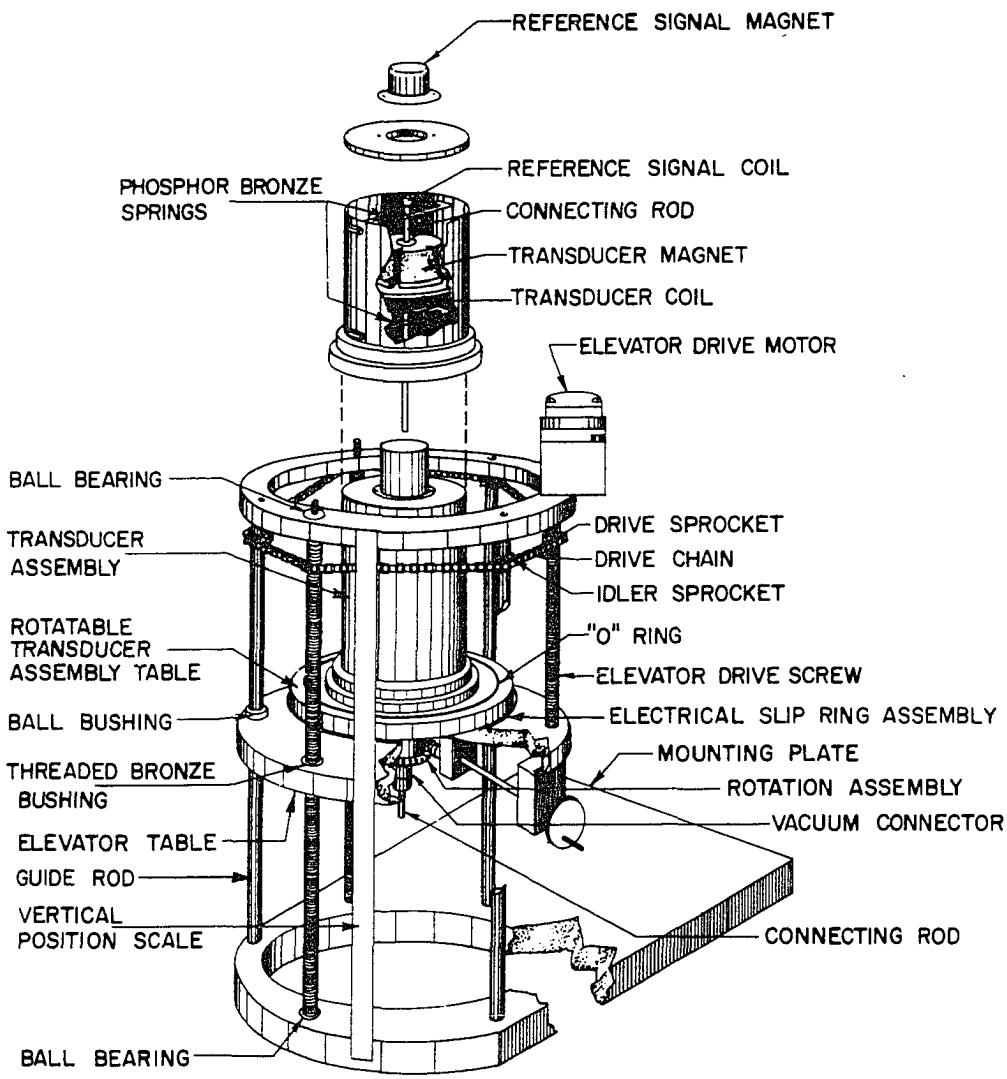

Figure 4. Transducer assembly and mounting system

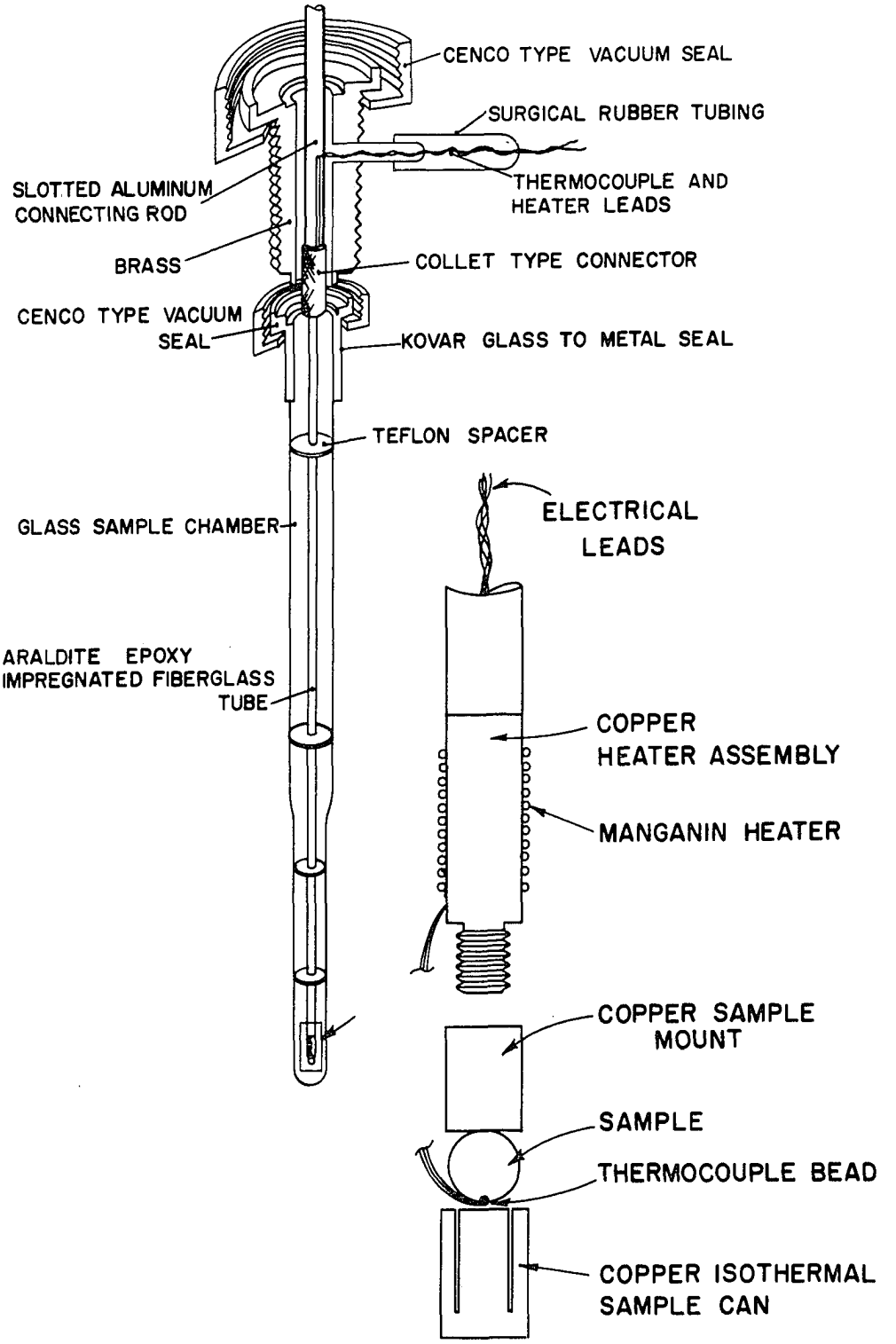

Figure 5. Sample chamber and sample rod assembly

sample rod and out through a surgical rubber tubing vacuum seal at the top of the sample chamber.

Each of the two pick-up coils used to sense the sample signal was 5/16 inch in diameter and 3/4 inch long. Each coil contained 28,000 turns of no. 50 gauge formvar-covered copper wire. The coils were positioned with their axes aligned vertically and with one coil located exactly in the center and flush against the face of each magnet pole piece.

The voltage induced in the pick-up coils was made insensitive to small changes in sample position by centering the sample with respect to the pick-up coils. This was done by applying a field so that a magnetic moment was induced in the sample. Then the sample was moved in the Z, or vertical, direction until a maximum signal was found. Then the sample was moved parallel to the X direction(i.e., parallel to the applied field) until a minimum in the signal was obtained. Finally the sample was moved parallel to the Y direction until a maximum was reached. Figure 6 shows the position sensitivity in the three directions.

Rotation of the transducer assembly table, sample chamber, and thus the sample about the Z axis was provided to allow for careful alignment of the crystallographic axis parallel to the field. This was done by applying a field and rotating the sample until a maximum or minimum signal was found depending upon whether an easy or hard direction of magnetization was parallel to the field. It was found that the crystallographic axis could be alligned parallel to the field to within better than $\pm 1^{\circ}$ in this manner.

a. Calibration Calibration of the VSM consisted of two problems. Before the magnetization of any sample could be determined, it was necessary to calibrate the reference signal with a standard of known

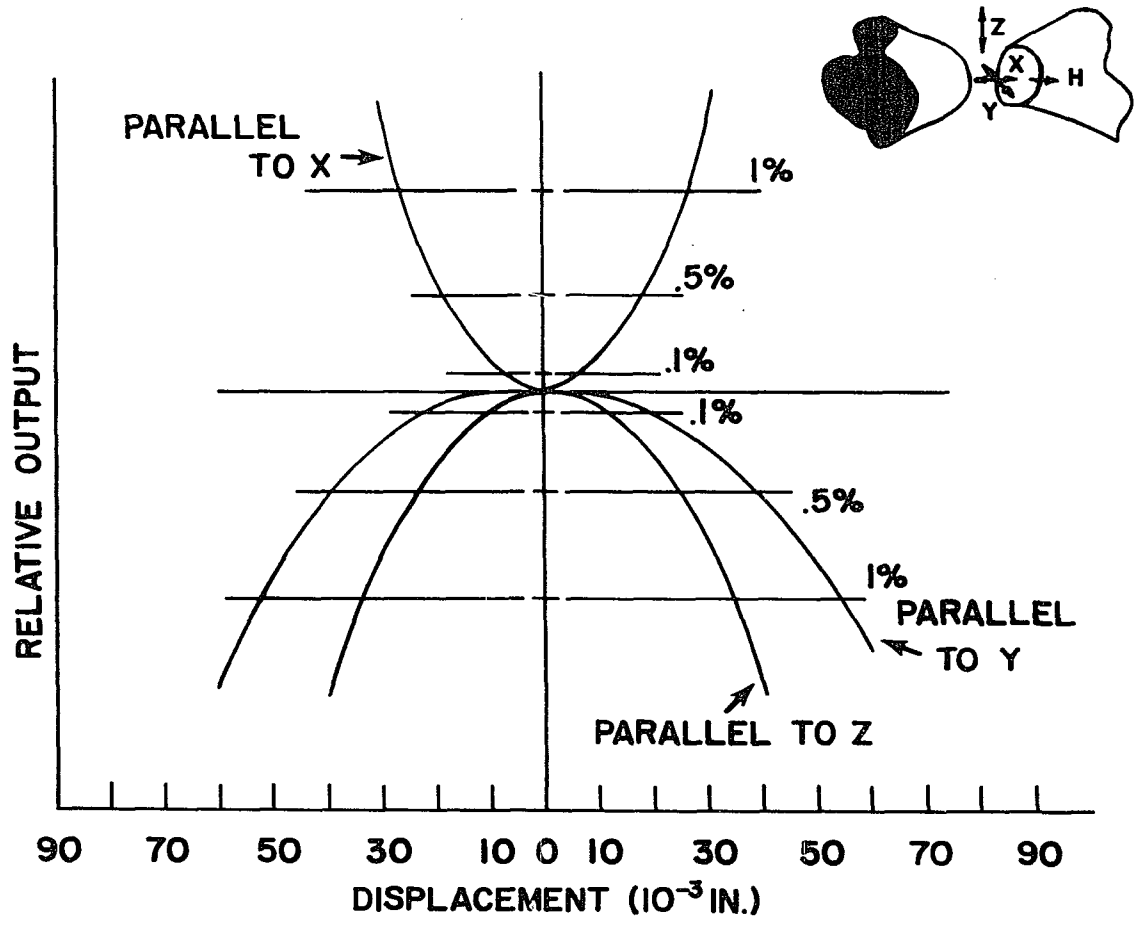

Figure 6. Position sensitivity of the sample with respect to the pick-up coils in three directions

magnetization. In addition, an abnormal increase in the measured magnetic moment was observed at high fields. This phenomenon, known as the image effect, is illustrated in Figure 7. It was necessary to find a way to take this into account.

Neglecting the image effect for the moment, the reference signal was calibrated by taking advantage of the saturation moment of nickel. Nickel saturates in a field of a few hundred oersteds beyond which its moment remains constant to better than 0.2% for the fields considered (31). The saturation value at 288°K used for the calibration was 55.05 emu/g. given by Danan (32).

In order to make sure no spurious effects were caused by the presence in the cryostat of either liquid nitrogen or liquid helium or both, the calibration was also carried out at these two bath temperatures. The values obtained agreed with the accepted values (33, 34) to within 0.2% which was the order of experimental error.

Once the reference signal was calibrated, a precision potentiometer voltage divider was used to accurately determine the fraction of the reference signal needed to balance the sample signal. Hence the magnetic moment of any sample was determined according to the equation

$$(DR)(C) = m$$

where DR was the dial reading on the potentiometer and C was the calibration constant previously determined from a standard of known magnetic moment, m.

The problem of the image effect was handled merely by calibrating and subtracting the effect from all measurements. In order to be certain

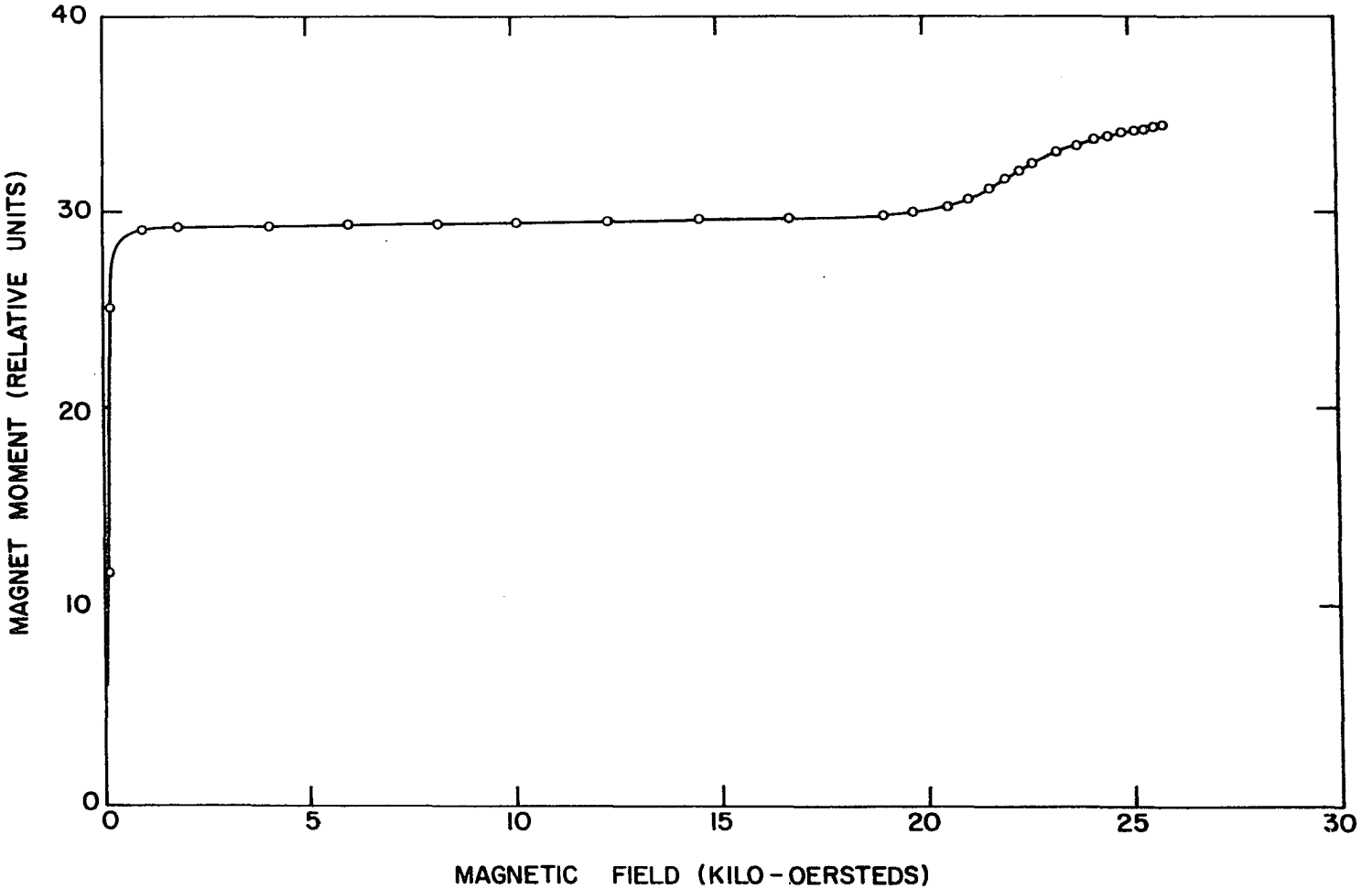

Figure 7. Magnetic moment vs. internal field for a small nickel sphere. Abnormal increase in moment above 20 kilo-oersteds is due to image effect.

that the contribution to the signal due to the image effect was strictly proportional to the magnetic moment of the specimen, several different size samples of nickel, one of iron, and a single crystal of erbium with c//H[1] at 4.2°K were used for the calibration. Scatter to the extent of about ±5% of the correction was observed in these data. Thus, in a region where the image effect contribution was 10% for example, the uncertainty in the magnetic moment was ±0.5%. The results of the image effect calibration are shown in Figure 8.

3. Cryostat

The cryostat used in this study is shown schematically in Figure 9. The tail section of the all glass dewar had an outside diameter of 26mm and an inside diameter of 10.2mm. Since the tail section of the sample chamber had an outside diameter of 6mm, adequate clearance was provided for centering of the sample with respect to the pick-up coils. Movement of the sample chamber was independent of the dewar.

Sample temperature was measured with a gold - 0.03 atomic percent iron vs. copper thermocouple in the range from 1.2 to 20°K. The thermocouple was calibrated to ±0.01°K by the author. Helium vapor pressure was used for the calibration below 4.2°K. Above 4.2°K it was calibrated vs. a germanium resistance thermometer which in turn had been calibrated against a helium gas thermometer. From 20°K to room temperature, a gold - 2.1 atomic percent cobalt vs. copper thermocouple was used. The calibration for this thermocouple was obtained from the National Bureau of

---

[1]This notation is used throughout this thesis to denote which of the crystallographic axes is parallel to the field.

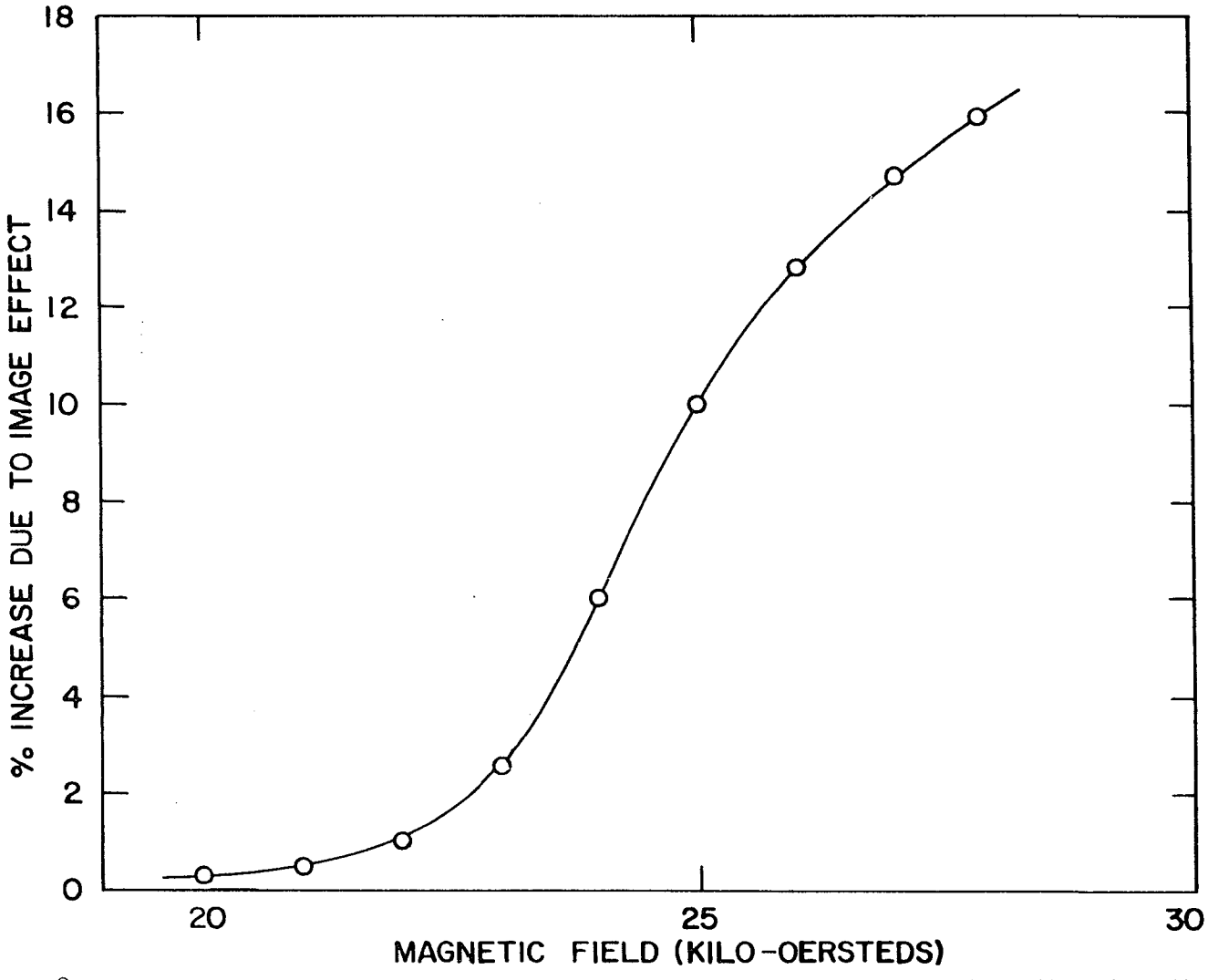

Figure 8. Image effect calibration as a function of field. Obtained from the high-field portion of curves of the sort shown in Figure 7

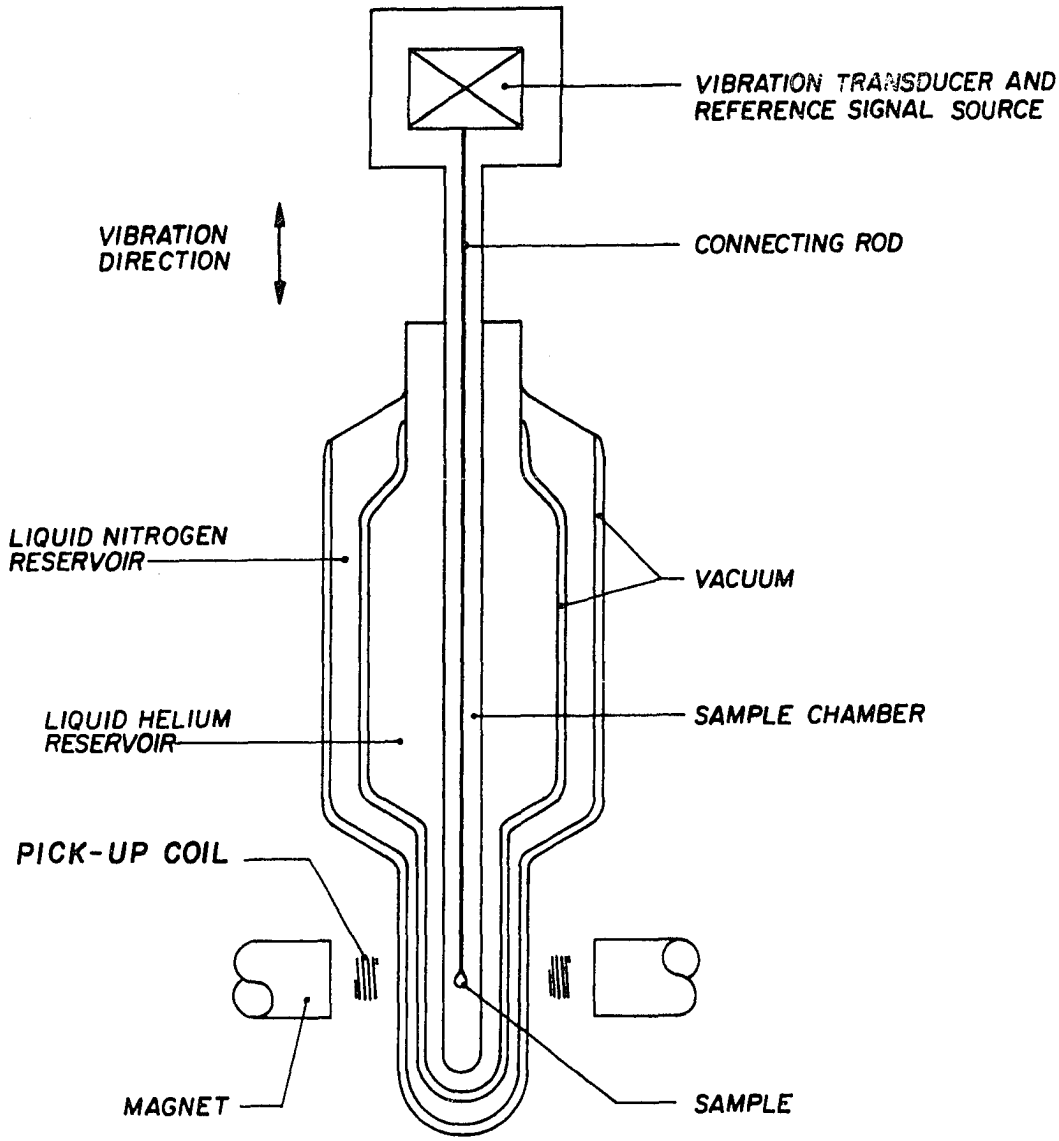

Figure 9. Schematic diagram of cryostat

Standards (35a). The particular thermocouple used in this study differed somewhat from the above calibration. However, it was found that a linear correction to the NBS calibration could be made with an accuracy of $\pm 0.1^{\circ}K$. This was determined by checking the thermocouple against another thermocouple which did fit the NBS calibration.

Heat was supplied to the sample by passing a DC current through a heater element consisting of 50 ohms of no. 41 gauge manganin wire wound noninductively on the heater assembly. Power was supplied simply by a storage battery together with a voltage divider and a variable resistor in series with the heater. The temperature was controlled by hand by careful adjustment of the heater current. It was found that the temperature could easily be maintained to within $\pm 0.05^{\circ}K$ by this method.

Some difficulty was experienced at first with thermal inequilibrium between the sample and the thermocouple. This was finally overcome by placing the thermocouple bead directly on the sample as shown in Figure 5. The isothermal sample can was placed over the sample so that the bottom of the can forced the thermocouple bead tightly against the sample.

4. Magnet

The magnet was a Harvey-Wells Model L-158 water cooled laboratory electromagnet. It featured a 15 inch pole diameter with hyperco pole tips tapered to 6.25 inches. The magnet was capable of producing fields in excess of 27,000 oersteds with an air gap of 1.8 inches. The fully transistorized magnet power supply regulated the current to the magnet to a few parts in 10^6.

a. Calibration The voltage across a temperature controlled manganin reference resistor in series with the magnet was calibrated against the field of the magnet as determined by nuclear magnetic resonance. In order to establish a definite hysteresis curve, it was necessary to saturate the magnet at maximum power three or four times. Once the hysteresis loop was well defined, it was possible to determine the field to 0.1% from the calibration. It was found that the calibration was equally reproducible when the field was approached from either zero or maximum power although the calibrations were slightly different in the two cases.

B. Mutual Inductance Bridge

The mutual inductance bridge (MIB) used in this study was the one described in detail by Gerstein (35b). Briefly, it consisted of two sets of induction coils, the "sample coils" and the "external coils". A 33 cycle per second current was supplied to the primary of both sets of coils. This resulted in a field in the core of the sample coils of about 10 oersteds. With a specimen in the core of the sample coils, the mutual induction between the primary and secondary was different than the mutual induction with no specimen present. This difference in mutual induction was directly related to the susceptibility of the specimen. The measurement was made by having the secondary of the sample coils as one arm of a bridge and the secondary of the external set as another arm. By adjusting the mutual inductance of the external coils, a null could be obtained which was amplified and displayed on an oscilloscope which served as the null detector.

The sample coils of the apparatus were placed in a cryostat. This permitted susceptibility measurements in the range 1.3 to 300^{o}K.

III. EXPERIMENTAL PROCEDURE

A. Vibrating-Sample Magnetometer

1. Discussion of sample geometry

When one makes magnetic measurements, he wishes to represent some of his data as a function of magnetic field. Unfortunately, it is the so-called internal field, and not the applied field, which is characteristic of the sample material. The internal field, H, can be quite different from the applied field, H_o. For a specimen whose magnetic moment per unit volume is given by M, the internal field is given by

$$H = H_o - DM . \qquad (3\text{-}1)$$

D is called the demagnetizing factor and the quantity DM the demagnetizing field. Everything else being equal, one would like to make D, and thus the demagnetizing field, small so that the correction to the applied field is small. Since D is a function of sample geometry, some thought must be given to the shape of sample that is to be prepared.

If one has a homogeneous isotropic medium, the demagnetizing factor is well known for ellipsoidal specimens, of which the sphere is an ideal case, and to a fairly good approximation for long thin cylinders where the field is parallel to the cylinder axis (33). For a cylinder whose length to diameter ratio is 10, the demagnetizing factor is smaller than that for a sphere by a factor of about 10. Therefore, it would appear that the cylinder is the better choice of sample geometry. However, there are a number of other things to be considered, particularly when single crystals are to be used.

The main advantage of cylinders is the small demagnetizing factor. However, when single crystals are used, one must be able to cut out the sample without damaging the crystal. Small diameter cylinders are very difficult to cut without damaging the crystal, so parallelepipeds are normally used. In that case, the demagnetizing factor can only be approximated. This is not so serious as it sounds since the demagnetizing factor is small and, therefore, any error is not particularly significant.

There is another advantage to cylinders (or parallelepipeds). The torque exerted on an anisotropic sample can be quite large when other than the easy direction of magnetization is parallel to the field. Considerable difficulty may be experienced with spherical samples ripping loose from the mount. This is easily overcome with cylinders.

A serious disadvantage to cylinders occurs when the working volume in the cryostat is limited. For the apparatus used in this study, the length of the cylinder would be limited to about 4mm. In order to achieve a favorable length to diameter ratio, the mass would be so small as to considerably reduce the sensitivity of the measurements.

Finally, a separate sample is needed for each crystallographic axis which is to be measured if cylinders are used. All three axes can be measured with one sample if spheres are used. Spheres allow two crystallographic axes to be measured with one mounting of the sample. Other axes can be measured by simply remounting the same sample.

After considering all these things, spherical samples were used in this study.

It was mentioned above that the demagnetizing factor is accurately known only for isotropic specimens. The rare-earth metals are extremely anisotropic. This posed a problem in the present study which is discussed in Section III.A.4.a.

2. Sample preparation

a. Preparation of single crystals A single batch of each of the metals, erbium, yttrium, and lutetium, was used as the starting material for all of the specimens used in this study. These metals were produced in this laboratory. The analytical data for each of the metals are shown in Table 1. The alloys were prepared by arc-melting the two components together on a water-cooled copper hearth in a purified argon atmosphere. The button was turned over and remelted a minimum of five times to insure homogeneity. The last melt left the specimen roughly cylindrical to facilitate the cutting of a spherical sample after the single crystals were grown.

Single crystals were grown from these arc-melted specimens by a strain-anneal method similar to that described by Nigh (6). In the present case, however, the arc-melted specimen was sealed inside a well outgassed tantalum crucible which was filled to about half an atmosphere with helium gas. This resulted in considerably less sublimation of the components during annealing. Also, it was found that less contamination of the sample occurred than if it were hung directly inside the vacuum furnace.

The crucible containing the sample was placed in a vacuum furnace where it was heated to a temperature about 200°C below the melting point

Table 1. Impurity values for starting metals

Element	H	N	O	C	F	Mg	Al	Si	Ca	Ti	Cr	Fe	Ni
Er	2	5	43	40	50	-< 1	-< 30	100	90		-< 30	-< 20	30
Lu	-	5	83	53	2	-< 3	-< 30	-< 20	< 25	-< 50	-< 30	-< 20	-< 20
Y	14	21	298	86	18	<30						78	22

Element	Cu	Ta	W	Y	Nd	Sm	Gd	Tb	Dy	Ho	Er	Tm	Yb
Er		-< 300	-< 300	-< 100					-< 100	< 100		-< 10	< 50
Lu	< 20	-< 300	-< 300	-< 100							-< 10	-< 10	-< 10
Y	300	-< 400			-< 200	-< 200	-< 30	-< 200	< 200	-< 100	100		<100

All values are in parts per million by weight

-< element not detected, number indicates detection limit of method and therefore impurity can only be said to be less than that amount

< detected, but less than

blank element not investigated

Considering the possibility of sample inhomogeneity, impurity values, where detected, are probably ±20% although the analytical methods are better than that for any one particular sample

of the sample. Although yttrium is the only one of the three metals for which a high-temperature allotrope has been observed in the pure metal, magnesium alloys of the other two metals do have such an allotrope (36). The possibility of interference by such an allotrope in the present alloys was avoided by staying well below the melting point of the sample. This temperature was maintained for 18 to 36 hours and then cooled over a period of about 30 minutes to room temperature. This resulted in large grains which usually extended entirely across the diameter of the cylinder and, in one case, up to 20mm in length.

b. Cutting and polishing of spheres Spherical crystals about 4mm in diameter were cut from the grains described above with a spark-cutter. This was accomplished by using a lathe to rotate the cylinder about its longitudinal axis and advancing a tantalum tube, which served as the cutting tool, along a direction perpendicular to the axis of rotation of the cylinder. The surface of the spheres were rather rough and pitted after spark-cutting. Therefore they were polished to smoothness and nearly perfect sphericity in three stages.

The sample was first placed in a one-inch diameter circular race. Air was forced tangentially into the race so that the sample rolled rapidly around the inside surface which was lined with sandpaper. Ten to twenty hours were required for the surface of the sample to become relatively smooth. In the author's opinion, it might be better to leave out this step. It is felt that the surface would be strained less and therefore less electropolishing later on would be required if this step were omitted.

The samples were then further polished using two copper rods which had been drilled out slightly to form a sort of pipe as shown in Figure 10. The sample was held between the ends of the two rods, one of which was turned rapidly with a lathe. The other rod was held by hand and worked about so that the sample moved in a random manner. A 0.3 micron diamond paste, commonly used for polishing metallographic specimens, served as the abrasive. This stage of the polishing was continued until the sample was spherical to within about 0.1%, i.e., from 0.0001 to 0.0002 inch as measured by a micrometer. This process took about an hour.

The sample was then polished electrolytically to remove the worked surface so that the Laue x-ray camera could be used to align the crystal. The electrolyte used was a 5 to 10% solution of 70% perchloric acid in methanol at $-78^{\circ}C$. A pair of tweezers was used to hold the sample while polishing. With the tweezers, and thus the sample, as the anode, the current was turned on with a current density of about 100 ma/cm^2 for about ten seconds. Then the sample was dropped and picked up again in a random manner so that the tweezers came in contact with a different portion of the sample surface, and the current was turned on again. This procedure was repeated 15 or 20 times. It was found that this method left the surface of the sample free from ridges or pits which would have occurred if the sample was held in one position during the polishing process.

Since the sample being polished was a single crystal, the surface was removed faster along some crystallographic directions than others. However, it was found that the sample was still spherical to within about 0.0005 inch after polishing.

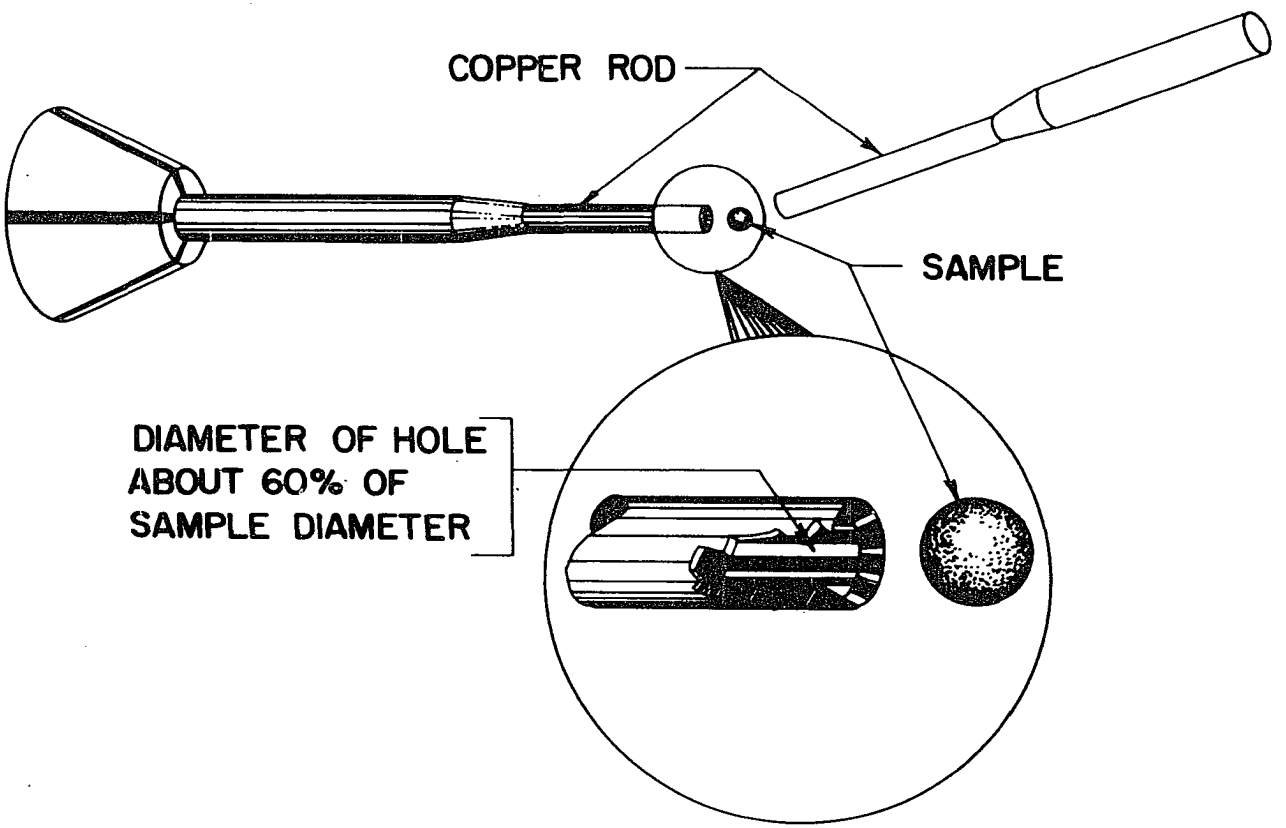

Figure 10. Apparatus used for polishing spherical samples

c. Density measurements The quantity, M, in Equation 3-1 is in units of emu per unit volume. All the magnetic results are in units of emu per gram. Therefore, it was necessary to know the density of the samples in order to calculate the demagnetizing field.

The density was determined for each sample after polishing with the copper rods, which is described above, and before electropolishing. The diameter was measured to ±0.0002 inch. This, together with the weight, yielded the density.

d. Analytical description of samples The analytical results for each of the starting metals are shown in Table 1. All impurity values are given in parts per million (ppm) by weight. Hydrogen, nitrogen, and oxygen impurities were determined by a vacuum fusion technique. The carbon and fluorine results were determined by a wet chemical analysis method. The other impurities were determined by spectrographic analysis.

After the single crystals were grown, a portion of each of the crystals was reanalyzed for hydrogen, nitrogen, and oxygen. These results are shown in Table 2.

It was feared that some contamination of the sample might occur during the cutting and polishing processes. Since analysis would destroy the sample, this possibility was investigated using several erbium samples whose original impurity levels were about the same as the actual samples. They were subjected to the same cutting and polishing procedure and then analyzed for impurities. These results show that there was some contamination by hydrogen, nitrogen, oxygen, and carbon due to spark-cutting. However, this was only a surface contamination since polishing of the surface removed the impurities.

Table 2. Impurities and composition of samples used in this study

Element	Er	$Lu_{25}Er_{75}$	$Lu_{50}Er_{50}$	$Lu_{75}Er_{25}$	$Y_{25}Er_{75}$	$Y_{50}Er_{50}$	$Y_{75}Er_{25}$
			VSM Samples				
H	3	5	6	1	1	1	2
N	7	-	-	-	4	5	6
O	116	179	206	98	88	101	147
Calc. % Er		75.5	50.5	25.4	74.4	50.7	24.6
Anal. % Er		75.3	50.6	26.1	77.2	50.3	25.2
			MIB Samples				
Cal. % Er		74.7	49.7		75.2	52.5	
Anal. % Er		75.1	49.3		75.9	52.9	

Hydrogen, nitrogen, and oxygen values are in parts per million by weight, and are ±20%. See explanation with Table 1. Percent erbium values are in atomic percent. Analytical values are ±0.5% of value listed.

The bulk composition of each specimen was determined by two methods. It was calculated by assuming the entire weight loss from both the arc-melting and the annealing processes described above was due to sublimation of erbium. This assumption is justified because of the very much higher vapor pressure of erbium (37). The bulk composition was also determined by a visable-light absorption technique. This method was used to analyze only for erbium in each case. These results, along with the calculated values, are shown in Table 2.

The homogeneity of portions of three of the crystals, $Y_{75}Er_{25}$, $Lu_{25}Er_{75}$, and $Lu_{50}Er_{50}$, was determined with a microprobe analyzer. In each case, the composition across the specimen was found to vary by less than 0.5% which was the detection limit of the analyzer. From these results it was assumed that the other alloys would also be homogeneous and they were not analyzed by the microprobe analyzer.

The lattice parameters were determined for each of the samples by a powder x-ray diffraction method. This was done to confirm that the alloys were solid solutions. The measured lattice parameters fell on a smooth curve between the two pure metals with a slight positive deviation from Vegard's law. The results for the crystallographic c/a ratio are shown in Table 3.

3. Magnetic measurements

A Laue x-ray camera was used to align the sample so that both the c-axis and one of the basal-plane axes would be in the horizontal plane when the sample was in position in the cryostat. G. E. Adhesive No. 7031 was then used to glue it to the sample mount as shown in Figure 5. The sample chamber and sample rod assembly were then placed in the cryostat where the sample was cooled to 4.2°K. The sample was then centered with respect to the pick-up coils and also with the desired crystallographic axis parallel to the field as described in Section II.A.2.

Measurements in the temperature range below 4.2°K were made by pumping out the reservoir above the liquid helium level. Temperatures as low as 1.2°K were obtained in this manner. In the temperature range from 4.2 to about 78°K, measurements were made with the inner reservoir filled with

liquid helium. From 78°K to room temperature, the inner reservoir was filled with helium gas and the chamber between the inner and outer reservoirs was filled with nitrogen gas. The outer reservoir, of course, contained liquid nitrogen. It was found that these exchange gases provided sufficient cooling without having to fill the inner reservoir with liquid nitrogen in this temperature range.

For measurements up to a few degrees above bath temperature, the sample chamber was filled with helium gas at a pressure of about 100 microns. At higher temperatures, the sample chamber was pumped out to a pressure of the order of 10^{-4} Torr. It was found that pressures in the sample chamber below about 200 microns had no effect on the measurements.

All magnetic measurements were made isothermally as a function of field in the entire temperature range 1.2 to 300°K. After each isotherm, the sample was warmed to a few degrees above the Néel temperature, cooled to 4.2°K in zero magnetic field (actually ~50 oersteds), and then warmed to the desired temperature for the next isotherm. A field was applied only after the desired temperature was reached. One exception to this was for pure erbium whose Néel temperature is ~85°K. In this case, for isotherms above 78°K, the sample was cooled only to 78°K before warming to the next isotherm. The above statements are true, of course, only for isotherms up to the Néel temperature. Above the Néel temperature, the sample was warmed directly to the next isotherm without first cooling to bath temperature.

Most samples were run twice. Between runs, the sample was removed from the apparatus and realigned with the Laue x-ray camera. For each of Figures 11 to 49, the separate runs are shown with different symbols.

4. Treatment of data

a. Demagnetizing field correction In Section III.A.1., the necessity of correcting magnetic data for the demagnetizing field was discussed. It bears repeating that this correction is essential so that the data is dependent only on the sample material and not on the particular sample geometry.

For an isotropic sphere, it can be shown (38) that the demagnetizing factor is equal to $4\pi/3$. However, the rare-earth metals are extremely anisotropic and, under these circumstances, the demagnetizing factor cannot be accurately calculated even for a sphere. Even so, as a trial, the c//H magnetic data for erbium was corrected using $4\pi/3$ for the demagnetizing factor. As the following discussion shows, $4\pi/3$ is obviously not a good value.

In the antiferromagnetic region, if a sufficiently large field is applied along the easy direction of magnetization, a critical field is found where the moments spontaneously align and the specimen becomes ferromagnetic. There should be a nearly discontinuous transition from the antiferromagnetic to the ferromagnetic state, at least at temperatures only slightly above the Curie temperature. This discontinuous transition has been observed experimentally for dysprosium (39, 40), holmium (41), and erbium (24) as well as calculated theoretically for dysprosium (42). The experimental work on holmium and erbium was done with parallelepiped samples where the correction for the demagnetizing field is small. The small demagnetizing field minimizes any error in its calculation. Therefore, one would expect the results to be fairly accurate. However, by

using $4\pi/3$ for the demagnetizing factor, the erbium curve in the present study bent back on itself in this region (i.e., three values of magnetic moment were observed for a given field in the neighborhood of the transition). This, of course, is absurd.

The reason for the triple-valued curve is that the data was over-corrected for the demagnetizing field, i.e., the demagnetizing factor was too large. The correct demagnetizing factor is not the theoretical value, apparently, because of the large anisotropy. Now one might expect the anisotropy to be a function of temperature with, perhaps, a very rapid change in the neighborhood of the various magnetic transitions. Thus the demagnetizing factor may be a function of temperature, and, in particular, it may be different in the different magnetic regions. Unfortunately, there is no way of accurately determining what the demagnetizing factor should be except in the antiferromagnetic region. Here, the fact that the antiferromagnetic-ferromagnetic transition should be discontinuous provides a method for experimental determination. It is possible to choose a demagnetizing factor such that the curve starts out vertically at the transition and then bends forward slightly as the moment approaches the saturation value. This is a reasonable sort of curve, and at the very least it gives a much better value than $4\pi/3$ for the demagnetizing factor.

Fortunately, it is only in this region where the use of the wrong demagnetizing factor would result in any appreciable error in the final results. In this region, the critical field at the antiferromagnetic-ferromagnetic transition, when plotted vs. temperature and extrapolated to zero field, yields the Curie temperature. This temperature is effected somewhat by the choice of demagnetizing factor. In other regions,

different demagnetizing factors result only in slight changes in the shape of the curves. See, for example, Figure 11 where the curves in the ferromagnetic region show that erbium begins to saturate at fields somewhat higher than found by Green et al. (24).

At any rate, the most satisfactory solution seems to be to experimentally determine the demagnetizing factor in the antiferromagnetic region and use this value at all temperatures. This experimental fit should be made at temperatures just slightly above the Curie temperature for pure erbium. For the alloys, which have no Curie temperature, the fit should be made at the lowest temperatures, i.e., in the neighborhood of $4.2^{\circ}K$.

The discussion so far has been concerned with the easy direction of magnetization. It is obvious that if the demagnetizing factor is different from $4\pi/3$ along the easy direction, it must also be different along the hard directions. This follows from the fact that the sum of the demagnetizing factors along three mutually perpendicular directions must add up to 4π (43). Since there is almost no basal-plane anisotropy in erbium or any of the alloys in this work, one can write

$$D_a = D_b = 1/2(4\pi - D_c) .$$

Thus the demagnetizing factors along the three principle crystallographic axes were determined for the various samples in this study and are listed in Table 3.

It is interesting to note that there is apprently a different effective anisotropy for rare-earths whose easy direction of magnetization is in the basal plane than for those whose easy direction is the c-axis. The

magnetic properties of dysprosium (40) and of some terbium-holmium alloys (44) have been measured using spherical single crystals. Use of $4\pi/3$ for the demagnetizing factor in these cases resulted in curves which bent back on themselves to the extent of only 300 or 400 oersteds. With erbium, whose easy direction is the c-axis, on the other hand, the error was of the order of 2,000 oersteds.

b. Computer treatment of data In this study, where the demagnetizing factors were large due to the use of spherical samples, the field correction was several percent at temperatures as high as the Néel temperature. Even in the paramagnetic region it was not completely negligible. Therefore, data for all the isofield plots of magnetic moment vs. temperature had to be corrected for the demagnetizing field. This must be done by plotting each isotherm of magnetic moment vs. internal field and extracting the isofield data from the graph. To do all this by hand, however, proved to be an extremely tedious and time comsuming job. Therefore, a computer program was written to handle this.

B. Mutual Inductance Bridge

1. Sample preparation

The spherical single crystals used for the VSM measurements proved to be too small to get reliable results with the MIB. Therefore, larger polycrystalline alloys were prepared from the same starting materials. For reasons discussed in Section IV.A.8., polycrystalline samples were satisfactory. They were arc-melted just as were the VSM samples except that no single crystals were grown. Also, no correction was made to the data for the demagnetizing factor. Therefore, the samples were used just

as they came from the arc-melter even though they were irregularly shaped.

The compositions of the alloys are listed in Table 2. Although the compositions were slightly different than the corresponding VSM samples, they are referred to in the text with the same symbols (i.e., $Y_{75}Er_{25}$ etc. is used for both the VSM and the MIB samples).

2. Magnetic measurements

The MIB data was taken in the range $4.2^{o}K$ to a few degrees above the Néel temperature. Although the temperature range below about $40^{o}K$ was the region of most interest, the Néel temperature measured with the MIB provided a good check with the VSM measurements. The sample was first cooled to $4.2^{o}K$, then warmed a few degrees where it was allowed to equilibrate a few minutes before taking the next susceptibility measurement, and so on.

IV. RESULTS

A. General

1. Condensation of data

A large amount of data was compiled during this study. In an effort to condense the thesis to a reasonable length, an attempt was made to hold the number of graphs to a minimum and still include all pertinent data. Accordingly, some of the curves which were drawn are not included because they are similar to ones already shown (e.g., b-axis curves are generally not included because they are nearly identical to the a-axis curves). The paramagnetic data (i.e., paramagnetic Curie temperatures and Curie constants) are listed in tabular rather than graphical form. For pure erbium, however, a graph of the paramagnetic data is also included to show the form. Also, such things as transition temperatures, which require graphical methods of determination, are merely stated and the graphs from which they were taken are not included.

2. Units

In order to make comparisons of the data for the different samples, it was necessary to normalize all the data to the amount of erbium present in the sample. This was done for both the VSM and the MIB data by assuming that the moment due to either the yttrium or the lutetium ions could be neglected for the purposes of this study. This is a reasonable assumption since neither yttrium nor lutetium have any unpaired electrons. In all cases, the magnetic moment (or susceptibility) of the sample was divided by the weight of erbium in the sample so that all numbers are

in terms of electromagnetic cgs units per gram of erbium.

3. Description of drift

The isothermal data shown in Figures 23, 24, 28, 29 30, 34, 38, 39, 42, and 44 include some points beside which is located either the symbol "L" or "S". This indicates that the magnetic moment was found to change with time. "S" indicates that the amount of change observed, after the temperature and field were established, varied from one to about five percent. "L" indicates a drift of five to more than 100 percent. The amount of this drift was largest and the rate of drift slowest at the lowest temperatures. The direction of drift was toward larger or smaller values of magnetic moment depending on whether the data was taken with increasing or decreasing field respectively.

The points were taken after a waiting period of the order of 30 minutes after which time the moment was usually still drifting slowly. Thus, there is some uncertainty in these points. In some cases, where the uncertainty was particularly great, a dashed line was drawn through the points in the isofield curves.

It would be natural to suspect that this drift was due to thermal inequilibrium. However, there are several things that negate this. Drift was observed at 1.2 and 4.2^{o}K (i.e., bath temperature) where thermal inequilibrium was nonexistant. The drift was reproducibly observed in different regions of temperature and field for the c//H data for all the alloys. It was either not observed or negligible for pure erbium and for the basal-plane data for all of the alloys. The drift was in opposite directions for increasing and decreasing fields while the temperature of

the sample was approached from below in both cases.

The most plausible cause of the drift seems to be atom movement. In erbium metal, a discontinuous change in the crystallographic c/a ratio occurs at the Curie temperature (45). Possibly a similar distortion is brought about by the application of a field in the alloys since drift was observed only in the regions where an abrupt change in moment occurs, such as the transition to ferromagnetism. At any rate, it is not likely that such a long relaxation time could be due to anything electronic or to domain wall movement.

B. Vibrating-Sample Magnetometer Data

1. Pure erbium

The c//H data for pure erbium are shown in Figures 11 to 14. Some small differences were noted between this and previous work. In particular, transition temperatures of 86.5 and 18.2°K were observed for the Néel temperature and the Curie temperature respectively. Previously reported values (13, 24, 25) are about 85 and 19.7°K respectively. In addition, the saturation magnetization found in this study was 276.0 emu/g. compared to 267 emu/g. previously reported (24, 25).

The saturation magnetization was found by first plotting moment vs. reciprocal field for the different isotherms and extrapolating to $1/H = 0$, i.e., infinite magnetic field. The values for the saturation moment thus obtained were plotted vs. $T^{\frac{3}{2}}$ and T^2 and extrapolated to 0°K. Figure 14 shows the data fit a T^2 plot somewhat better.

The Curie temperature was obtained in this study by extrapolating the critical field vs. temperature curve to zero field. The critical field is

the field at which the moments spontaneously align themselves and the sample becomes ferromagnetic. Unfortunately, the observed critical field is dependent upon the demagnetizing factor which, as discussed earlier, is somewhat uncertain. However, a reasonable level of confidence can be placed in the Curie temperature obtained by this method since a very sharp peak was also observed in the a//H data at 18.0°K and in the b//H data at about 18.5°K.

Figure 13 shows a rounded peak corresponding to the transition from one antiferromagnetic structure to another. This transition exhibits considerably more field dependence than does the Néel temperature. When plotted against field and extrapolated to zero field, a transition temperature of 50.5°K was obtained. On the other hand, when the moment vs. transition temperature plot was extrapolated to zero moment, a temperature of 52.3°K was obtained. Also, the a-axis data shown in Figure 21 exhibit a change in slope, which is field independent below 10 K-Oe., at about 52°K.

The discrepancy in the two methods of determining the transition temperature is due to the presence of a spontaneous moment in the range 45 - 55°K. This was observed by extrapolating the moment vs. field curves to zero field. A maximum spontaneous moment of about 3.7 emu/g. was found at 48.5°K by this method. Also, from the isofield data, by plotting the moment at the peak vs. field and extrapolating to zero field, a spontaneous moment of about 3.4 emu/g., was obtained. The values, 3.7 and 3.4 emu/g., are well within experimental error of one another.

To obtain the correct zero field transition temperature, it seems that the peak should be extrapolated to zero field. However, the value

obtained by extrapolating to zero moment agrees better with other workers (13, 21, 25).

Figure 13 also shows a broad peak which occurs only below about 4 K-Oe., in the neighborhood of 26°K. The actual maximum of the peak occurs at about 28°K. This has also been reported by Bozorth and Gambino (13).

When attempts were made to measure the basal-plane magnetization of erbium, the torque exerted on the sample broke it loose from the mount. This was finally overcome by reducing the sample size from about 0.2g. to about 0.05g. and filling the isothermal sample can with Dow Corning Stopcock Grease which acts as a good adhesive when frozen. These samples were designated "crystal #2" and "crystal #2a" respectively even though they were the same crystal. Another crystal of about 0.2g mass was designated "crystal #3" and was used primarily in the paramagnetic region where the torque was much smaller.

The basal-plane data for pure erbium are shown in Figures 15 to 21. Figure 16 shows a sort of "double step" in the isothermal a-axis data at 15°K. Associated with this is a very wide double hysteresis loop shown in Figure 15. The b-axis data in Figures 17 and 18 exhibit a similar "double step" but it appears to occur about 0.5°K higher temperature. Other isothermal data are shown in Figures 19 and 20. There are small differences in the a- and b-axis data below about 40°K.

The isofield basal-plane data are shown only for the a-axis in Figure 21. The b-axis curves are nearly identical except that the sharp peak occurs about 0.5 degrees higher.

Measurements for b//H were not made above 100°K because the a- and b-axis data are identical above 40°K.

The paramagnetic data for both the a- and c-axes of erbium are shown in Figure 22. This plot of reciprocal susceptibility vs. temperature shows that the straight lines for the a- and c-axes are parallel and that both axes obey the Curie-Weiss law above about 120°K. The paramagnetic Curie temperatures and the Curie constant in terms of the effective number of Bohr magnetons were determined by a least squares straight line fit to the data above 120°K. These numbers, as well as the temperature above which the straight line fit was made, are given in Table 3.

Graphs of the paramagnetic data for the alloys are not shown since they are very similar to the one for pure erbium. Table 3 gives the paramagnetic Curie temperatures, the Curie constants, and the temperatures above which the data fall on a straight lines for all the alloys.

2. $Y_{25}Er_{75}$

The c//H data for the $Y_{25}Er_{75}$ alloy are shown in Figures 23 to 25. The isothermal curves in Figure 24 show that the sample begins to saturate at about 21 K-Oe. at 4.2°K. A low-moment pseudosaturation region (plateau) exists up to about 45°K. Hysteresis curves are shown in Figure 23.

Because this alloy had only one plateau whereas the $Lu_{25}Er_{75}$ alloy exhibited two, it was decided to anneal these two samples and rerun a few isotherms. Both samples were annealed at 550°C for twelve hours.

Some of the $Y_{25}Er_{75}$ alloy data for the annealed sample are shown as run 2 in Figure 24. The shape of the curve is not appreciably different although the spontaneous moment, found by extrapolating the curve to zero

field, has been decreased by about 5%.

Isofield data in Figure 25 give a Néel temperature of 70.6°K. A dashed line was drawn to the point at 1.2°K and 3 K-Oe. because the large amount of drift observed lends considerable uncertainty to this point.

The basal-plane isotherms are shown in Figure 26. The b-axis moment is shown to be about 2% larger at low temperatures. The 4.2°K isotherms for both the a- and b-axes are represented by one curve at low fields. This was done merely because it is difficult to resolve the difference at low moments although it does exist. Within experimental error, the basal plane is isotropic above about 60°K.

A narrow hysteresis (shown only for the a-axis in Figure 23) was observed for both the a- and b-axes. This hysteresis gradually decreases to zero as the temperature is increased to about 18°K.

Since the a- and b-axes are nearly identical, only the a//H isofield data are shown in Figure 27. A peak is shown which extrapolates to a zero field temperature of 16.4°K. A slight change of slope occurs at the Néel temperature of 70.6°K.

3. $Lu_{25}Er_{75}$

The isothermal c//H data for the $Lu_{25}Er_{75}$ alloy are shown in Figures 28 to 32. Figure 28 shows that the sample saturates in fields greater than about 14 K-Oe. at a moment only slightly less than that of pure erbium. Figures 29 and 30 show two low-moment pseudosaturation regions. The first exists in the range 1.2 - ~30°K; the second in the range ~12 to ~38°K. The decreasing field curves in Figure 28 show the moment remains relatively constant at low fields with a value about equal to that at the

second plateau.

The isofield c//H data in Figures 31 and 32 give a Néel temperature of 68.4°K. In addition, a peak which exists only at intermediate fields occurs in the neighborhood of 20°K. This is the result of the two plateaus mentioned above. The peak is quite flat, particularly at fields in the neighborhood of 10-12 K-Oe., because the height of the second plateau is constant between about 14 and 18°K. The data for the annealed sample described earlier is shown as run 3 and is seen to reproduce quite well.

The zero-field temperature at which the transition from the first to second plateau occurs was found by two methods. First, the temperature at the midpoint of the flat peak was plotted vs. field and extrapolated to zero field. Secondly, the critical field for which the spontaneous transition occurs was plotted vs. temperature and extrapolated to zero field. Temperatures of 27.0 and 27.5°K respectively were obtained for the two methods. It seems somewhat questionable to do this since neither the peak nor the second plateau exist at low fields. However, for lack of a better way to define the transition temperature, this is what was done.

In the region below about 6 K-Oe. and below about 6°K, the amount of drift observed was very large and the rate of drift quite slow. Therefore, the data in this region is suspect and a dashed line was drawn through these points in Figure 32.

The basal plane data indicate a b-axis moment about 3.5% larger than the a-axis moment at 4.2°K. This anisotropy decreases to less than 1% above about 80°K. The isothermal curves are quite similar to those for the $Y_{25}Er_{75}$ alloy and are not, therefore, shown. Only the 4.2°K isotherm for the a-axis is shown in Figure 29. Figure 28 shows the 4.2°K a-axis hysteresis which gradually decreases to zero as the temperature is

increased to about 18°K.

Isofield data for the a//H direction are shown in Figure 33. The b//H curves are not shown because they are nearly identical to the a//H curves. A peak is observed which extrapolates to a zero-field temperature of 16.1°K. A slight change in slope is observed at the Néel temperature of 68.4°K.

4. $Y_{50}Er_{50}$

The isothermal data for both the c//H and the a//H directions are shown in Figures 34 and 35. This sample is not ferromagnetic even at the highest fields. However, a low-moment pseudosaturation region is observed below about 24°K, and at temperatures between about 10 and 30°K, a second pseudosaturation region is observed. This results in the peak shown in Figure 36 which exists only above about 7 K-Oe. The decreasing field data show a wide hysteresis at low fields in the temperature range where both plateaus exist. Two of these curves are shown in Figure 34.

The zero-field temperature for the transition from the first to second plateau was found by the same two methods described for the $Lu_{25}Er_{75}$ alloy. A temperature of 17°K was found by extrapolating the temperature at the peak vs. field to zero field. A temperature of 18°K was found by extrapolating the critical field vs. temperature curve to zero field.

At low temperature and low field, there was a large drift in the c-axis measurements. Therefore, a dashed line was drawn through these points in Figure 36 since there is considerable uncertainty in them.

Figure 36 shows the Néel temperature of this alloy to be 54.1°K.

There is about 1.5% anisotropy (b-axis moment larger) in the basal plane at 4.2°K. This decreases to zero above about 40°K. Only the a-axis isofield data are shown in Figure 37. A small peak occurs at 12.5°K and there is a slight cahnge in slope at the Néel temperature.

5. $Lu_{50}Er_{50}$

The c//H data for the $Lu_{50}Er_{50}$ alloy are shown in Figures 38 to 41. The moment begins to saturate at about 20 K-Oe. at 4.2°K. A tendency toward pseudosaturation is observed up to about 20°K. Hysteresis curves are shown in Figure 38. A rather wide loop occurs in the low-moment plateau region. The isofield data in Figures 40 and 41 show a Néel temp temperature of 49.2°K. There was some drift in the 1.2°K isotherm so dashed lines have been drawn to these points.

The a-axis data are shown in Figures 39 and 41. The basal plane is isotropic at all temperatures within experimental error. A very small rounded peak occurs in the 2 K-Oe. isofield curve at about 9°K. A change in slope occurs at the Néel temperature.

6. $Y_{75}Er_{25}$

The c//H data for the $Y_{75}Er_{25}$ alloy are shown in Figures 42 and 43. Although Figure 42 shows that the high-field moment at 4.2°K is nearly the saturation moment of pure erbium, the curves are indicative of those in the neighborhood of a Néel temperature. There is a very narrow hysteresis (about 400 oersteds wide at 4.2°K) below about 20°K. However, this is not shown in any of the figures. The isofield data in Figure 43 shows the Néel temperature to be 31.5°K.

Representative a//H data are shown in Figures 42 and 43. The b-axis was not measured in this alloy since measurements on the other five alloys indicated there would be very little, if any, basal-plane anisotropy.

7. $Lu_{75}Er_{25}$

The c//H data for the $Lu_{75}Er_{25}$ alloy are shown in Figures 44 and 45. The moment at 4.2°K at high fields is nearly the saturation moment of pure erbium. Here again, the curves are indicative of those in the neighborhood of a Néel temperature. The decreasing field data is nearly identical to that described for $Y_{75}Er_{25}$ alloy and is not shown. Figure 45 shows the Néel temperature to be 27.4°K.

Representative a-axis data are shown in Figures 44 and 45. About 1.5% basal plane anisotropy was observed (b-axis moment larger) but some of this may be due to experimental error. Figures 44 and 45 show the a-axis moment is less than the c-axis moment at all temperatures. This is not true for the $Y_{75}Er_{25}$ alloy.

8. Need for zero field measurements

The zero-field transition temperature from one antiferromagnetic spin configuration to the other for pure erbium was found to be 50.5°K in this study. Other workers have reported it to be 52 to 54°K (13, 21, 25). Recently, Child et al. (15) have made some neutron diffraction studies on yttrium-erbium alloys and have reported these same two configurations to be present in all the alloys they studied in the range 90 to 30 atomic percent erbium. If allowances are made for the errors they place on the transition temperatures, it is found that it varies in a manner somewhat like the variation of the Néel temperatures in these alloys.

In the present study, only two alloys, $Lu_{25}Er_{75}$ and $Y_{50}Er_{50}$, were found to have anomalies which might be attributed to the transition from one antiferromagnetic configuration to the other. However, these anomalies do not exist at zero field and apparently occur at different temperatures than those observed by Child et al. Thus it is questionable as to whether they correspond to the same transition. This was thought to be a little strange since the peak corresponding to this transition was quite prominent in the pure erbium data. Since the lowest field used in the VSM data was usually about 2 K-Oe., it was decided to run some of the samples at zero field on a mutual inductance bridge.

New samples were prepared for the MIB measurements since those used for the VSM measurements were too small. Since only anomalies indicating magnetic transitions were sought, and not quantitative results, polycrystalline samples were satisfactory and thus polycrystalline samples were used. The compositions of the alloys used for the MIB measurements are listed in Table 2.

C. Mutual Inductance Bridge Data

The MIB data are shown in Figures 46 to 49. In all four alloys, the Néel temperature observed is in reasonable agreement with the VSM data. The MIB data in the neighborhood of the Néel temperature were taken "on the run" as the temperature was slowly increased. This may have resulted in some thermal inequilibrium so that the observed Néel temperature may be slightly high. In all samples except the $Y_{25}Er_{75}$ alloy, the only other anomaly observed was a peak whose temperature corresponds well with the a-axis peak in the VSM data. The $Y_{25}Er_{75}$ alloy exhibits a change in slope

at about 16°K which is also in good agreement with the a-axis peak in the VSM data. However, it also has a peak at about 29°K which might be considered to correspond to the 27°K peak in the VSM data for the $Lu_{25}Er_{75}$ alloy.

Table 3. Summary of experimental results

Sample	c/a	D_c	D_a	T_c	T_a	T_{x1}	T_{x2}	T_N	T_N(calc.)	μ_{eff}	θ_c	θ_a	T_P
Er	1.572	3.10	4.70	18.2	18.2	28	50.5	86.5	87.3	9.93	59.0	30.5	120
$Y_{25}Er_{75}$	1.572	3.38	4.59		16.4		29.5	70.6	78.5	9.89	46.9	19.3	120
$Y_{50}Er_{50}$	1.572	$4\pi/3$	$4\pi/3$		12.5		17.5	54.1	55.2	10.05	33.5	8.1	90
$Y_{75}Er_{25}$	1.573	$4\pi/3$	$4\pi/3$					31.5	34.8	9.88	19.9	-2.2	60
$Lu_{25}Er_{75}$	1.574	3.60	4.48		16.1		27.5	68.4	72.2	10.00	49.3	21.3	120
$Lu_{50}Er_{50}$	1.578	$4\pi/3$	$4\pi/3$		9.0			49.2	55.3	9.97	36.0	12.6	90
$Lu_{75}Er_{25}$	1.581	$4\pi/3$	$4\pi/3$					27.4	35.6	10.03	20.6	0.6	60

All temperatures are in degrees Kelvin

c/a	Crystallographic c/a ratio
D_c	Demagnetizing factor used for c-axis data
D_a	Demagnetizing factor used for basal plane data
T_c	Curie temperature
T_a	Temperature of peak in basal plane isofield curves
T_{x1}	28°K peak in c-axis isofield curve of erbium
T_{x2}	Transition temperature from one antiferromagnetic structure to another in erbium (in the alloys, the anomaly at this temperature may be due to something else)
T_N	Néel temperature

Table 3 (Continued)

Sample	c/a	D_c	D_a	T_c	T_a	T_{x1}	T_{x2}	T_N	T_N(calc.)	μ_{eff}	θ_c	θ_a	T_P

T_N(calc.) Calculated Néel temperature

μ_{eff} Number of effective Bohr magnetons from paramagnetic data

θ_c Paramagnetic Curie temperature for c-axis

θ_a Paramagnetic Curie temperature for a-axis

T_P Temperature above which data obey Curie-Weiss Law

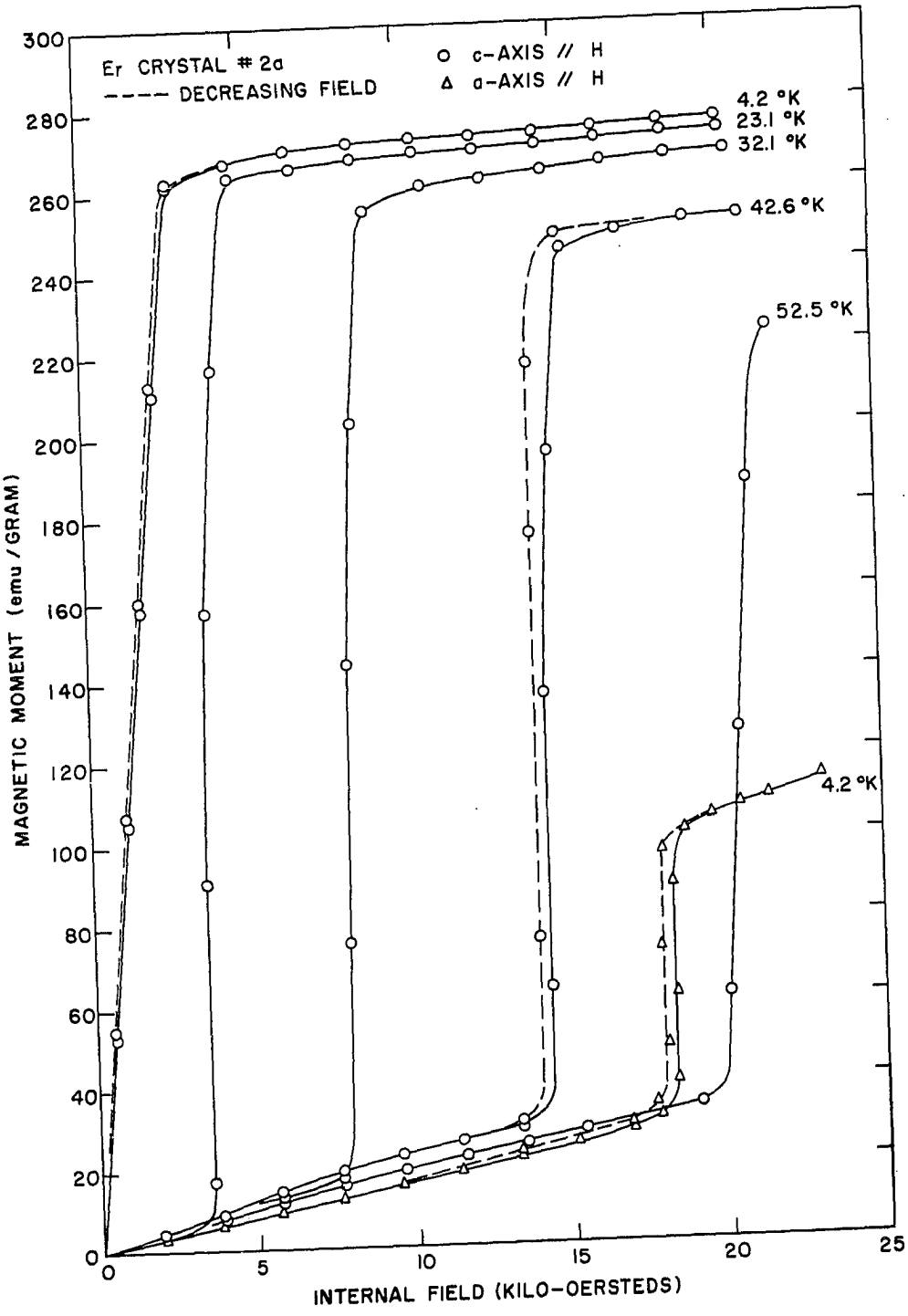

Figure 11. Magnetic moment vs. field for the a- and c-axes of erbium at various temperatures

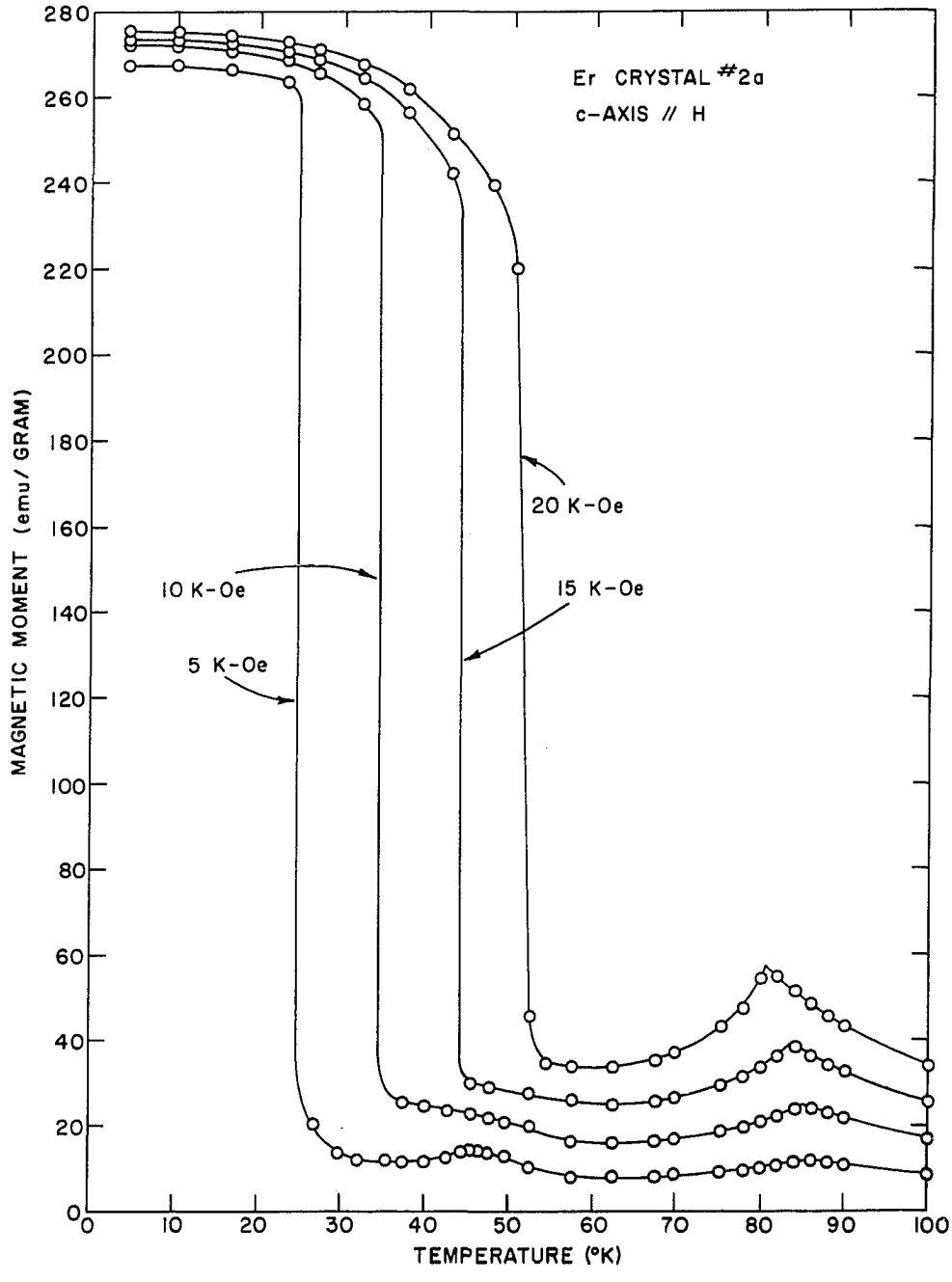

Figure 12. Magnetic moment vs. temperature for the c-axis of erbium at various constant internal fields

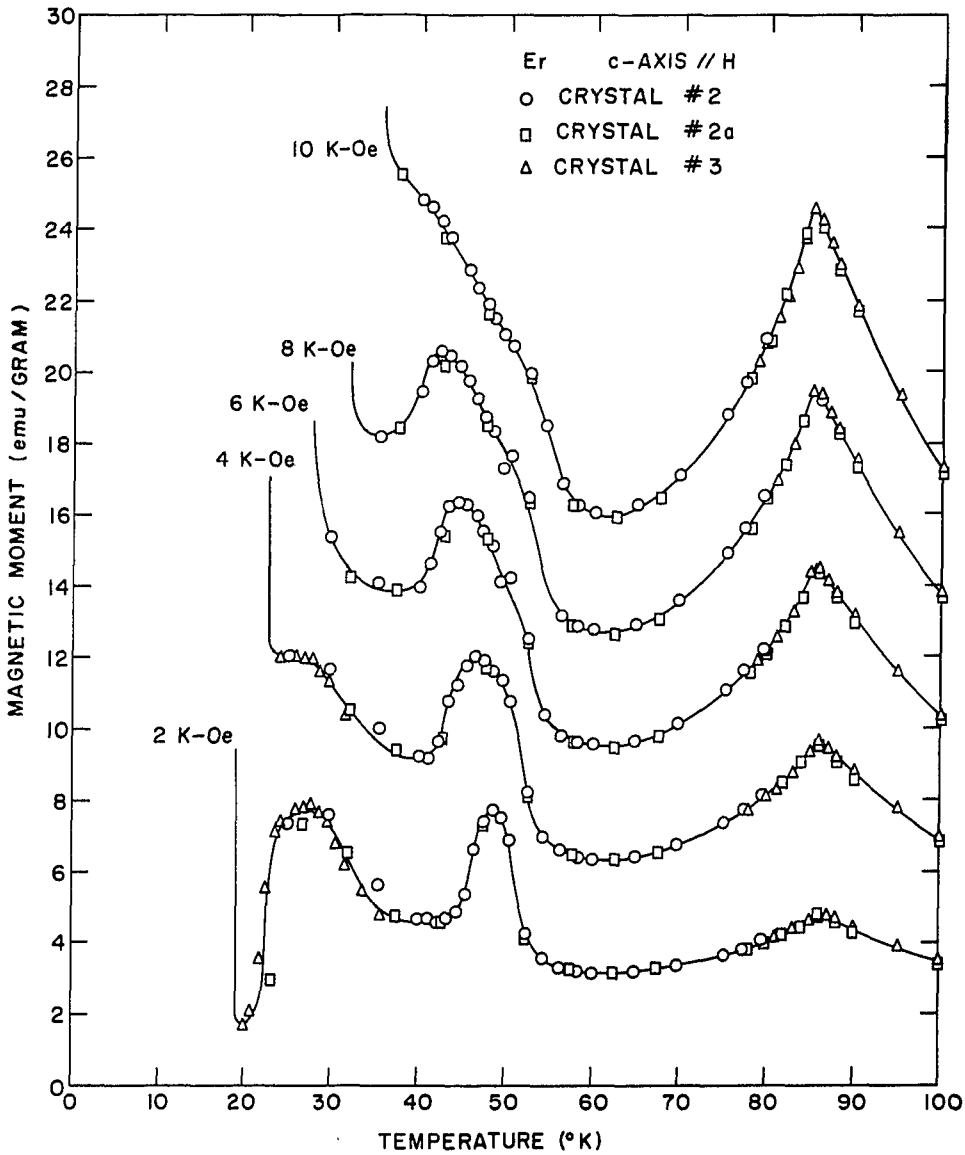

Figure 13. Magnetic moment vs. temperature for the c-axis of erbium at various constant internal fields (expansion of part of Figure 12)

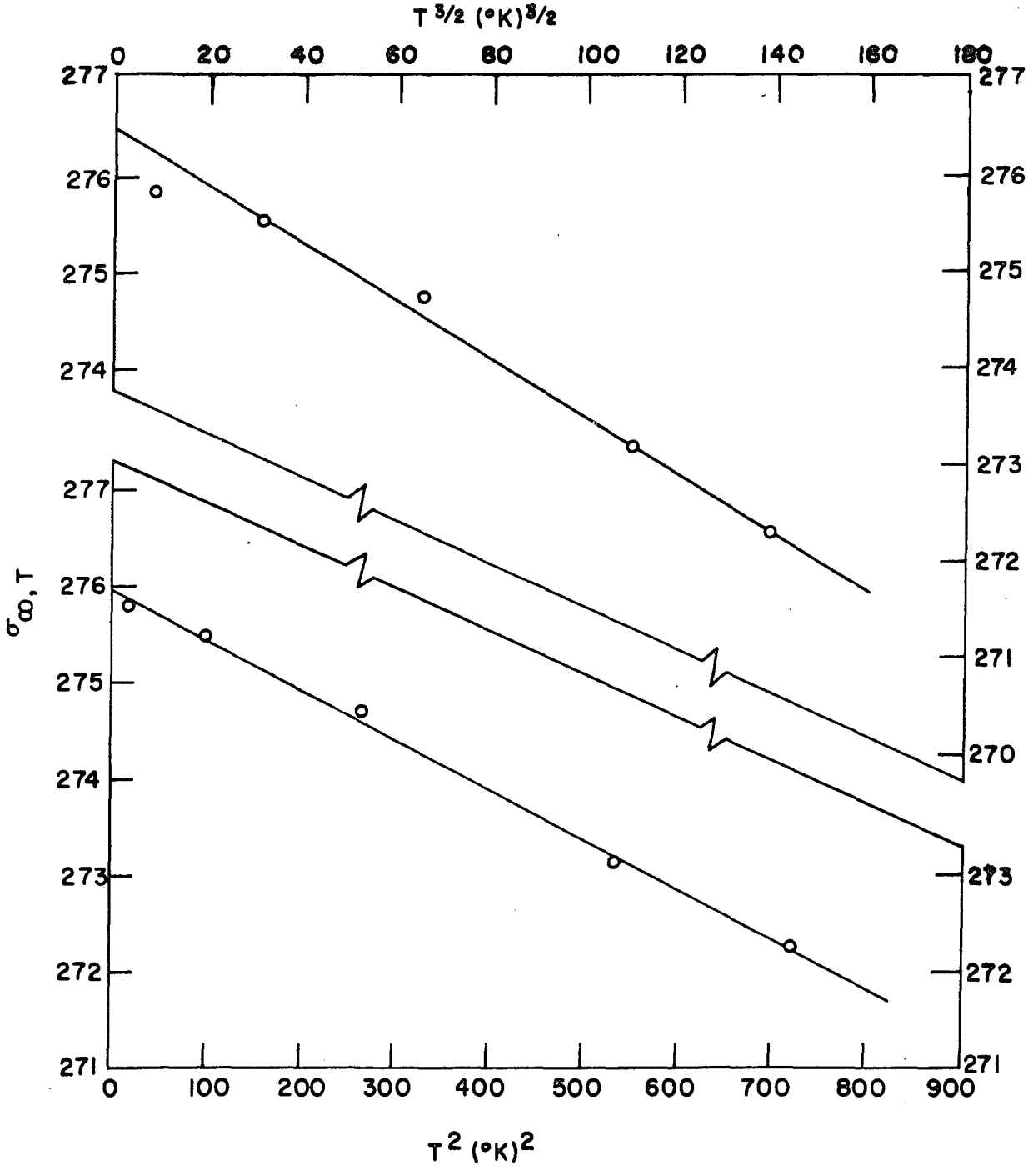

Figure 14. Saturation moment per gram vs. $T^{\frac{3}{2}}$ and T^2 for the c-axis of erbium

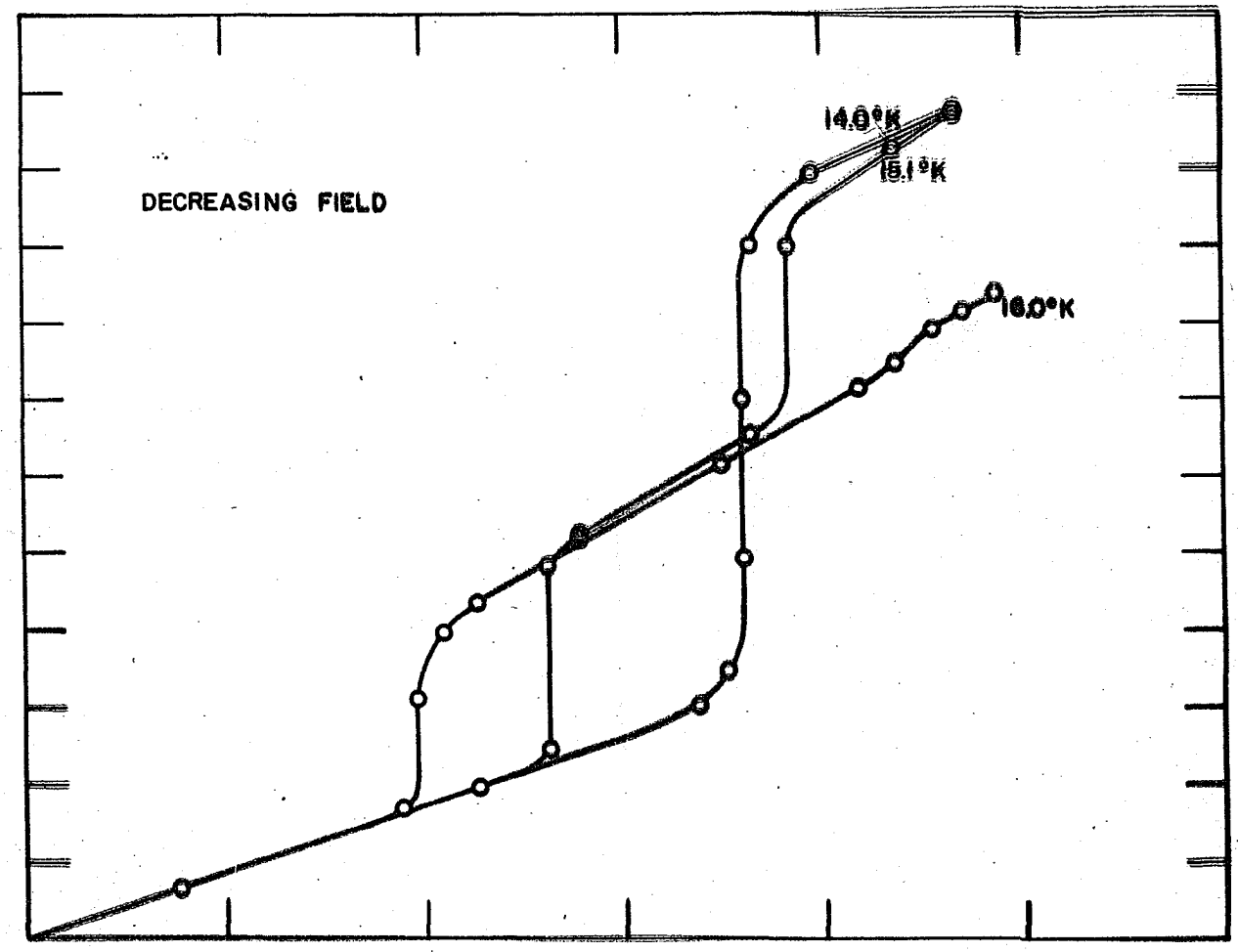

Figure 15.
(decreasing field curves)

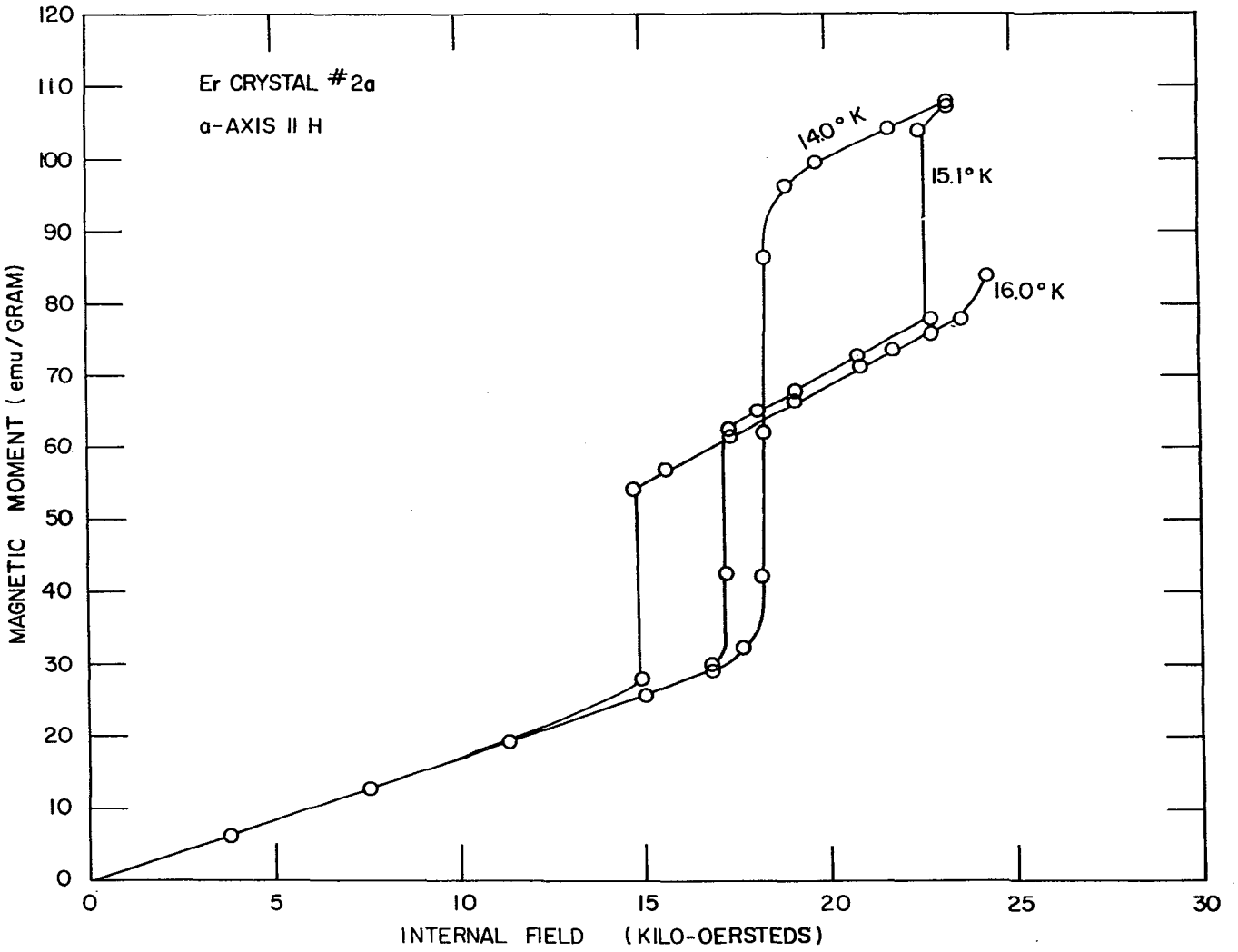

Figure 16. Magnetic moment vs. field for the a-axis of erbium in the neighborhood of 15°K

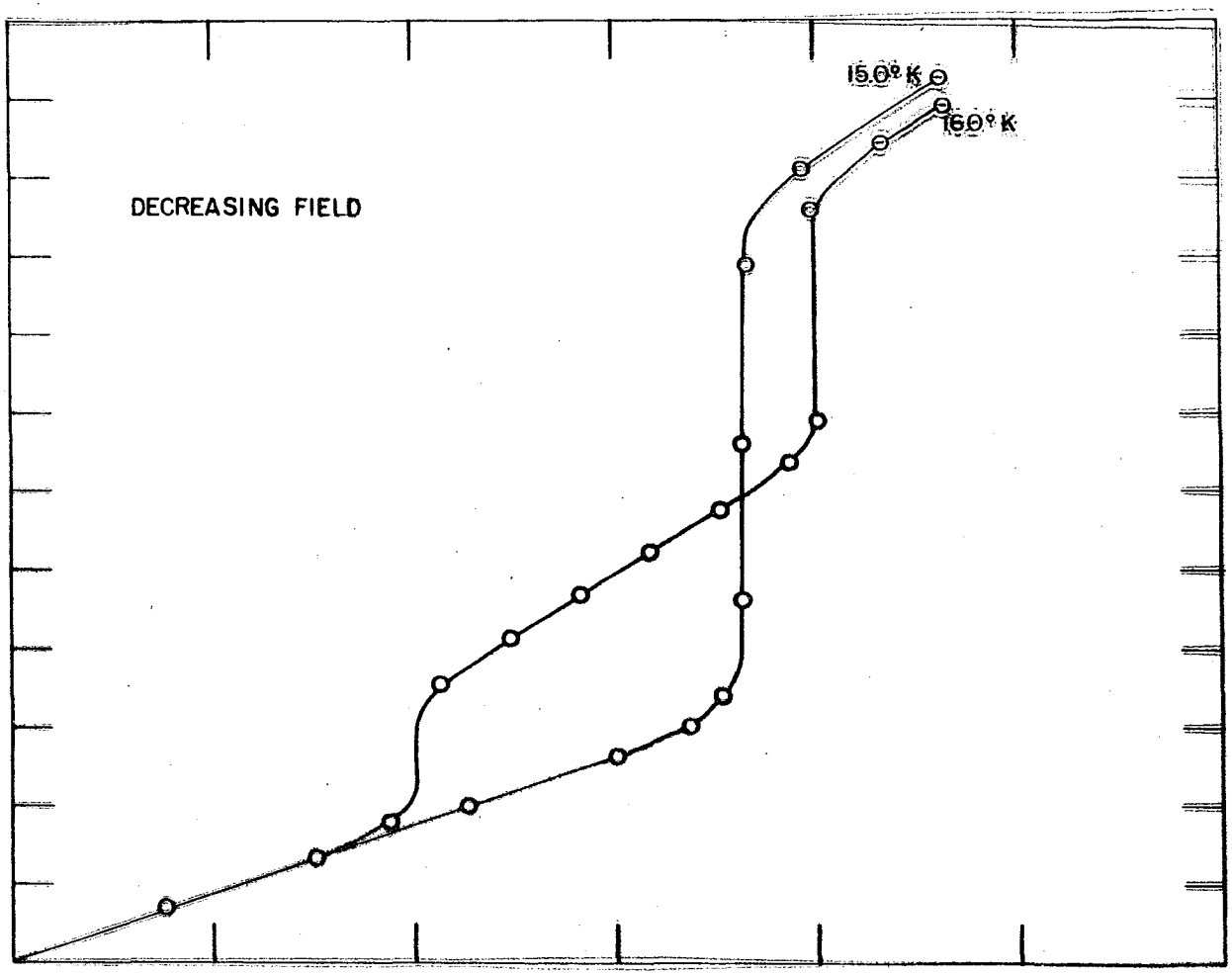

Figure 17.
(decreasing field curves)

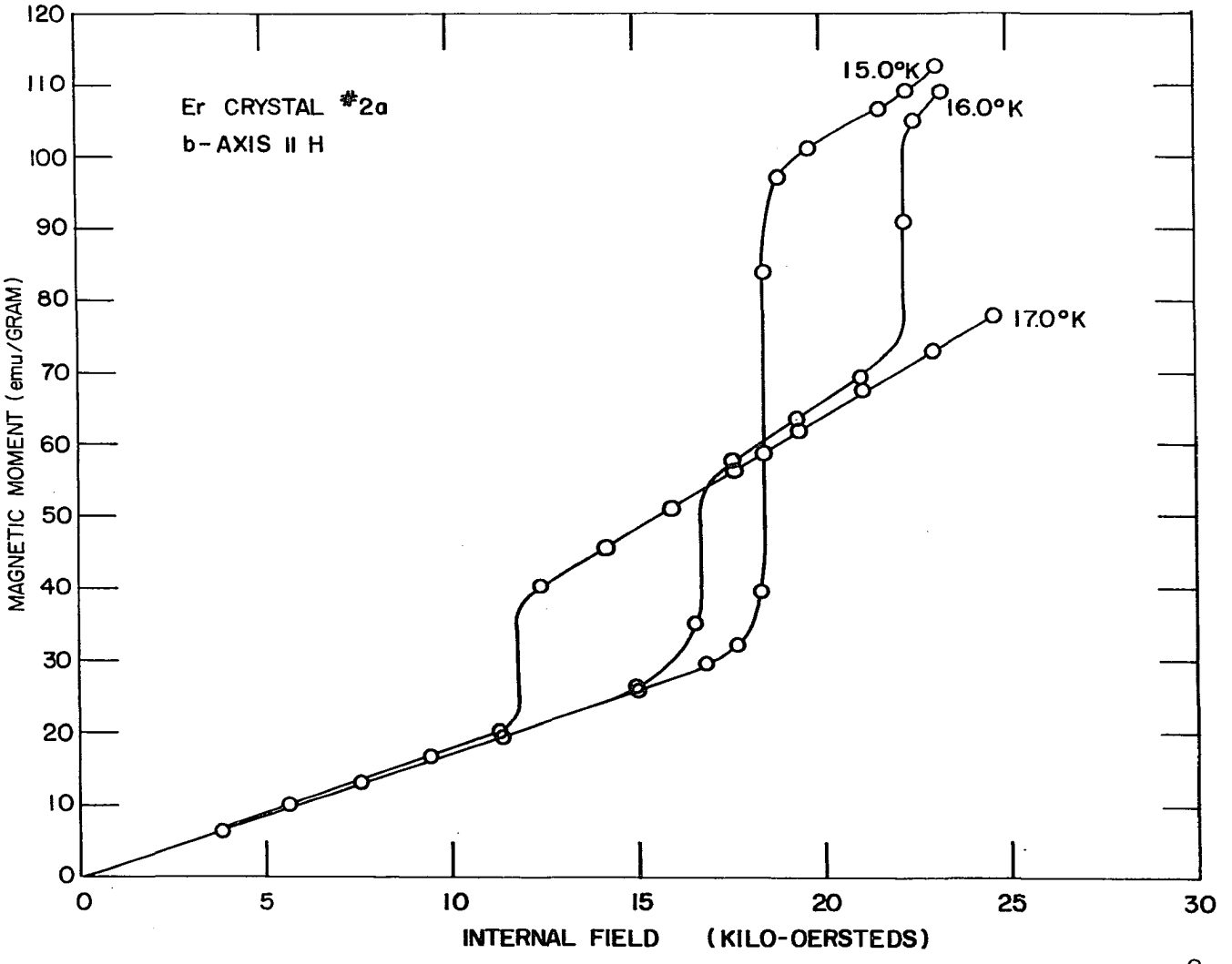

Figure 18. Magnetic moment vs. field for the b-axis of erbium in the neighborhood of 16°K

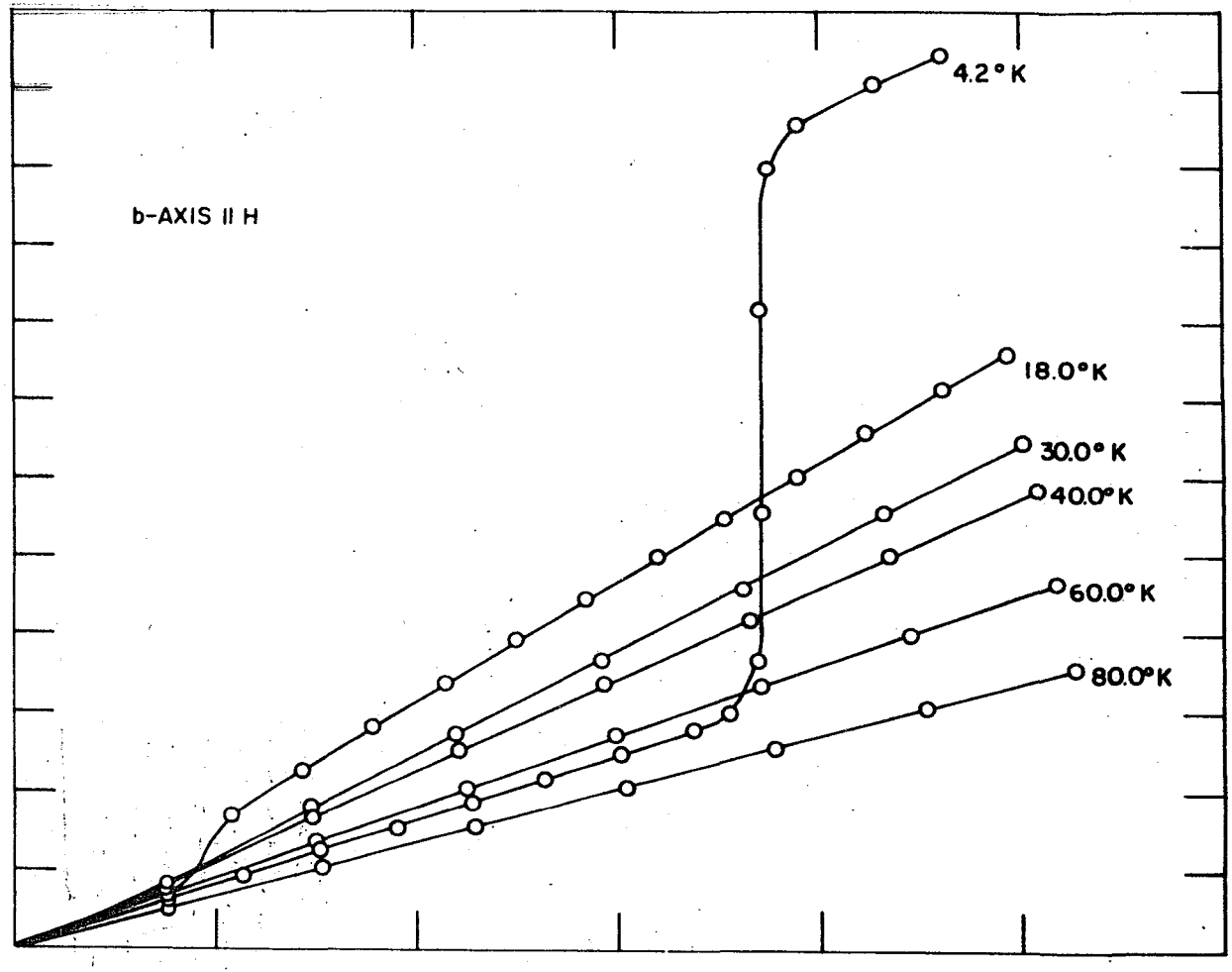

Figure 19. (b-axis parallel to H)

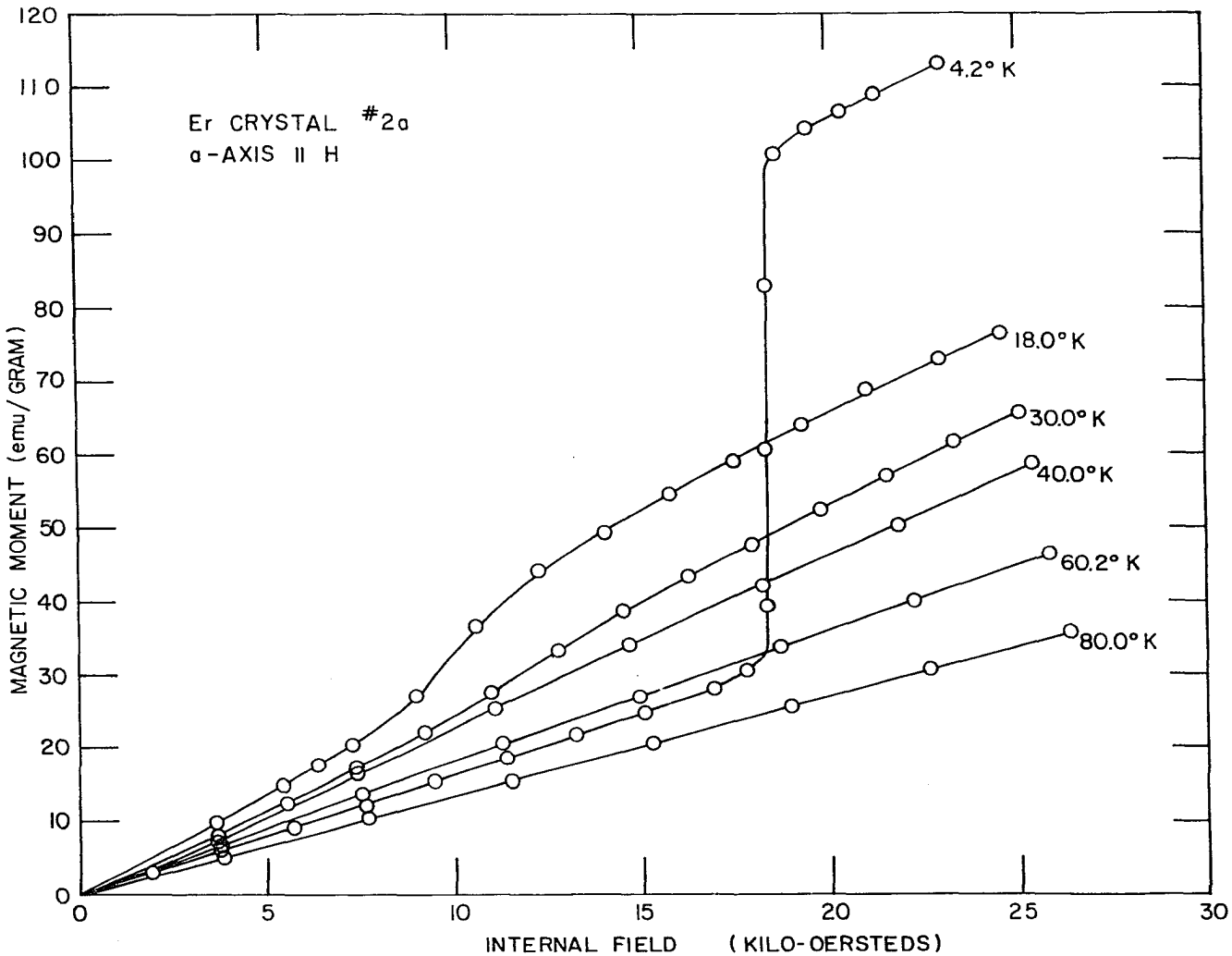

Figure 20. Magnetic moment vs. field for erbium at various temperatures (a-axis parallel to H)

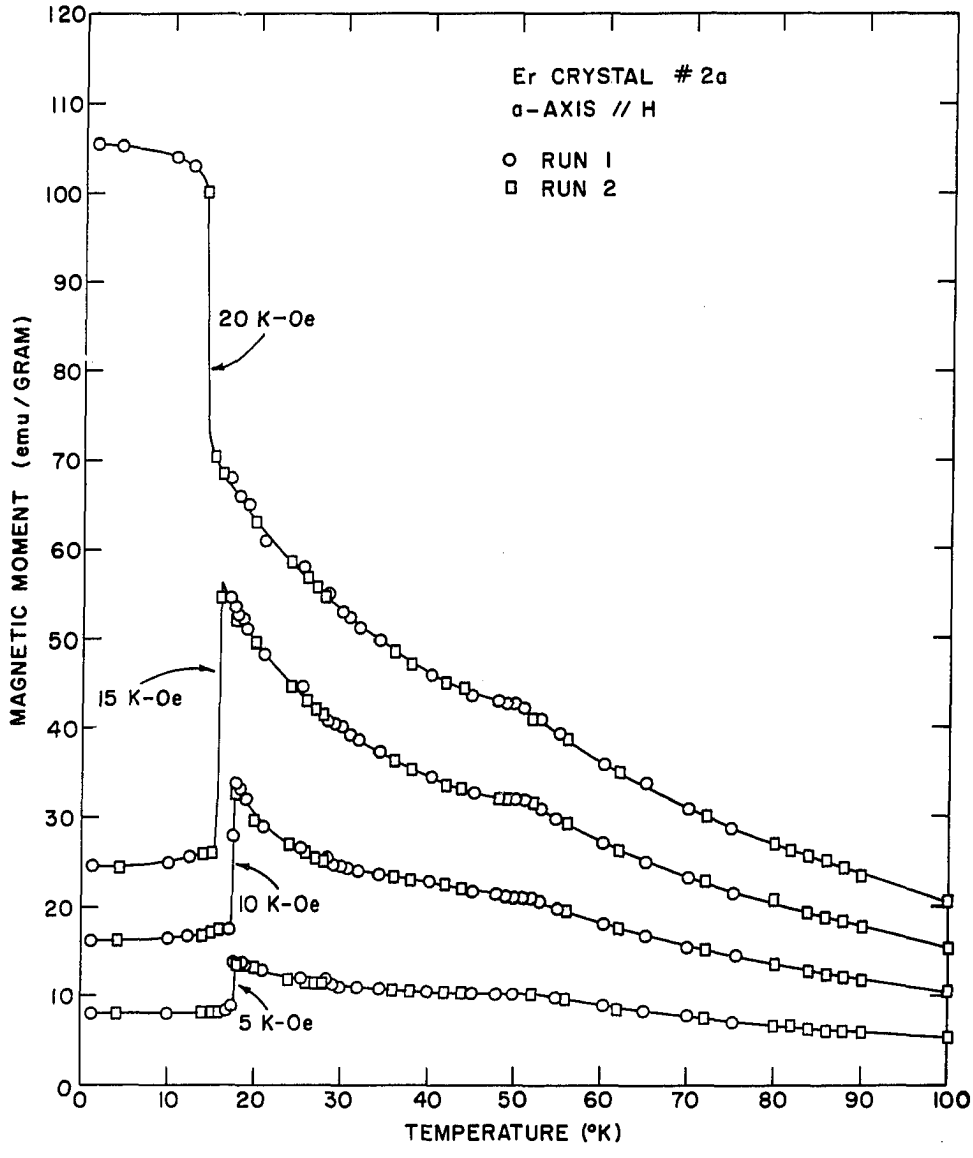

Figure 21. Magnetic moment vs. temperature for the a-axis of erbium at various constant internal fields

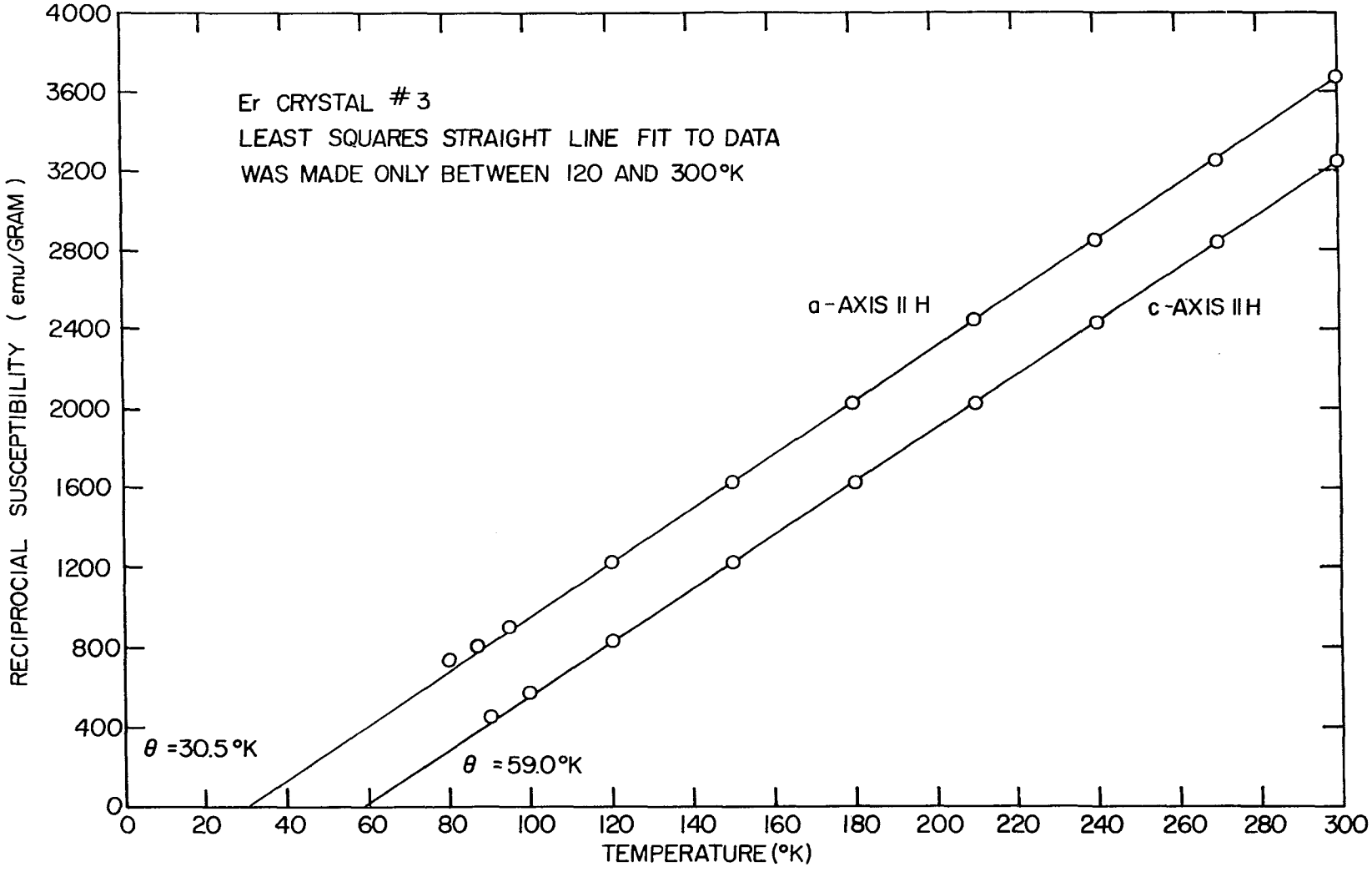

Figure 22. Reciprocal susceptibility vs. temperature for the a- and c-axes of erbium.

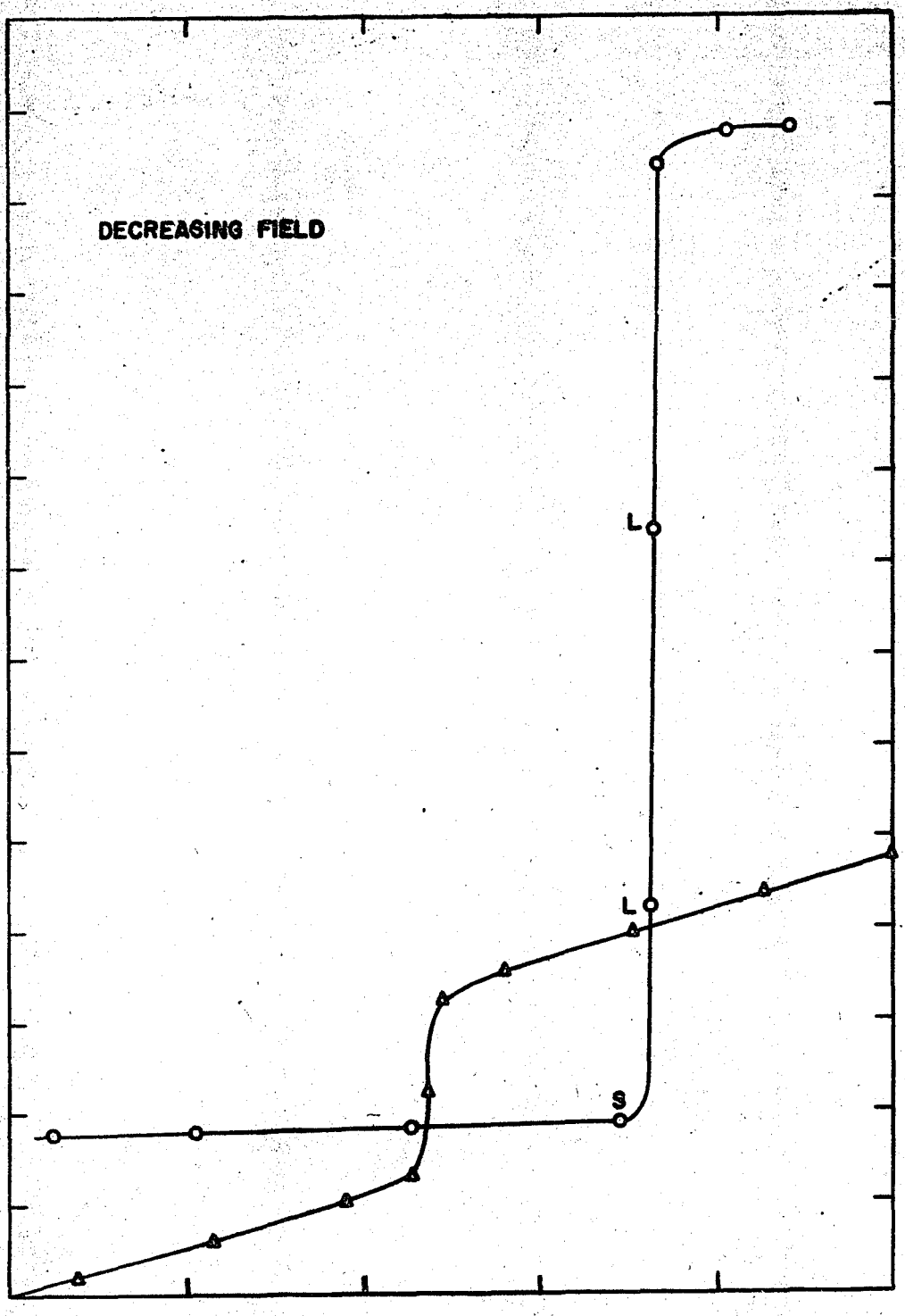

Figure 23. (decreasing field curves)

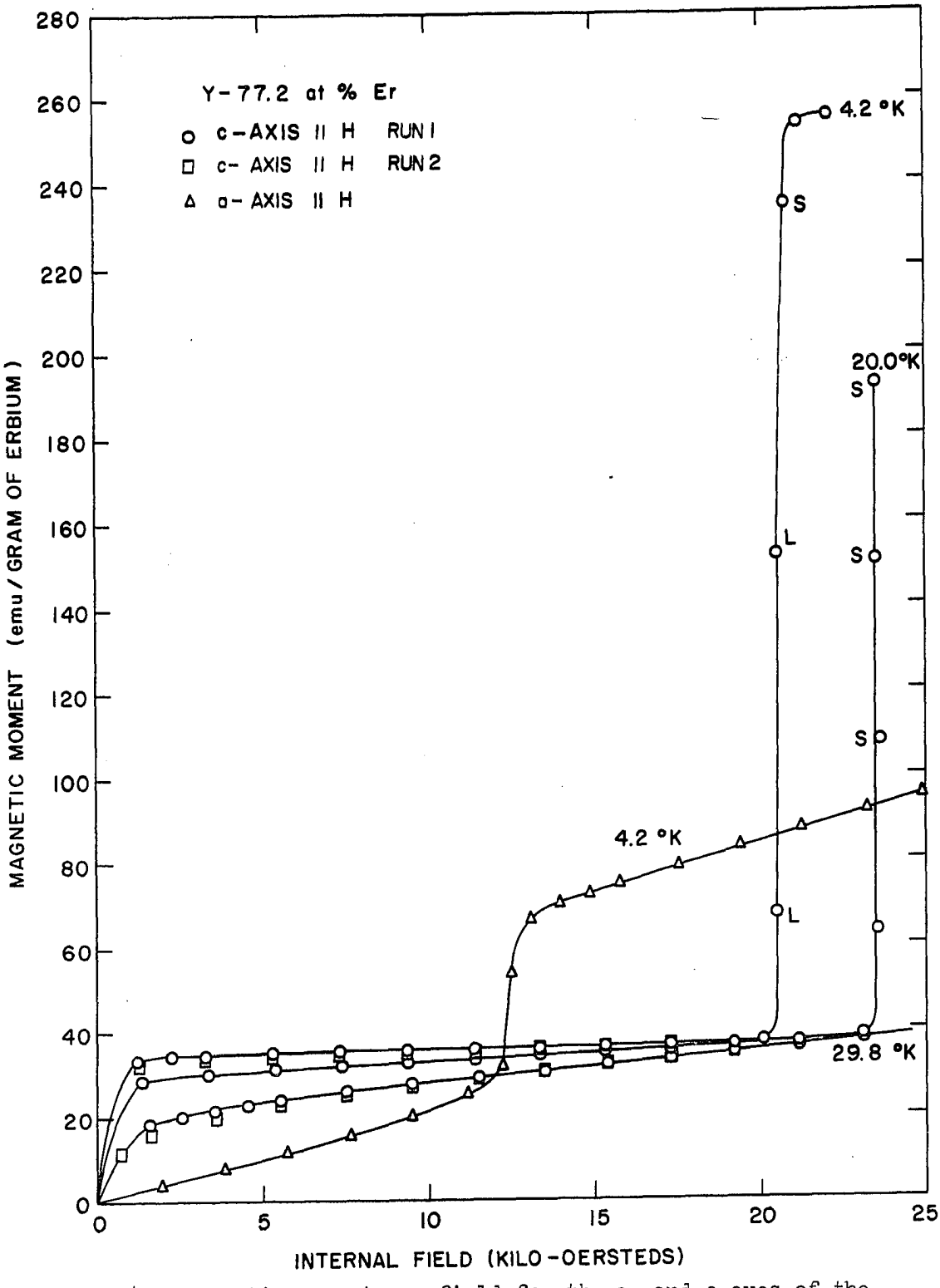

Figure 24. Magnetic moment vs. field for the a- and c-axes of the $Y_{25}Er_{75}$ alloy at various temperatures

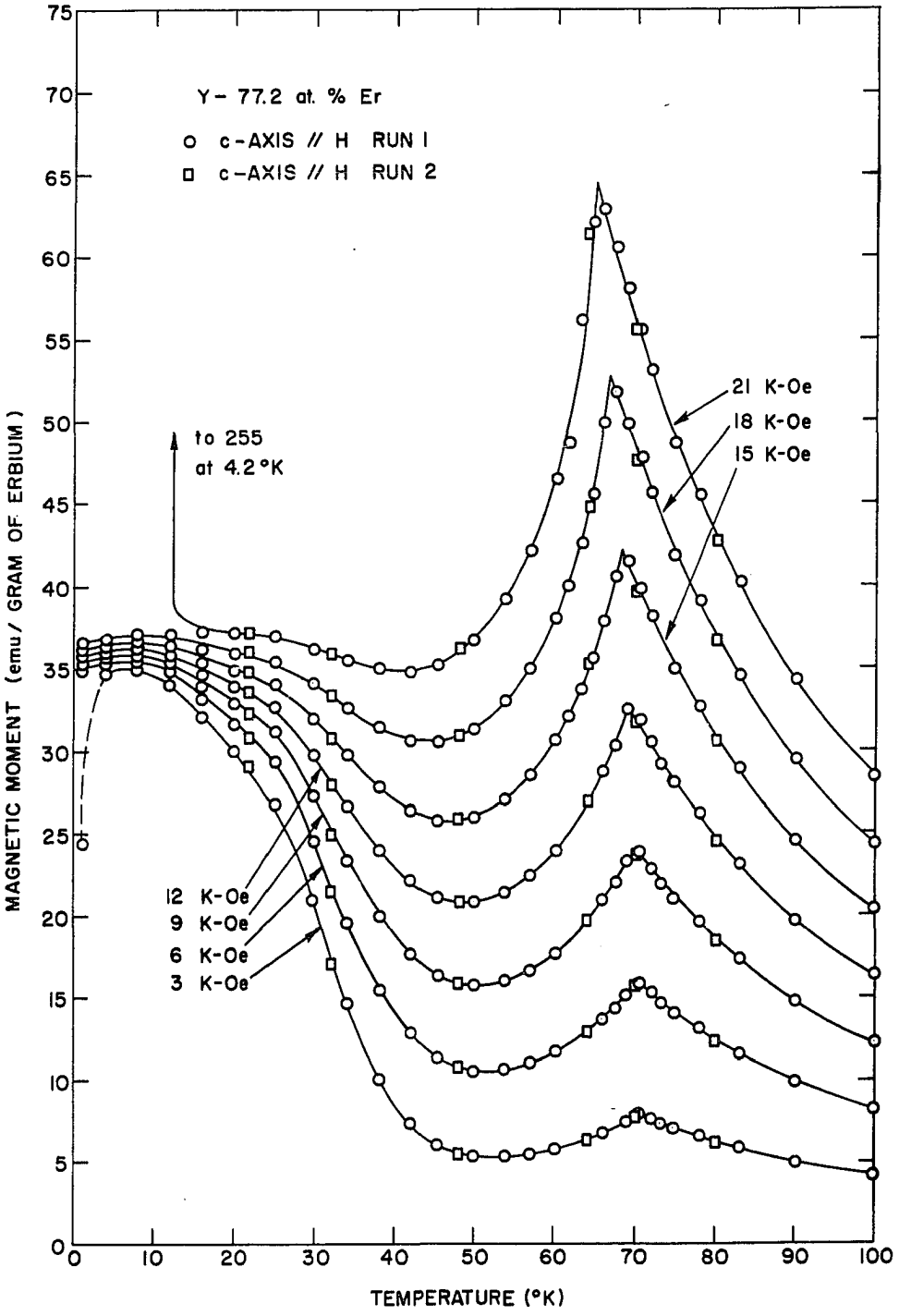

Figure 25. Magnetic moment vs. temperature for the c-axis of the $Y_{25}Er_{75}$ alloy at various constant internal fields
--- region of large drift

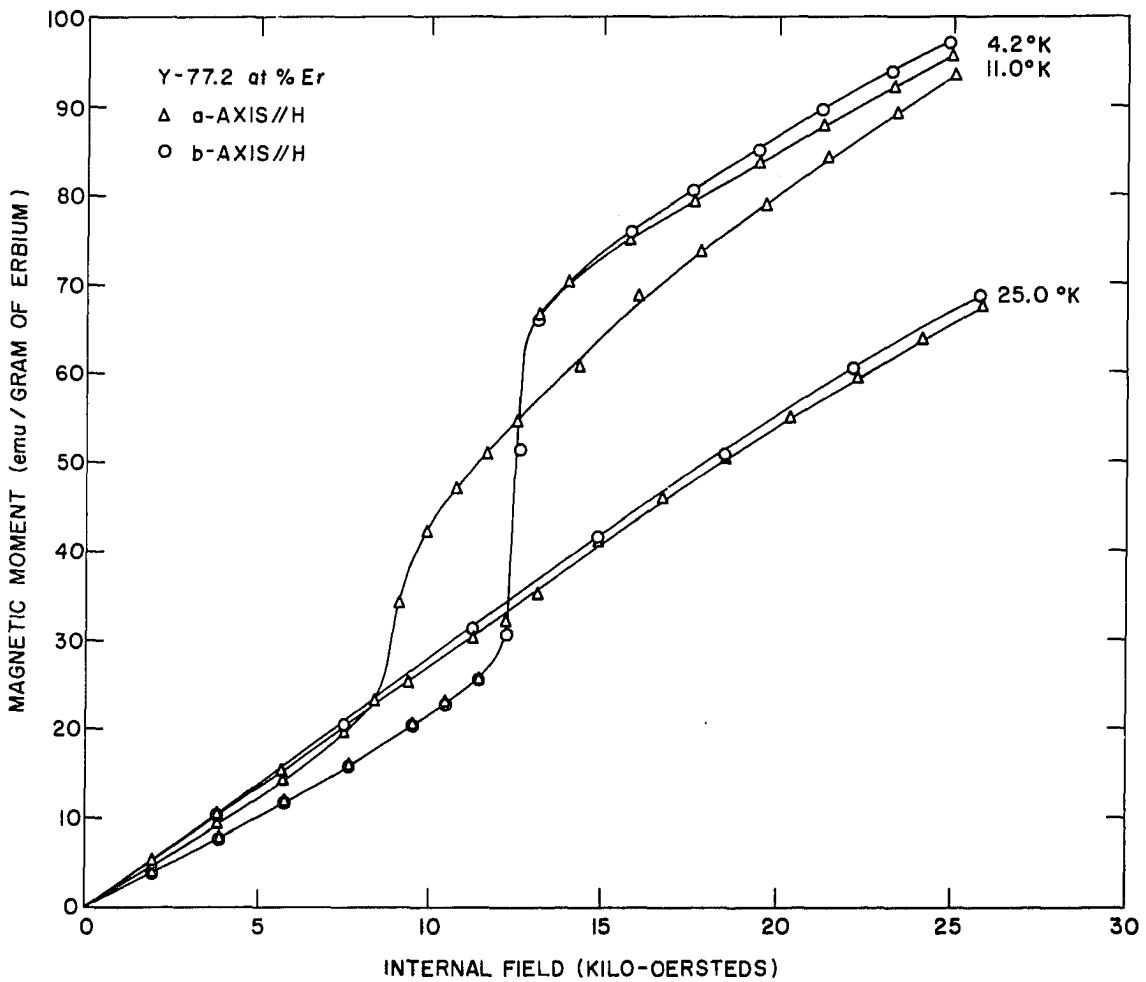

Figure 26. Magnetic moment vs. field for the a- and b-axes of the $Y_{25}Er_{75}$ alloy at various temperatures

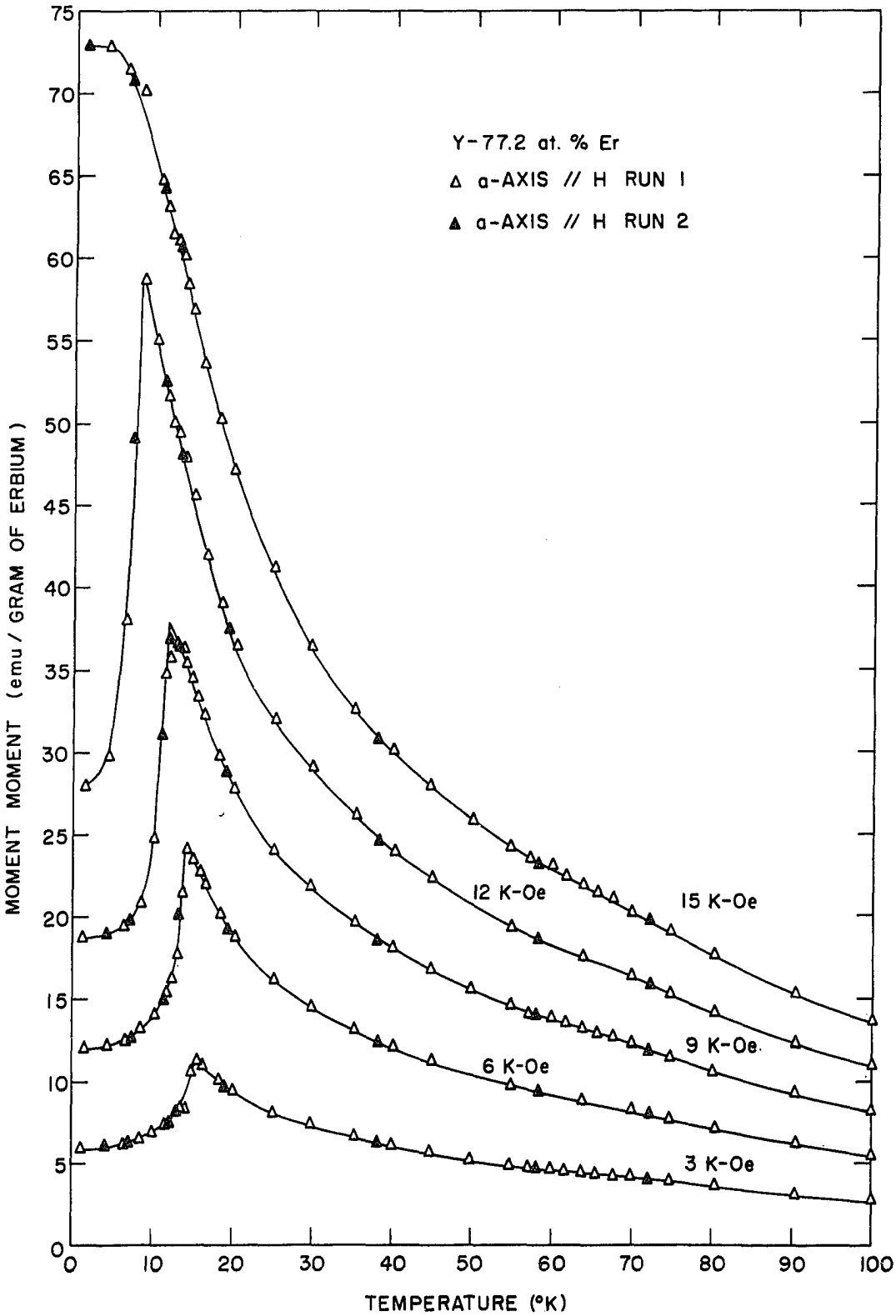

Figure 27. Magnetic moment vs. temperature for the a-axis of the $Y_{25}Er_{75}$ alloy at various constant internal fields

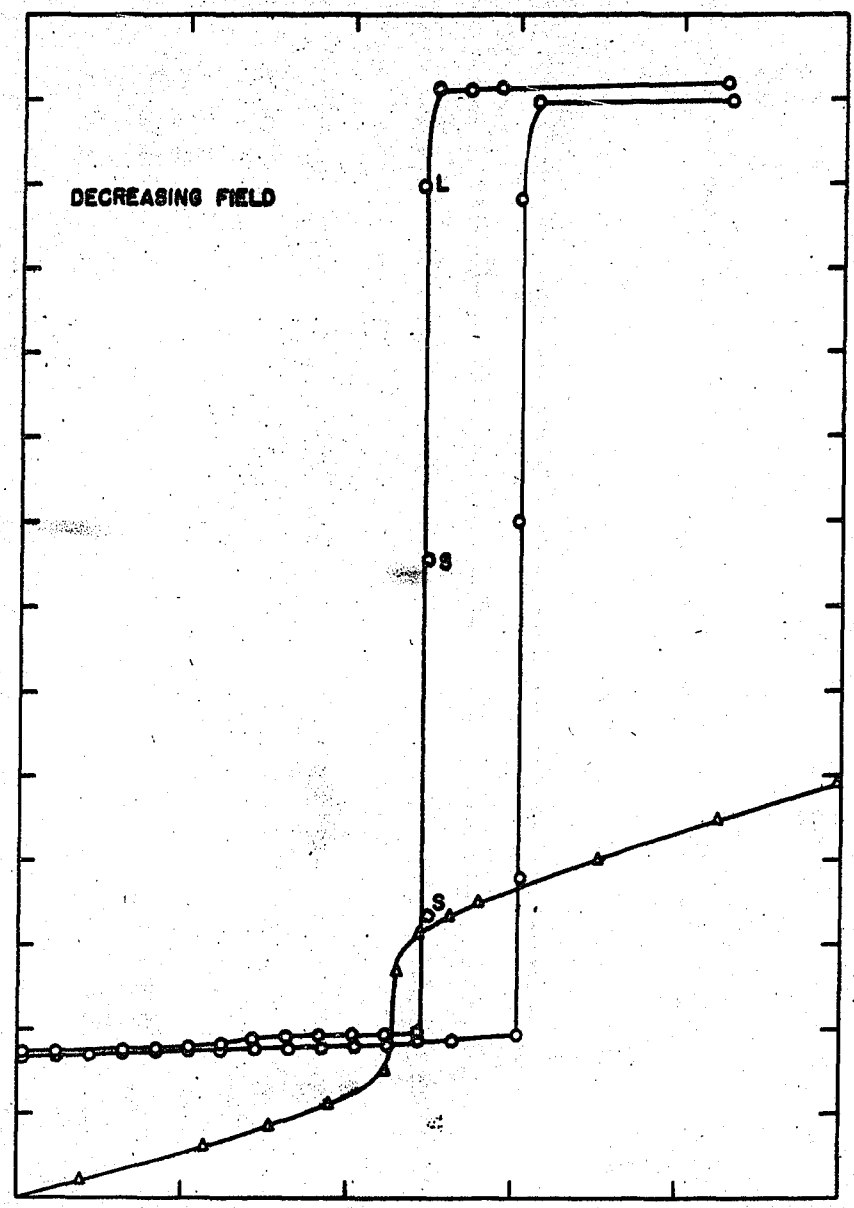

Figure 28. (decreasing field curves)

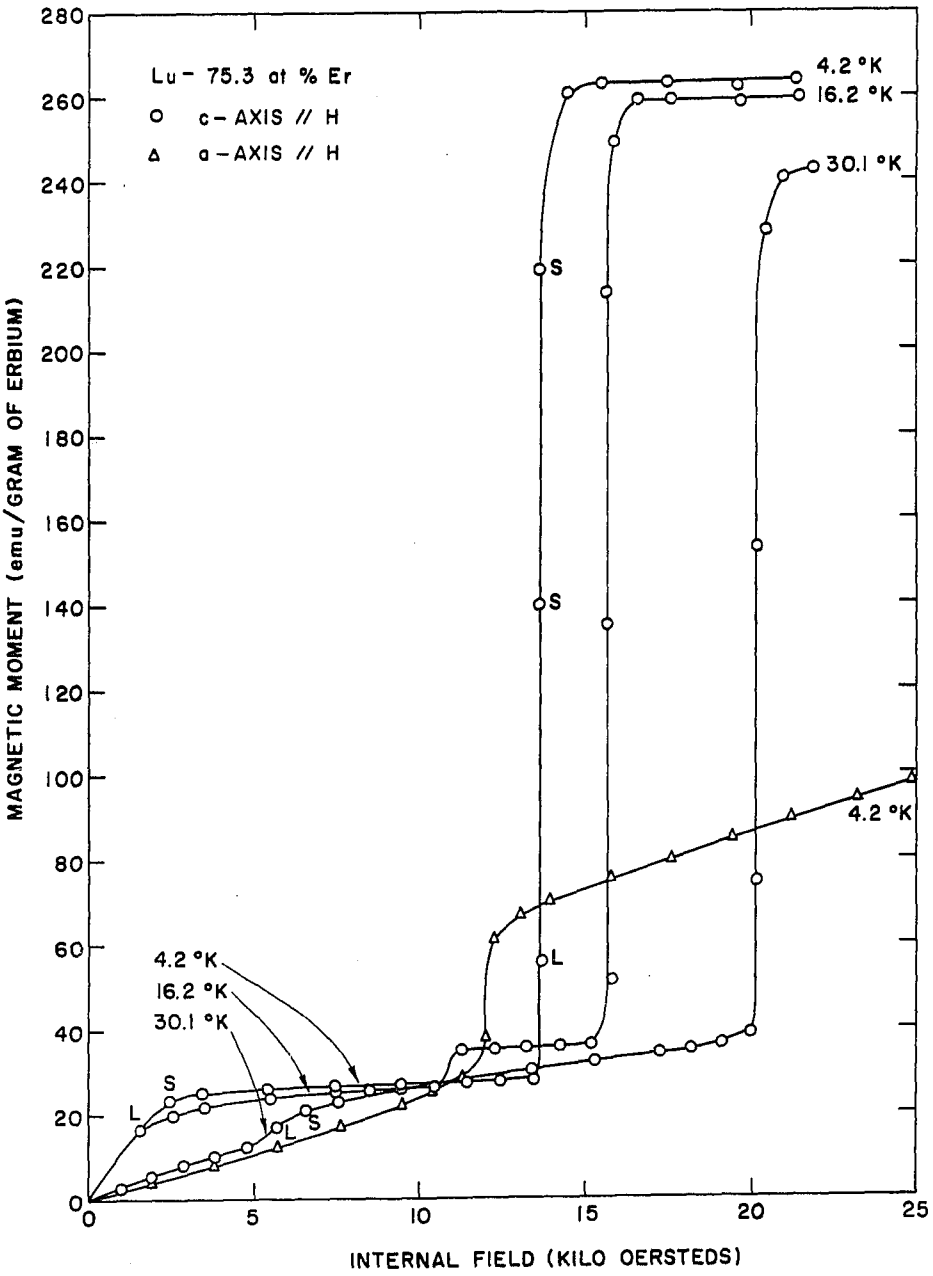

Figure 29. Magnetic moment vs. field for the a- and c-axes of the $Lu_{25}Er_{75}$ alloy at various temperatures

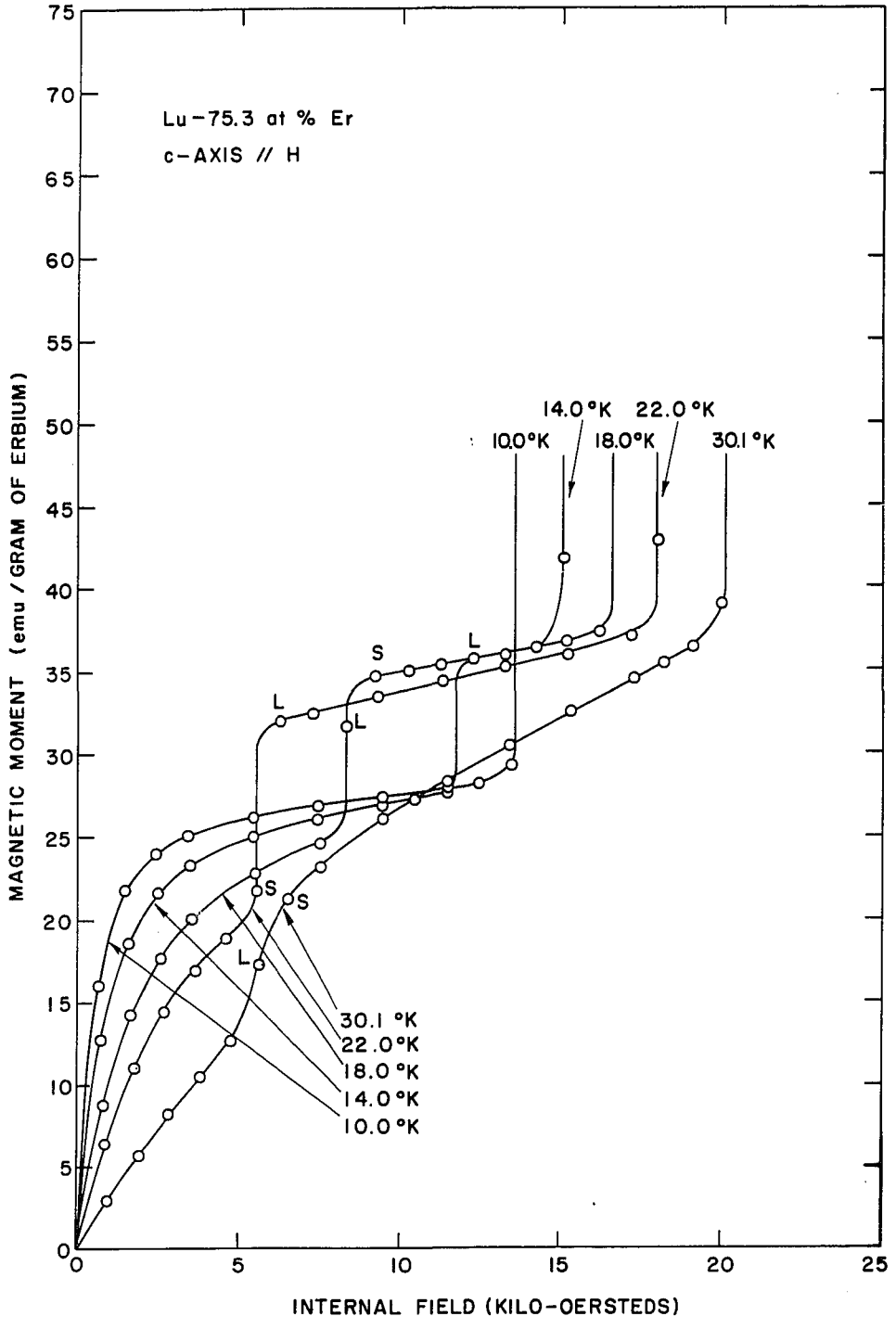

Figure 30. Magnetic moment vs. field for the a- and c-axes of the $Lu_{25}Er_{75}$ alloy at various temperatures (expansion of part of Figure 29)

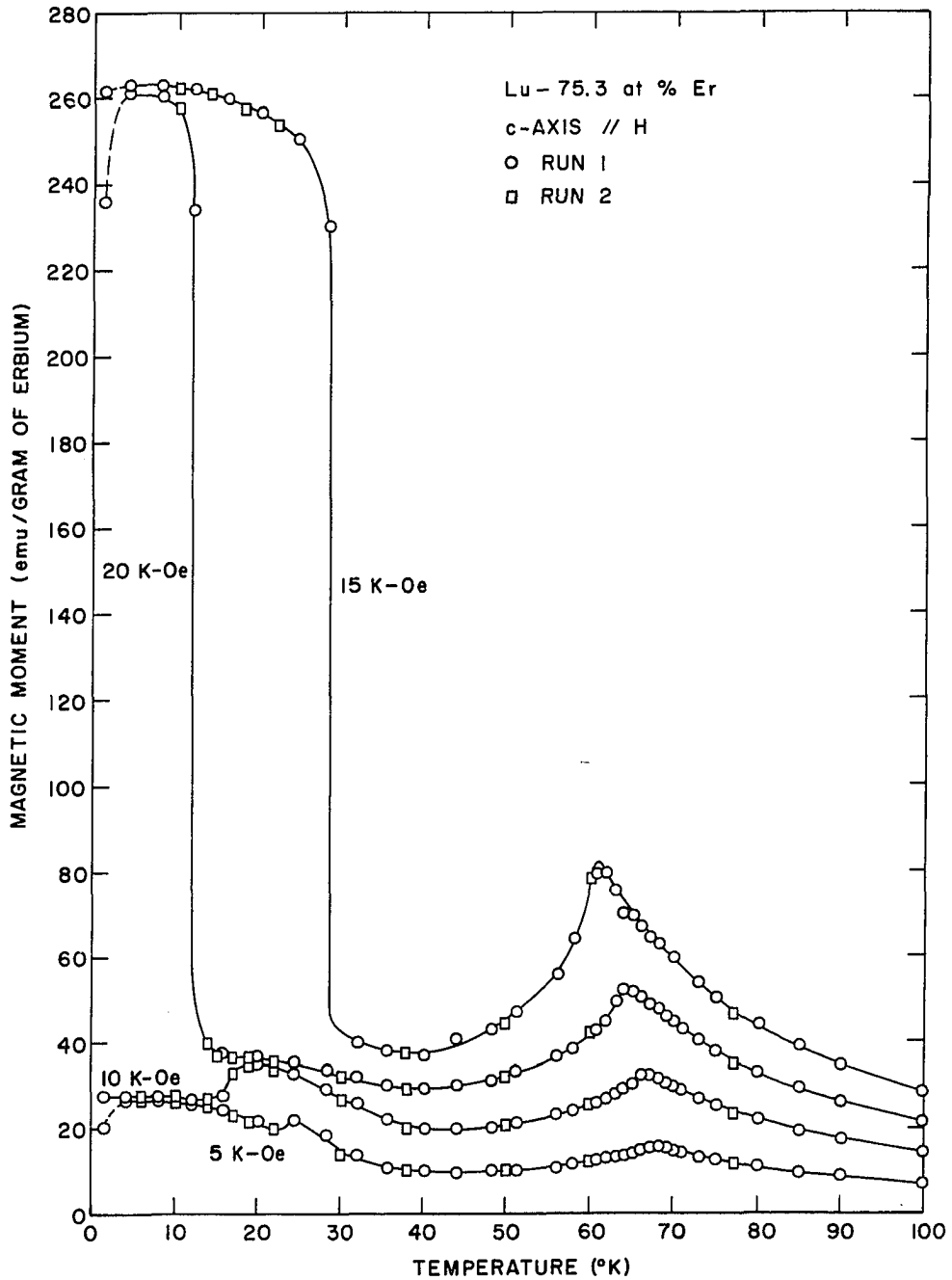

Figure 31. Magnetic moment vs. temperature for the c-axis of the $Lu_{25}Er_{75}$ alloy at various constant internal fields
--- region of large drift

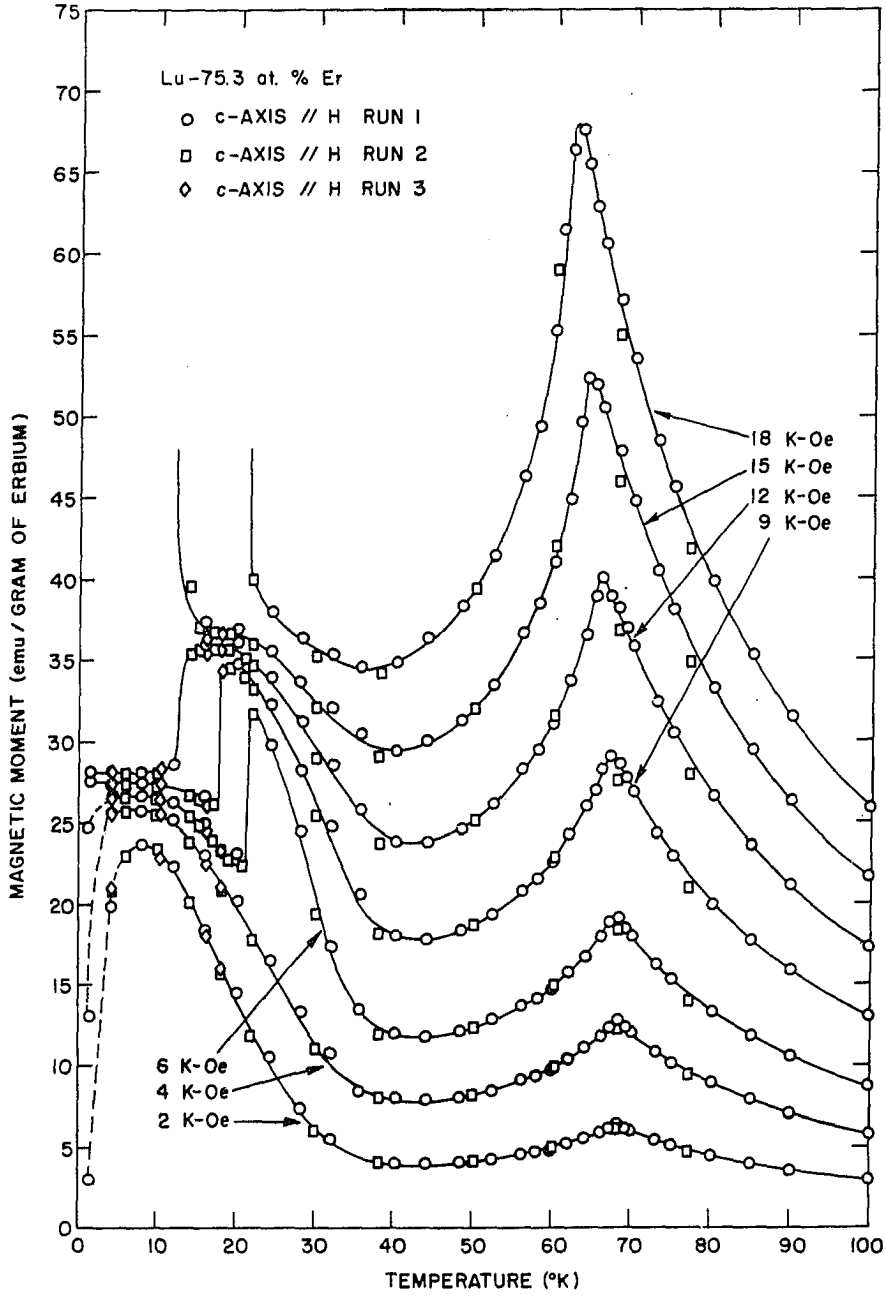

Figure 32. Magnetic moment vs. temperature for the c-axis of the $Lu_{25}Er_{75}$ alloy at various constant internal fields
--- region of large drift (expansion of part of Figure 31)

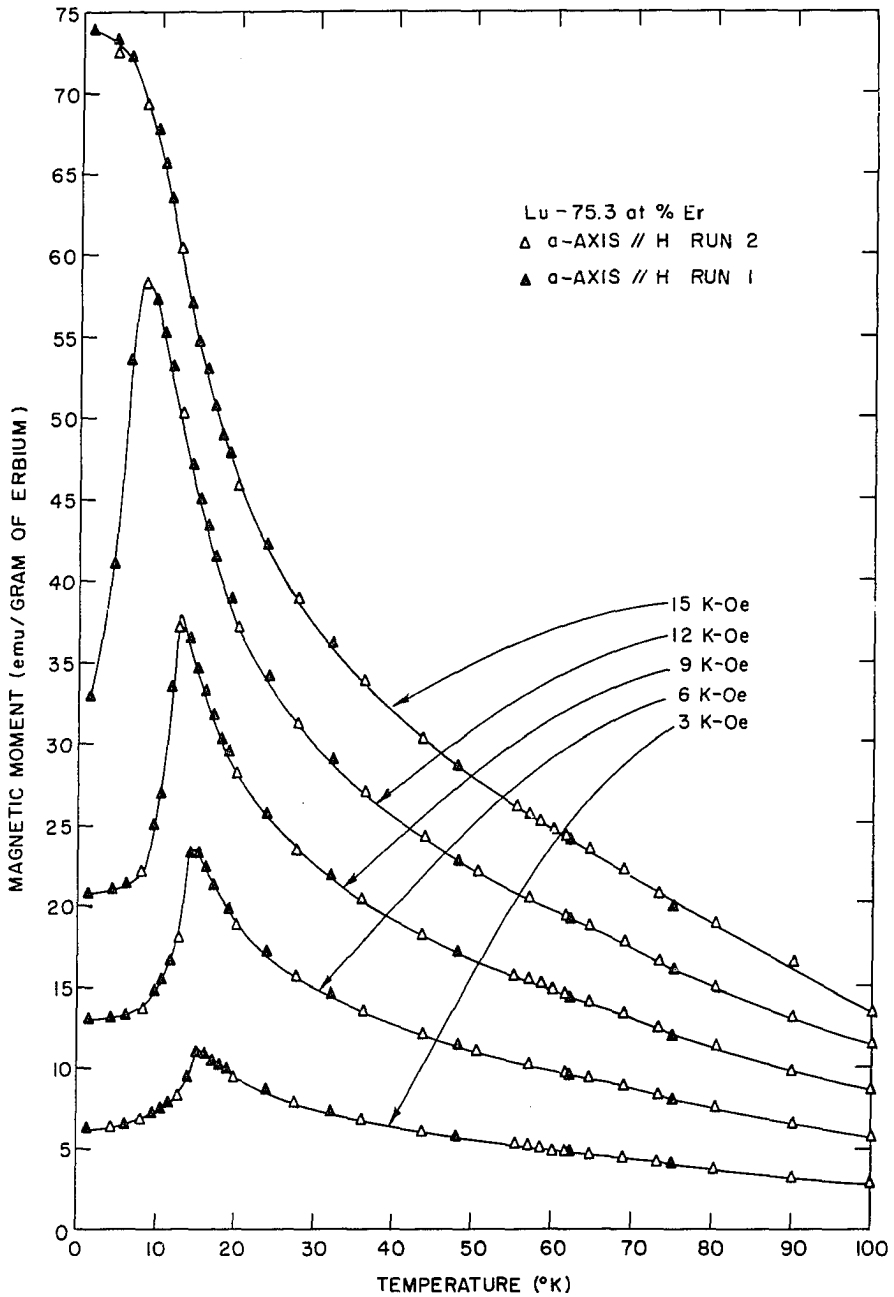

Figure 33. Magnetic moment vs. temperature for the a-axis of the $Lu_{25}Er_{75}$ alloy at various constant internal fields

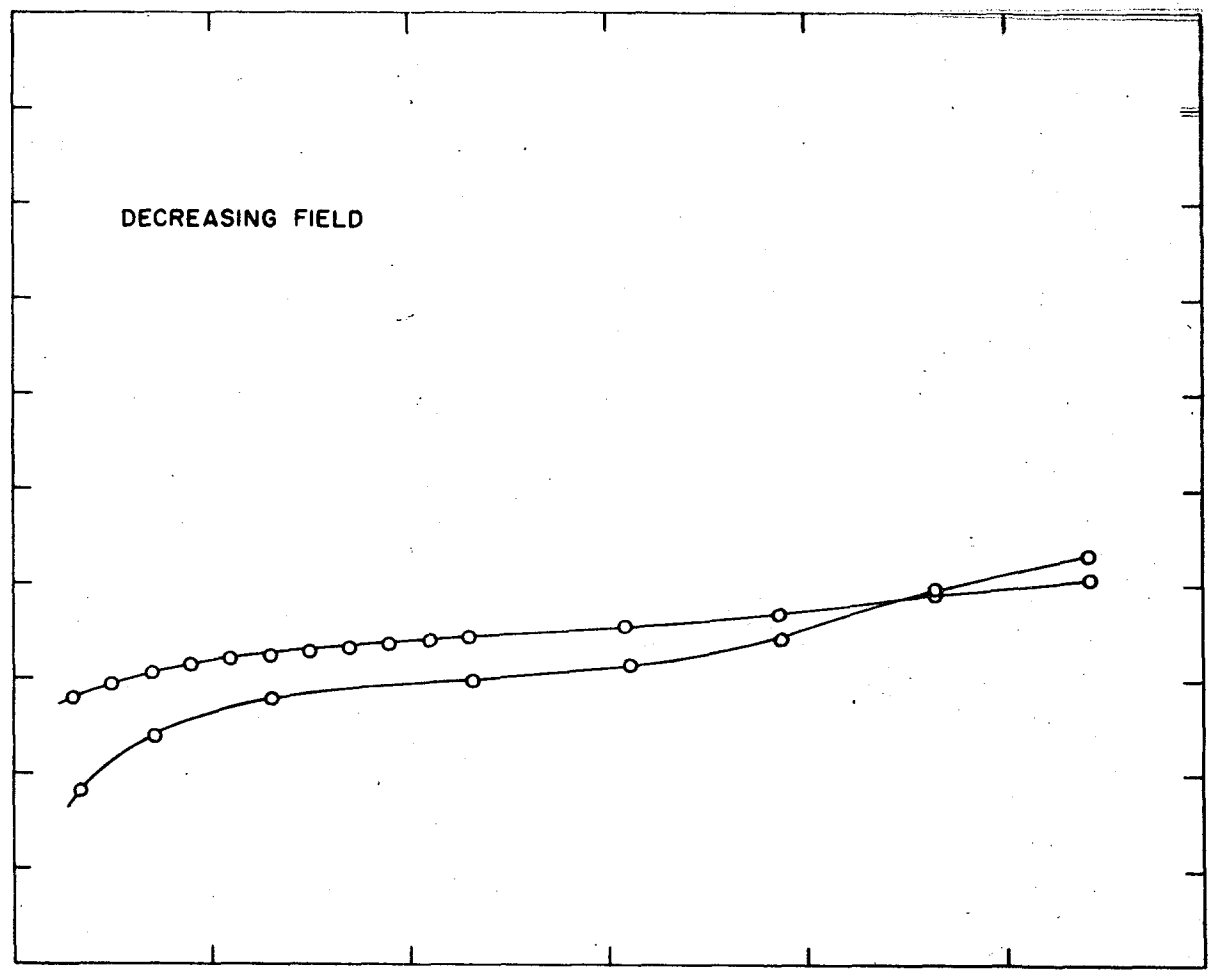

Figure 34.

(decreasing field curves)

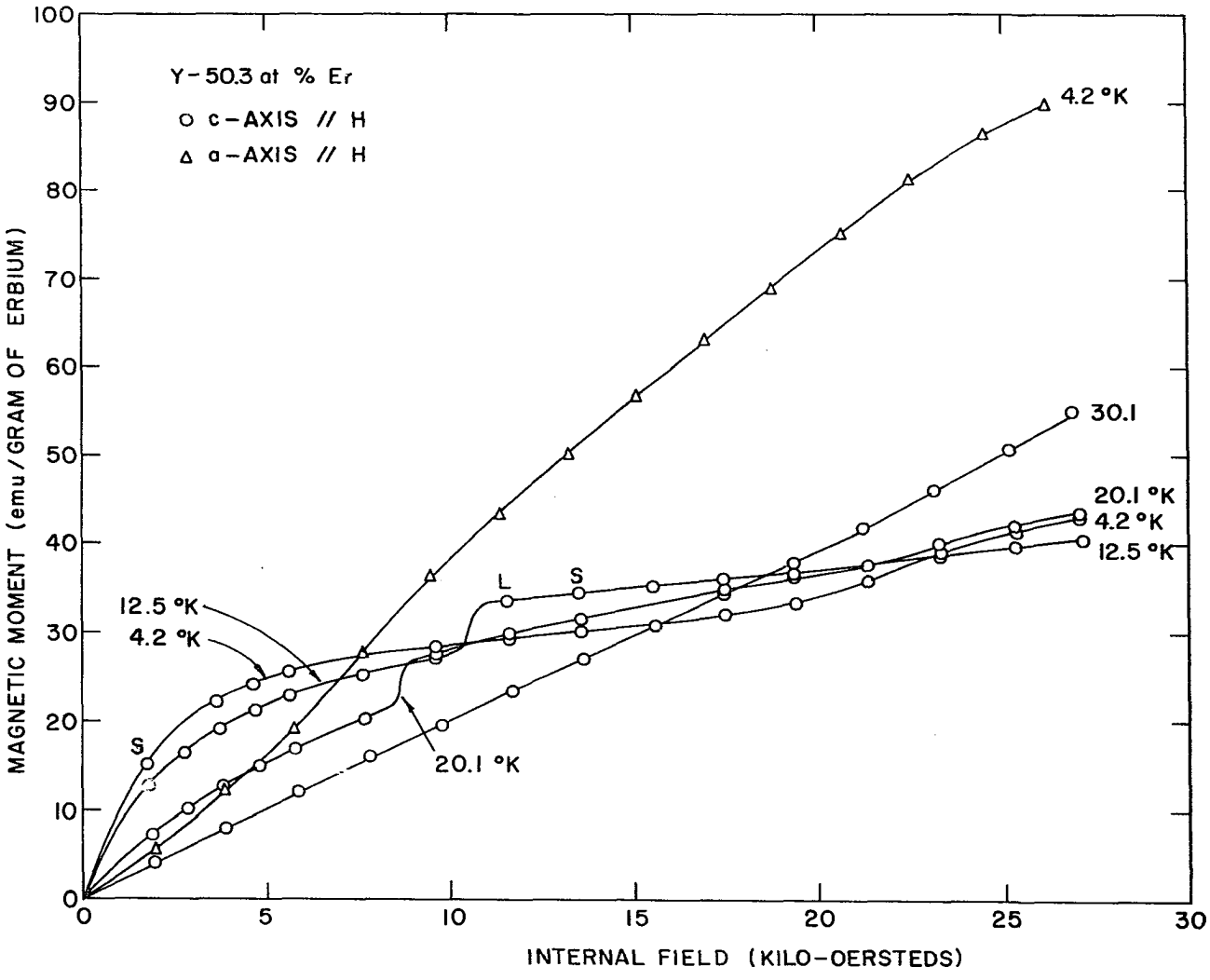

Figure 35. Magnetic moment vs. field for the a- and c-axes of the $Y_{50}Er_{50}$ alloy at various temperatures

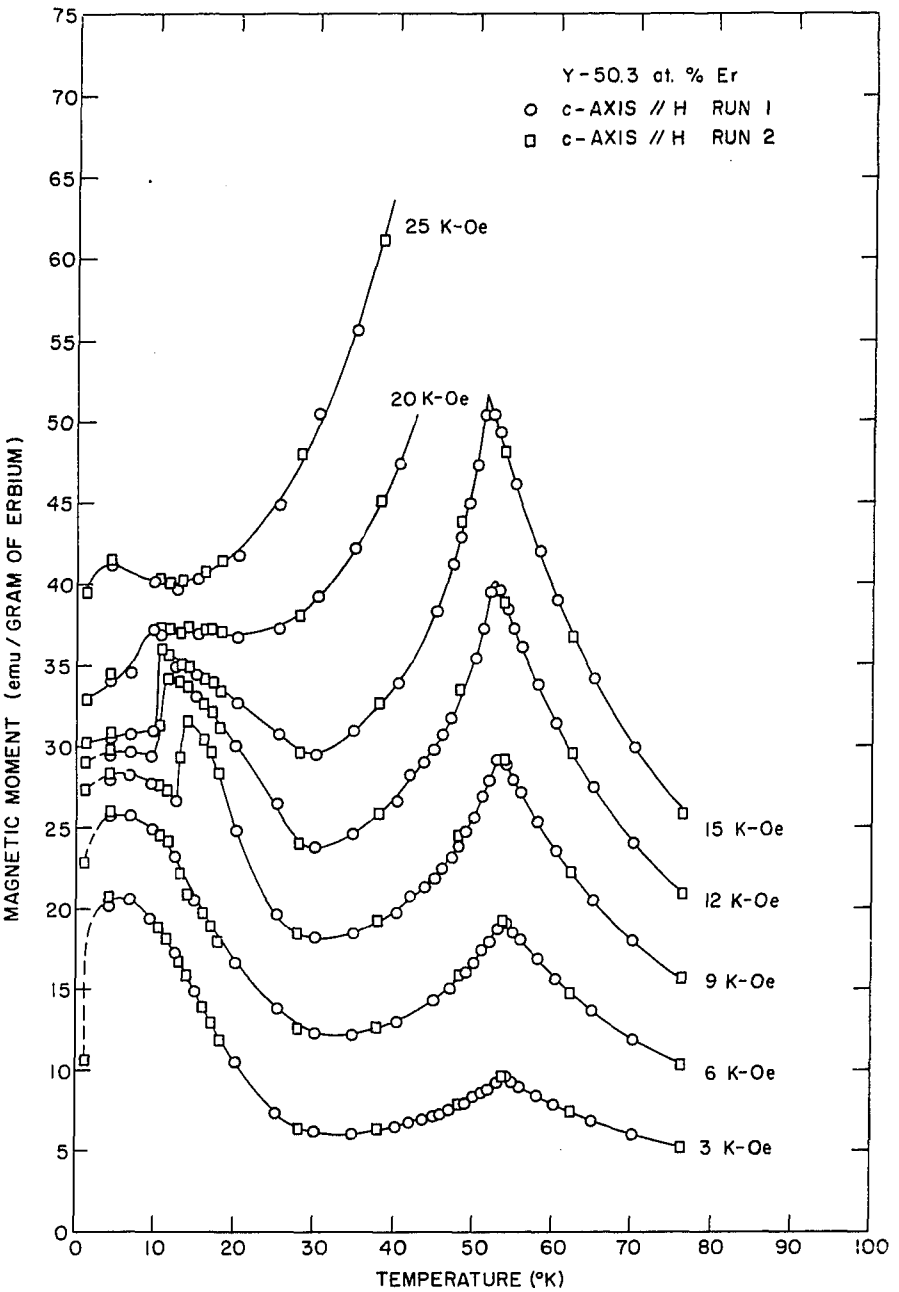

Figure 36. Magnetic moment vs. temperature for the c-axis of the $Y_{50}Er_{50}$ alloy at various constant internal fields. --- region of large drift

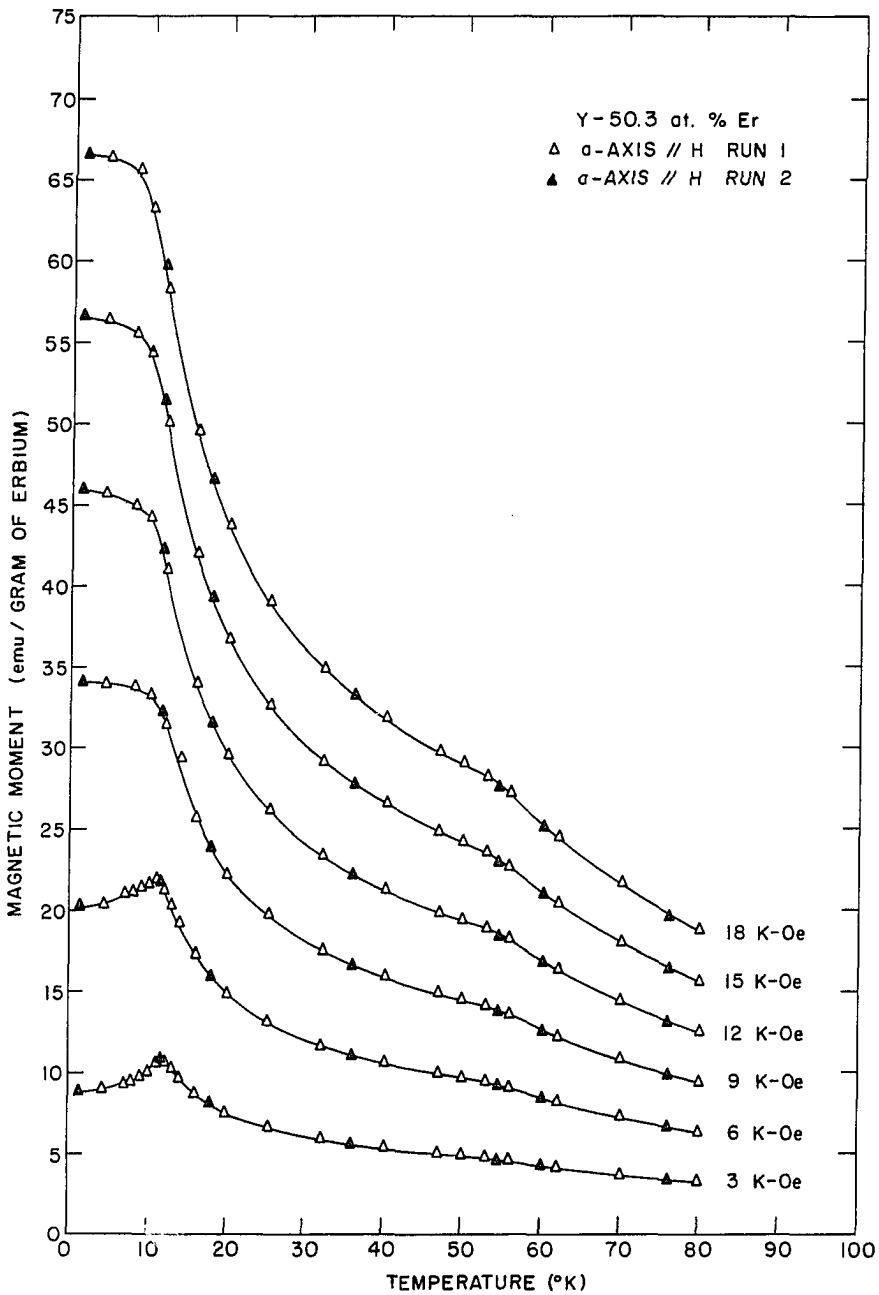

Figure 37. Magnetic moment vs. temperature for the a-axis of the $Y_{50}Er_{50}$ alloy at various constant internal fields

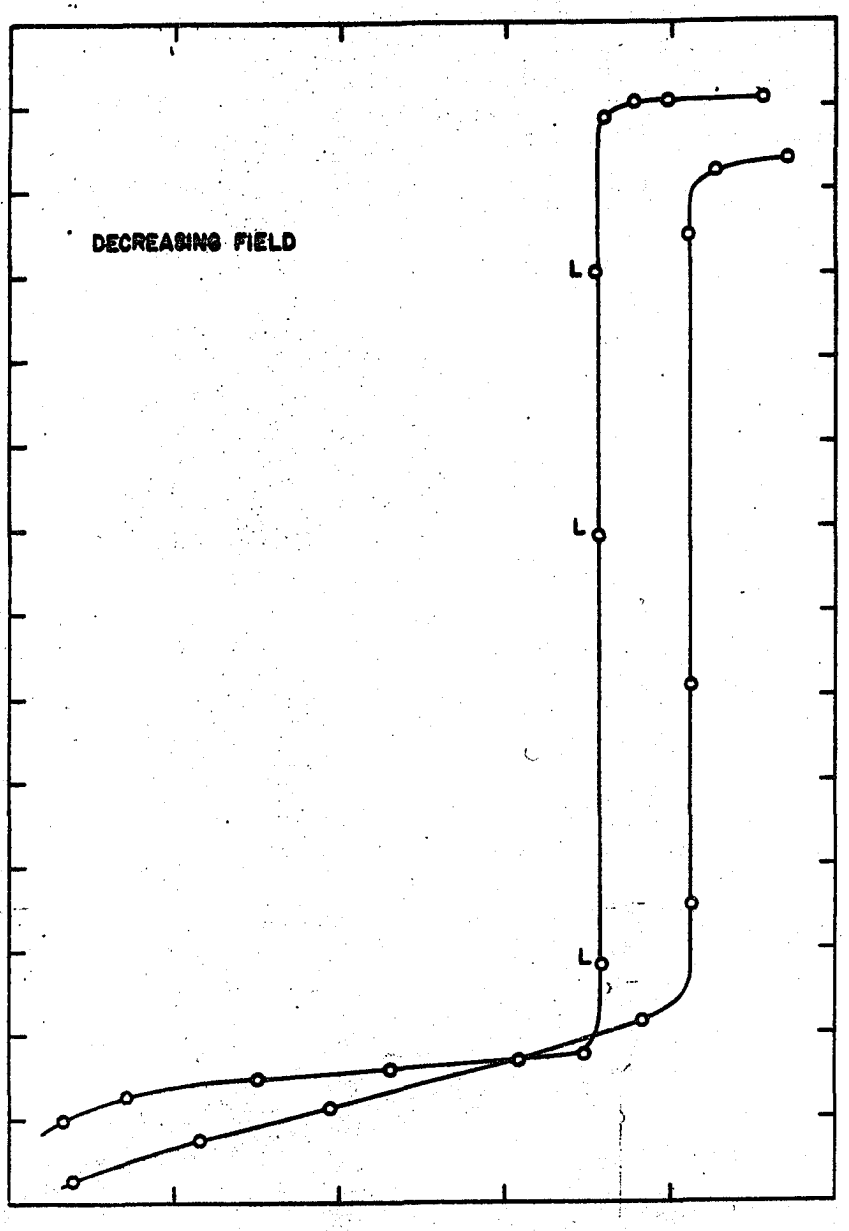

Figure 38. (decreasing field curves)

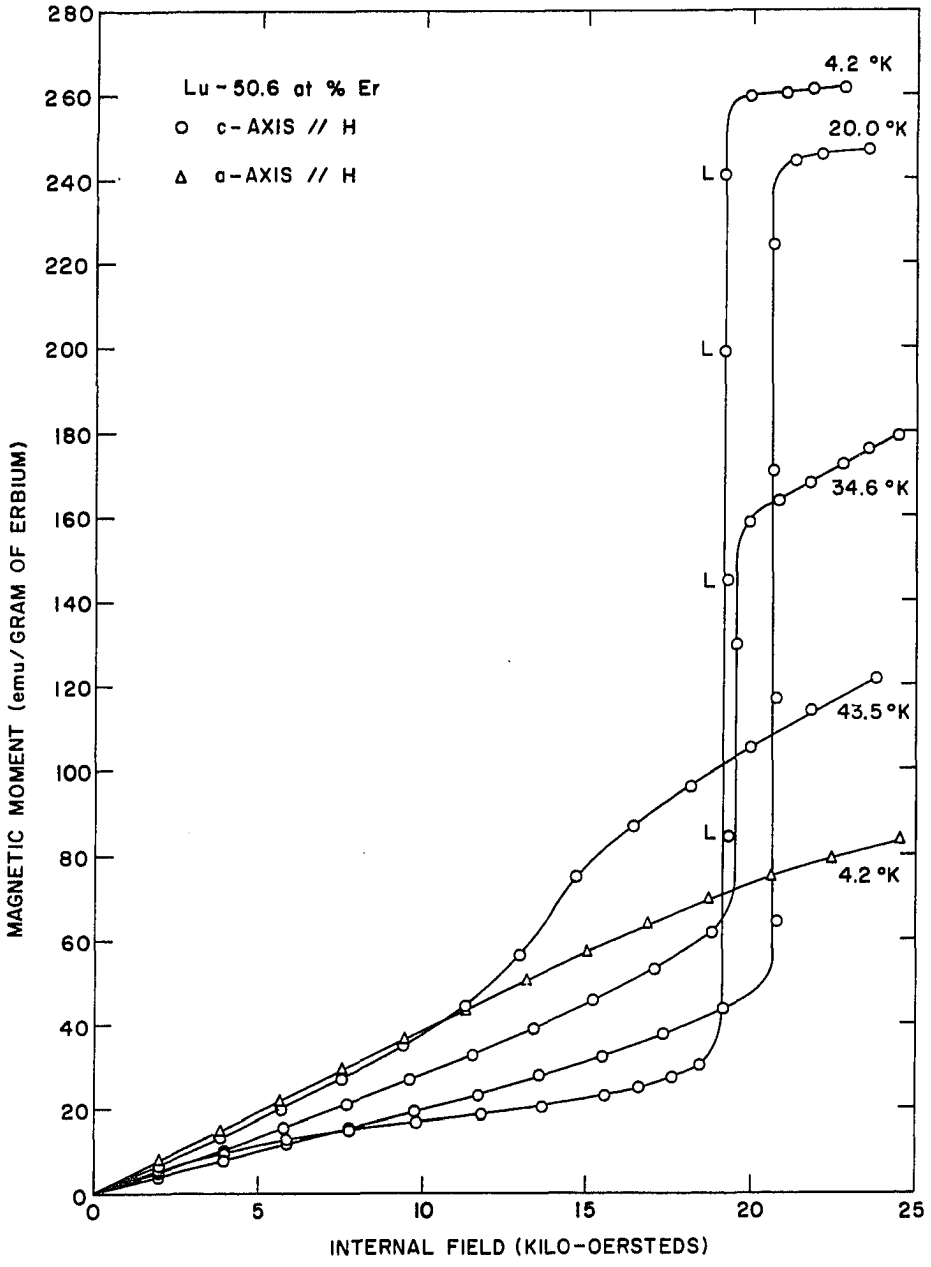

Figure 39. Magnetic moment vs. field for the a- and c-axes of the $Lu_{50}Er_{50}$ alloy at various temperatures

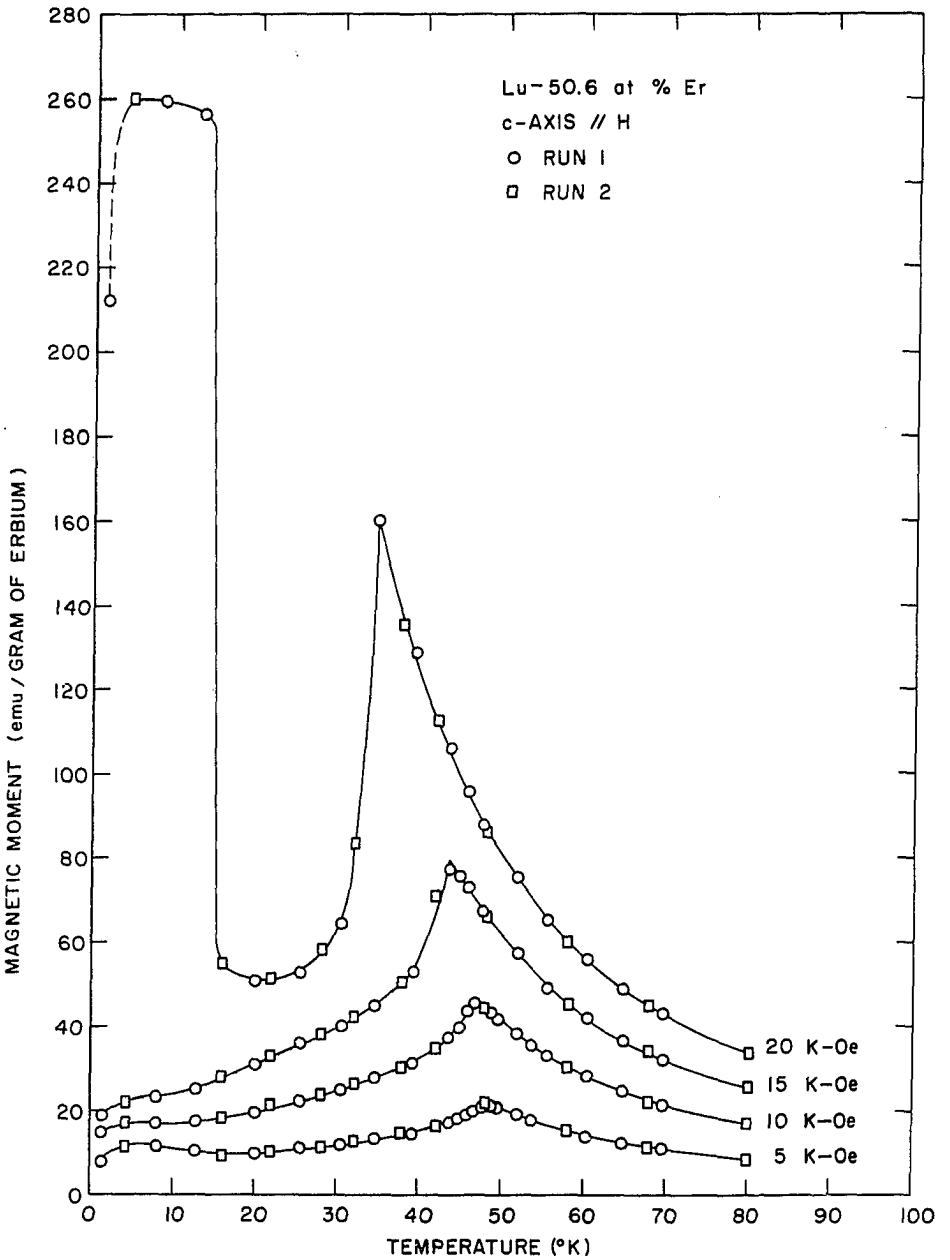

Figure 40. Magnetic moment vs. temperature for the c-axis of the $Lu_{50}Er_{50}$ alloy at various constant internal fields --- region of large drift

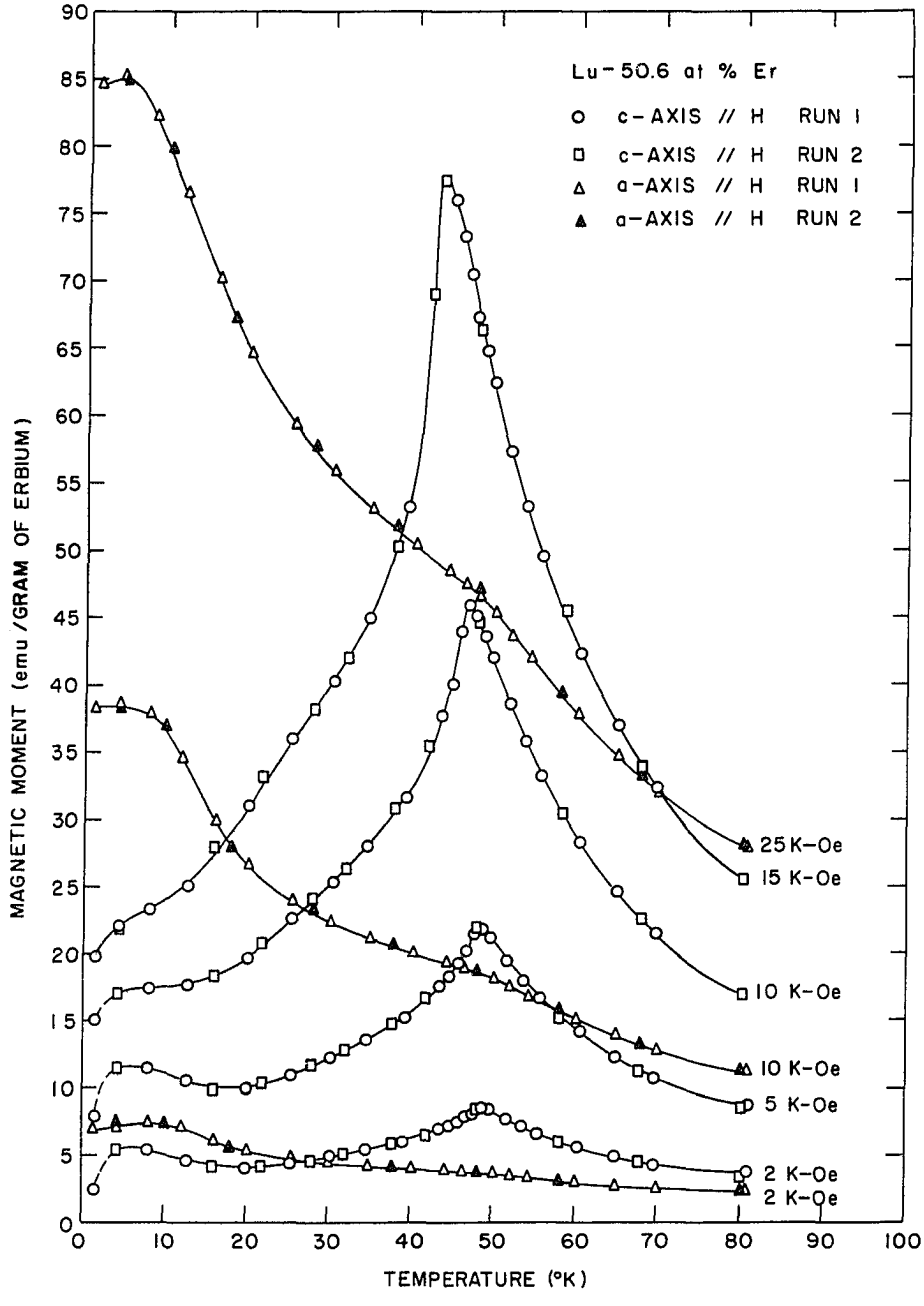

Figure 41. Magnetic moment vs. temperature for the a- and c-axes of the $Lu_{50}Er_{50}$ alloy at various constant internal fields --- region of large drift (c-axis curves are an expansion of part of Figure 40)

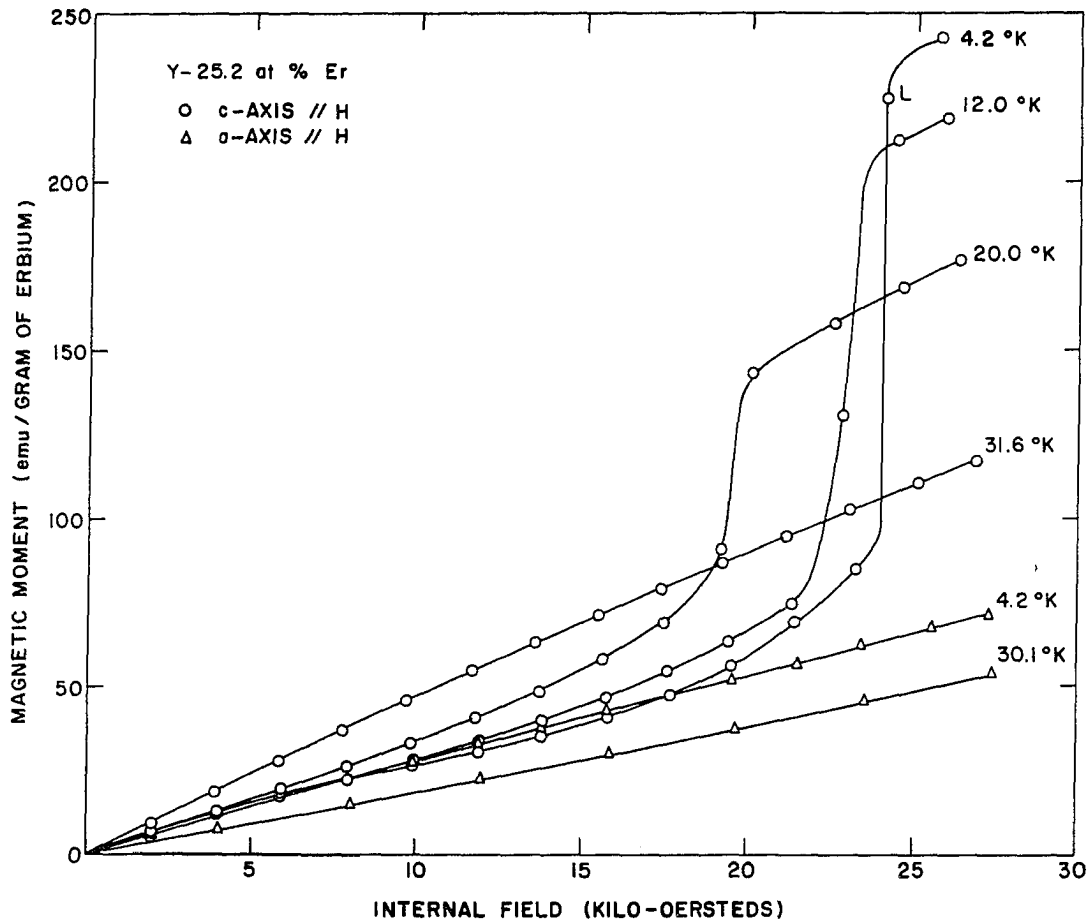

Figure 42. Magnetic moment vs. field for the a- and c-axes of the $Y_{75}Er_{25}$ alloy at various temperatures

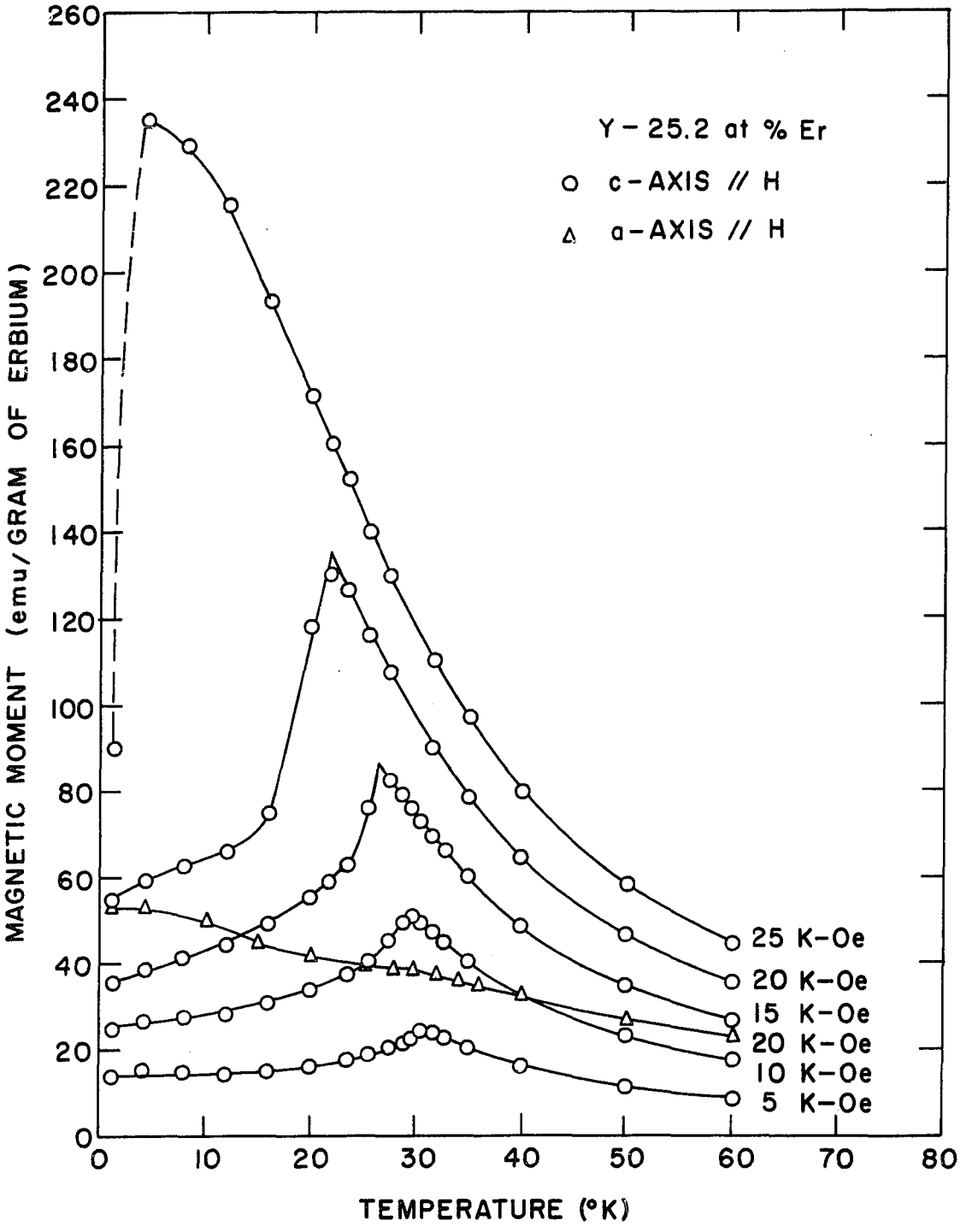

Figure 43. Magnetic moment vs. temperature for the a- and c-axes of the $Y_{75}Er_{25}$ alloy at various constant internal fields. --- region of large drift

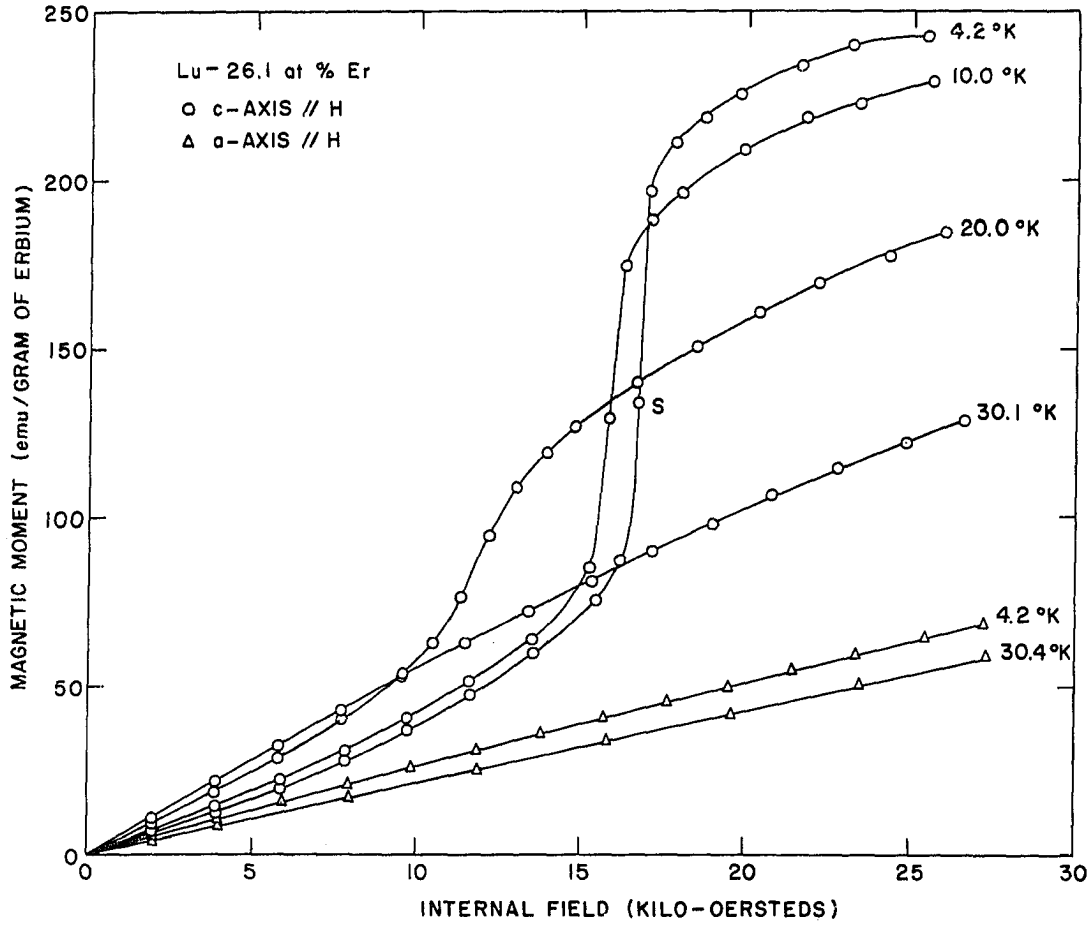

Figure 44. Magnetic moment vs. field for the a- and c-axes of the $Lu_{75}Er_{25}$ alloy at various temperatures

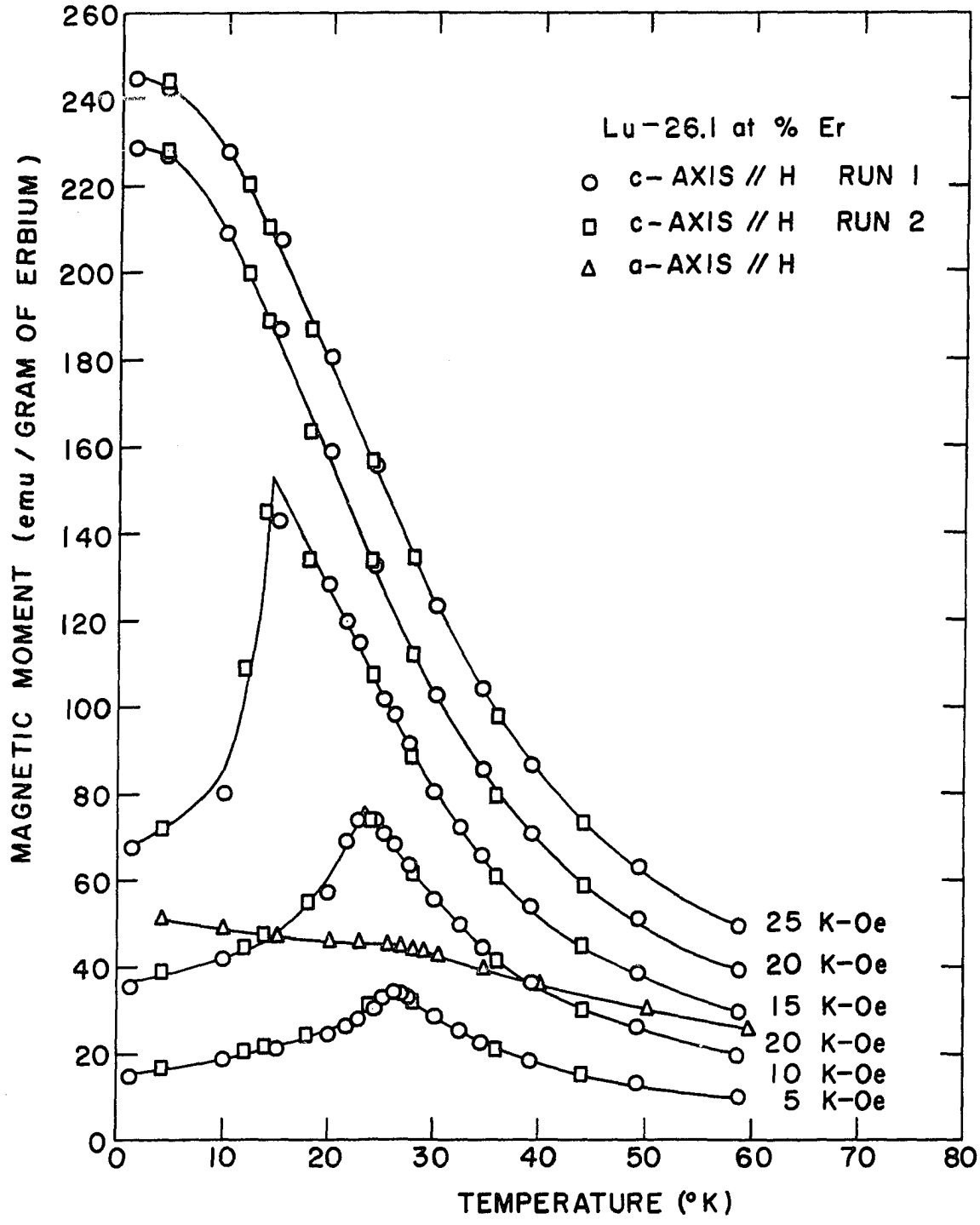

Figure 45. Magnetic moment vs. temperature for the a- and c-axes of the $Lu_{75}Er_{25}$ alloy at various constant internal fields

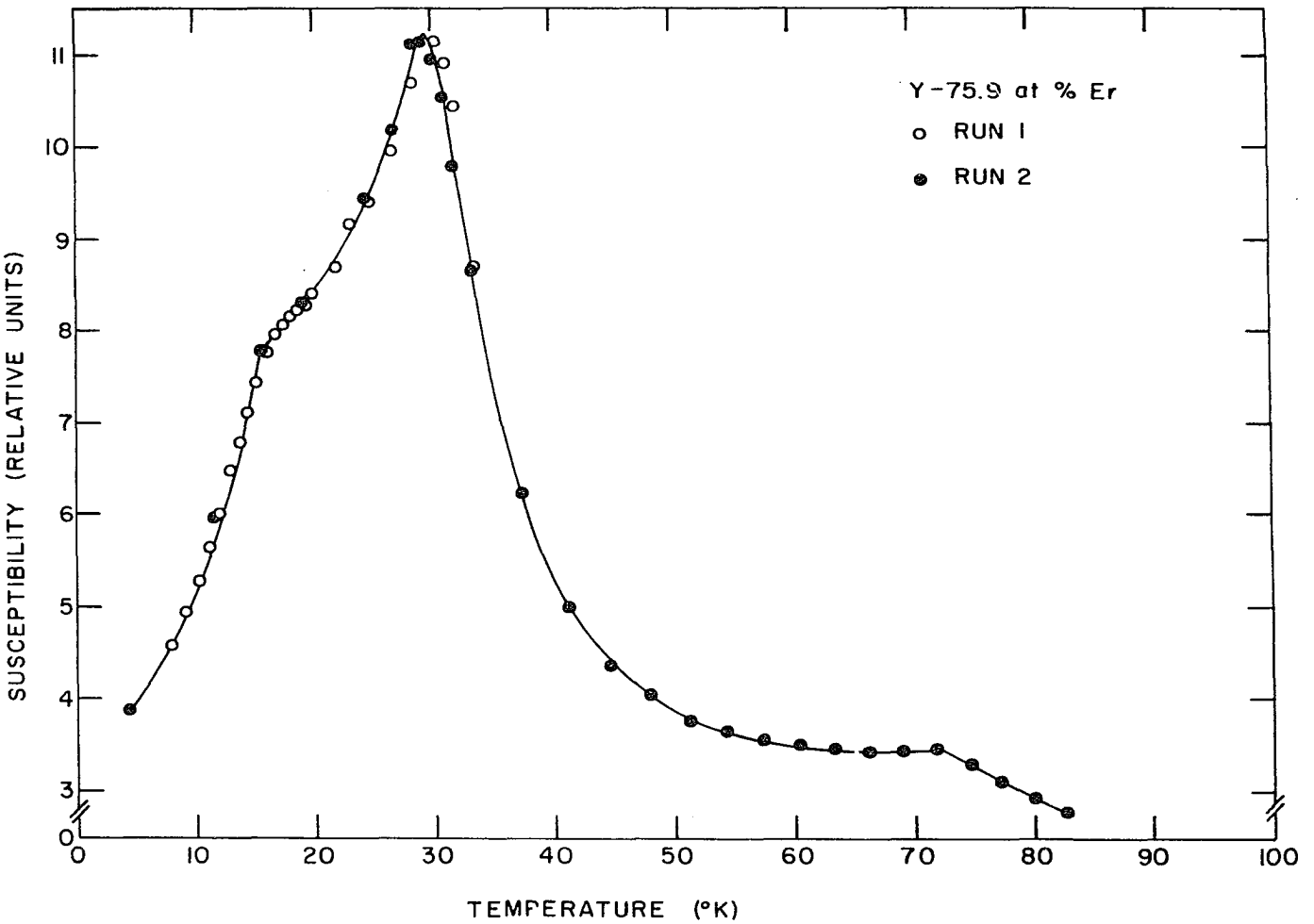

Figure 46. Susceptibility vs. temperature of the $Y_{25}Er_{75}$ alloy. Mutual inductance bridge data

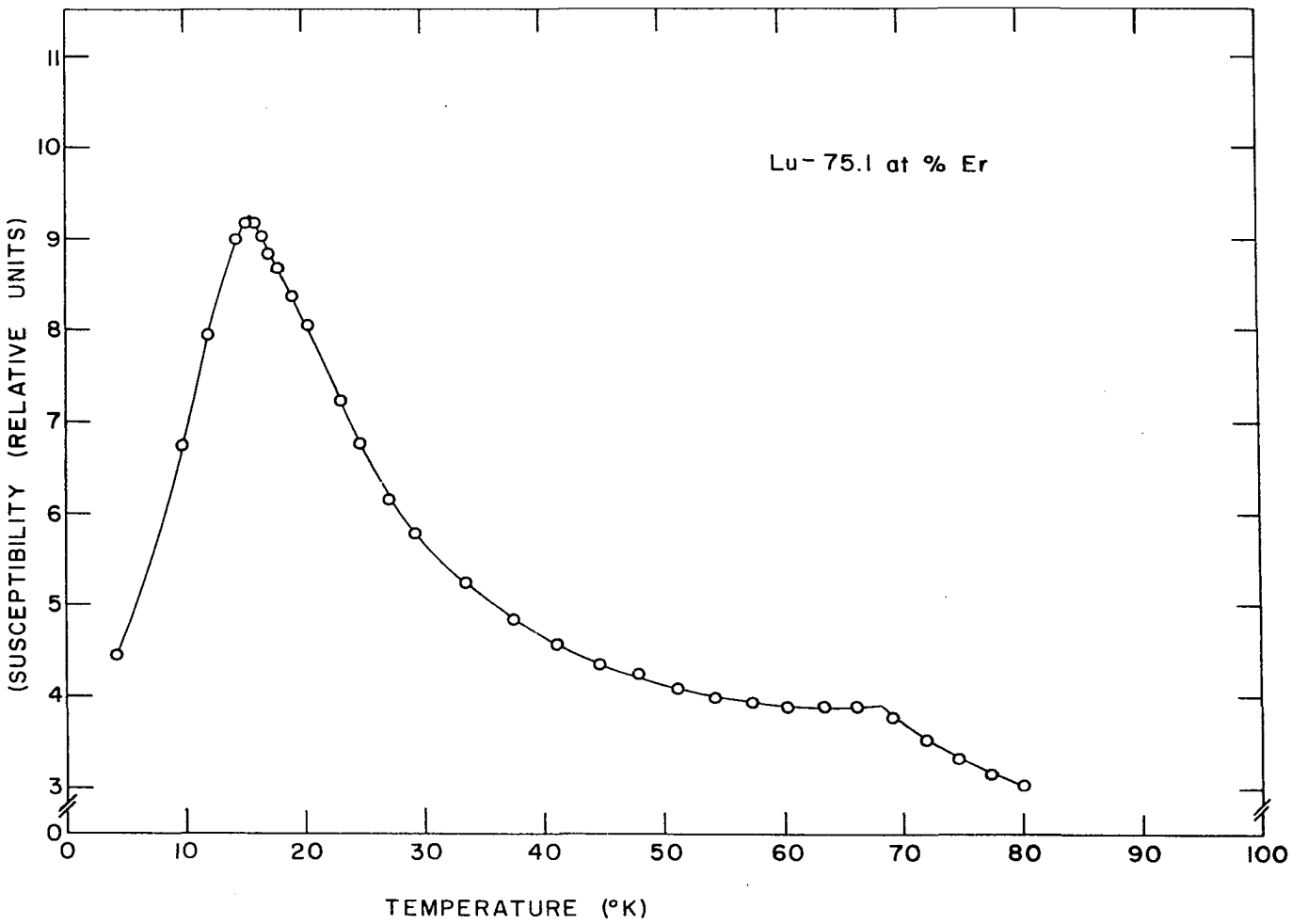

Figure 47. Susceptibility vs. temperature of the $Lu_{25}Er_{75}$ alloy. Mutual inductance bridge data

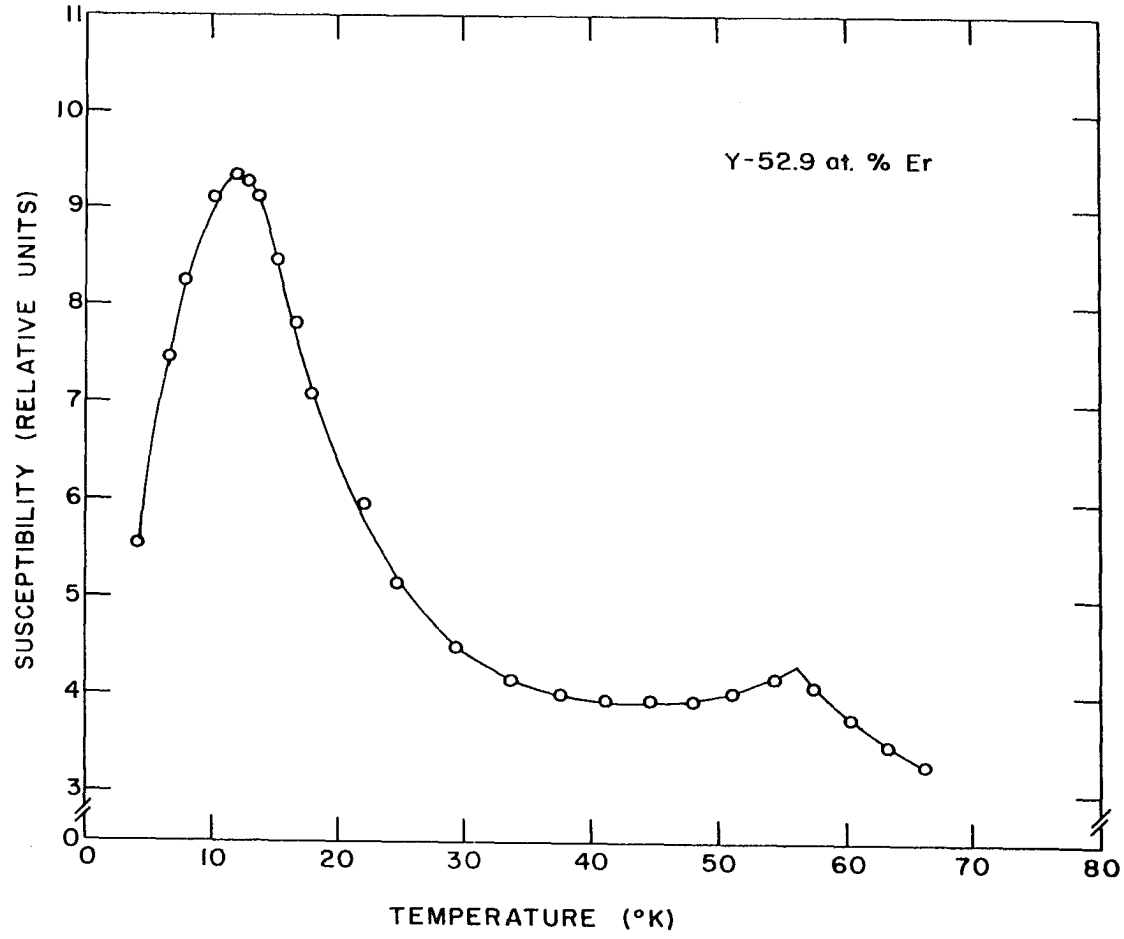

Figure 48. Susceptibility vs. temperature for the $Y_{50}Er_{50}$ alloy. Mutual inductance bridge data

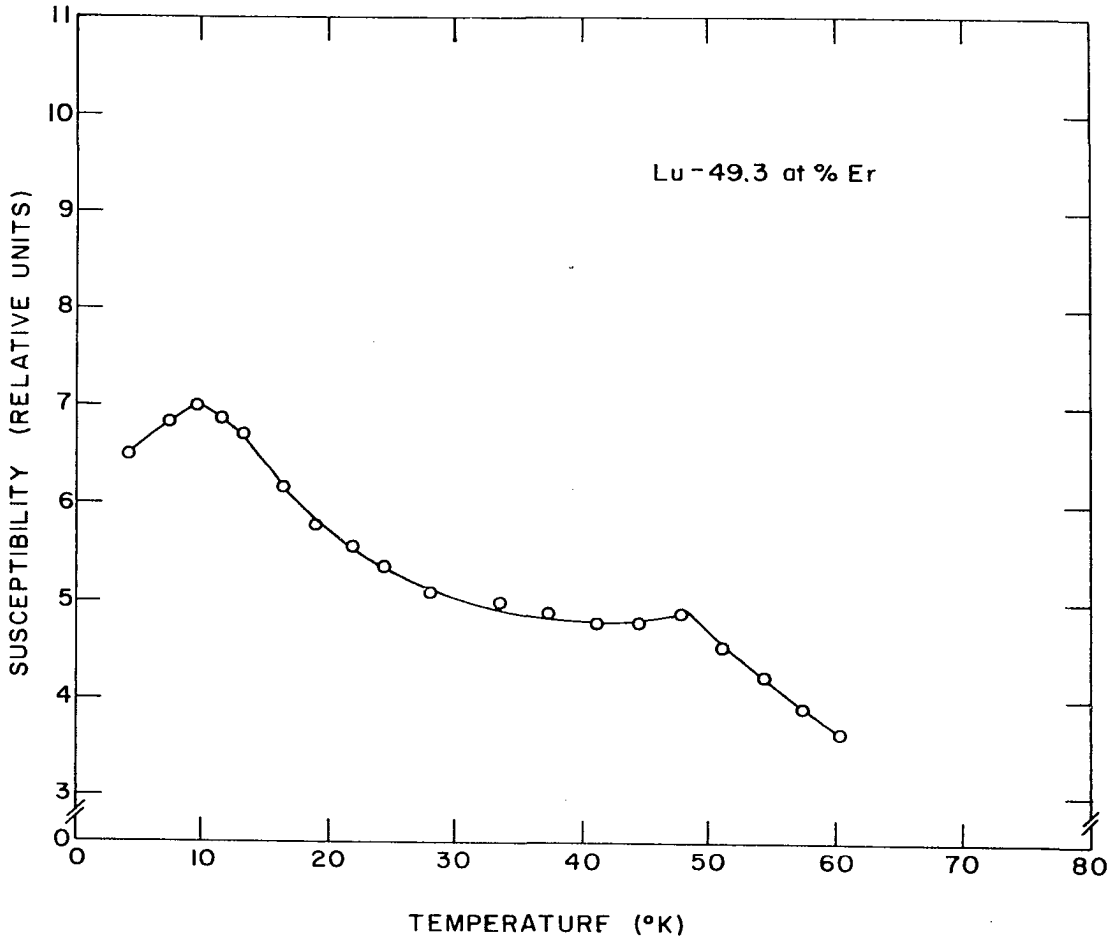

Figure 49. Susceptibility vs. temperature for the $Lu_{50}Er_{50}$ alloy. Mutual inductance bridge data

V. DISCUSSION

A. Magnetic Results

1. Pure erbium

As stated in Section IV.B.1., some small differences were noted between this and previous work on erbium. Some of these differences are possibly due to impurities. The major impurity differences between this work and that of Green et al. (24), is due to oxygen and tantalum. Green et al. reported 1200 ppm oxygen by weight and 0.5 - 2% tantalum compared to 116 ppm oxygen and less than 300 ppm tantalum for this work. This could be enough to account for most of the 3.3% difference in saturation magnetization if one assumes a negligible moment due to oxygen and tantalum. Impurity concentrations were not given explicitly in other work. It is not clear just how impurities should effect the Curie and Néel temperatures. If impurities are, in fact, the reason for the differences, the effect of a purer sample is to expand the antiferromagnetic region, at least in erbium.

The saturation magnetization of 276.0 ±2.0 emu/g. found along the c-axis in this study is to be compared with a theoretical value of 300.5 emu/g. In terms of the number of Bohr magnetons per atom, the theoretical value of Er^{3+} with its $4f^{11}$ electrons in the ground state, $^4I_{\frac{15}{2}}$, is, according to Equation 1-9, gJ = 9. The experimental value is equal to 8.26. The reason for the difference between experiment and theory is that a component of the moment lies in the basal plane. Thus, rather than the spins being parallel, the configuration is said to be that of a ferromagnetic spiral. Assuming no contribution from the conduction

electrons, the angle between the spins and the c-axis is given by $\cos^{-1} \frac{8.26}{9} = 23.3$ degrees.

The slope obtained by plotting inverse paramagnetic susceptibility vs. temperature gives an experimental effective Bohr magneton number of 9.93 ±0.1 which is in agreement with the values of 9.9 ±0.2 and 9.79 ±0.15 given by Green et al. (24) and Arajs and Miller (46) respectively. The theoretical value, according to Equation 1-7, is given by

$$\mu_{eff} = g[J(J + 1)]^{\frac{1}{2}} = 9.6$$

The excess over the theoretical value is usually attributed to polarization of the conduction electrons.

Neutron diffraction data (25) show three distinct regions of long-range magnetic order in erbium. These are represented schematically in Figure 1. The spin configurations are straightforward for both the high- and the low-temperature regions. In the intermediate region (20 to 52°K), the structure is less well understood. Figure 1d is not, in fact, a strictly correct physical picture of the structure.

This study indicates the presence of a fourth region of long-range magnetic order. This is shown by the peak at 28°K in the c-axis data in Figure 13 and also reported by Bozorth and Gambino (13). There was some thermal hysteresis in the neutron diffraction data (25) between 20 and 30°K but nothing that the authors attributed to a definite structure change. It is interesting to note that a similar peak occurs in holmium at 20°K (41).

With regard to the basal-plane data, two points, which may be related, are worthy of discussion. First, the isothermal data in Figures 15 to 20 show that both the a- and b-axis curves undergo a discontinuous transition

below about 15°K in the neighborhood of 18.5 K-Oe. In the neighborhood of 15 and 16°K for the a- and b-axes respectively, the transition takes place in two definite steps rather than one. It is interesting to consider these transitions in light of the work of Nagamiya et al. (47) and Kitano and Nagamiya (48). These authors have given a detailed theoretical treatment of the magnetization processes of various screw spin systems. When considering a ferromagnetic spiral, such as that which occurs in erbium, it is convenient to project all the spins to a common origin. One then thinks of the spin arrangement as being conical rather than spiral. Having done this, the above authors conclude that the conical spin arrangement may go through a number of intermediate stages in route to the ultimate parallel alignment. The initial effect of an applied field perpendicular to the cone axis is to produce a fan arrangement where the spins are no longer uniformly distributed on the cone but are pulled around toward the field direction somewhat. As the field is further increased, the magnetization process may include discontinuous transitions to structures which may or may not have some simple relation to the original cone.

For the moment, therefore, let us assume that the single-step transition shown in Figures 15 to 20 corresponds to a collapse of the conical structure into a parallel alignment of spins lying in the plane defined by the c-axis and the applied field, and with the angle between the c-axis and the spins remaining constant. If this assumption is correct, the moment at the knee should be a measure of the basal-plane component of the total magnetic moment. With this in mind, the moment at the knee was

determined for the b-axis (the b-axis data was used rather than the a-axis data since the b-axis moment is slightly higher in this region) by extrapolating the vertical and the high-field portions of the isotherms below 15°K to the point of intersection. By plotting these values vs. temperature squared and extrapolating to 0°K, a moment of 105 emu/g., or 3.14 μ_B per ion, was obtained. When this was combined with the c-axis saturation magnetization of 8.26 μ_B, a total moment of $\mu = [(8.26)^2 + (3.14)^2]^{\frac{1}{2}}\mu_B = 8.84\ \mu_B$ was found. This is in reasonable agreement with the theoretical value of 9.0 μ_B. However, one would expect the experimental value to be slightly greater than the theoretical value due to a small contribution from the conduction electrons. Therefore, the spins are probably aligned nearly, but not exactly, parallel.

As already described, the basal-plane component of the moment, as obtained from the b-axis data, is 3.14 μ_B. The basal-plane component obtained from the c-axis is given by $\mu = [(9.0)^2 - (8.26)^2]^{\frac{1}{2}}\mu_B = 3.57\ \mu_B$. Since the value obtained from the b-axis measurement is based on the assumption of a parallel alignment of spins, the value of 3.57 μ_B obtained from the c-axis data is probably a better one. Of course, conduction electron contribution was neglected in both cases. This would make the value of 3.14 μ_B too large and the 3.57 μ_B value too small. In addition, for the c-axis measurement, the possibility of forcing the spins toward the c-axis from their zero-field position was neglected and this would also make the value of 3.57 μ_B too small. Thus the correct basal-plane component may be somewhat larger than 3.57 μ_B.

The second point to be discussed about the basal-plane data concerns the isofield curves shown in Figure 21. For fields greater than about

18.5 K-Oe., the curves show an abrupt increase in moment as the temperature is lowered. Below 18.5 K-Oe., a sharp peak is observed. Below about 10 K-Oe., the temperature of the peak is field independent and occurs at 18.0°K which is the same as the Curie temperature as determined from the c-axis data. Thus these data show that for low fields the moment at 4.2°K, for instance, is less than the moment just above the Curie temperature. On the other hand, Cable et al. (25) have reported the zero-field basal-plane component of the moment to be 4.3 μ_B at 4.2°K and 3.6 μ_B at 20°K. One might be inclined to say that our data are in disagreement with the neutron diffraction data of Cable et al. However, the two types of measurements are basically different. Magnetization data gives a direct measurement of the net moment for the sample as a whole. Neutron diffraction, in principle, measures the moments of the individual ions, but the values obtained are based on rather complicated interpretations of an assumed model. Thus a direct comparison between the two types of measurements may not be completely justified for this reason as well as the fact that the neutron diffraction measurements were made at zero field while the magnetization measurements were not.

The a- and b-axis data are compared in Figures 15 to 20. Not explicitly shown is the fact that both the sharp peak in Figure 21 and the double step in Figures 15 to 18 seem to occur at about 0.5°K higher temperature along the b-axis. However, since the difference is about equal to experimental error, whether or not it is real seems questionable. Although the b-axis was run only once, the a-axis was run twice and the data were exactly reproduced in this respect. Other comments on the

basal-plane anisotropy are included in the discussion of the alloys.

2. Alloys

None of the alloys studied are ferromagnetic in zero field. This is in agreement with previous work (13, 15, 18) which show that of the order of 10% yttrium in erbium is enough to suppress ferromagnetism entirely. Presumably the same is true of lutetium in erbium.

The Néel temperatures are proportional to the 2/3 power of the average de Gennes factor (17) and are given by Equation 1-12. The de Gennes factor, G, used in this equation for both yttrium and lutetium is zero. The values found for the constant, A, are 49.0 and 53.5 for the yttrium-erbium and the lutetium-erbium alloys respectively. Conversely, the Néel temperatures are lower than predicted by the universal constant, A = 46.7, found by Bozorth and Gambino (13). This deviation is greater for the lutetium-erbium alloys. See Table 3.

The paramagnetic Curie temperatures and the Curie constants in terms of the effective number of Bohr magnetons per erbium atom are given for all the alloys, as well as for pure erbium, in Table 3. Although the Curie constants vary slightly from one sample to the other and even between the different axes of the same sample, they are all within experimental errorr of 9.97 $\pm 0.1 \mu_B$.

The four alloys $Y_{25}Er_{75}$, $Y_{50}Er_{50}$, $Lu_{25}Er_{75}$, and $Lu_{50}Er_{50}$, all have peaks in the basal-plane data at 16.4, 12.5, 16.1, and about 9°K respectively. These anomalies are also observed in the MIB data. It seems likely that these peaks are related to the 18°K peak in the basal-plane data for pure erbium. Presumably some ordering takes place which is

reflected in the basal-plane data. In pure erbium, this ordering is related to the ferromagnetic-antiferromagnetic transition.

There are anomalies in the c-axis data shown in Figures 32 and 36 which extrapolate to a zero-field temperature of 27.5 and 17.5°K for the $Lu_{25}Er_{75}$ and the $Y_{50}Er_{50}$ alloys respectively. On the other hand, the temperatures of these anomalies are found to be 48 ±3 and 38 ±3°K respectively if the data is extrapolated to zero moment rather than zero field. In addition, a peak is observed at 29°K for the $Y_{25}Er_{75}$ alloy in the MIB data. Just what these are due to is not clear. A possible candidate seems to be a transition similar to the structure change which occurs at 52°K in pure erbium.

Child et at. (15) have carried out neutron diffraction studies on some yttrium-erbium alloys and have reported transitions characterized by an ordering of the basal-plane component of the moment into a spiral at the lower temperatures, just as takes place in pure erbium at 52°K. However, since their work was done on polycrystalline samples, they say it would not be possible to detect a squaring up of the c-axis component of the moment in the alloys, such as takes place in pure erbium, even though it may occur. This leaves room for uncertainty as to just what happens at this transition in the alloys. At any rate, they plotted transition temperatures of alloys containing 90, 70, 50, and 30 atomic percent erbium vs. de Gennes factor, and apparently drew a line proportional to the 2/3 power of the de Gennes factor through their data points. From this graph, transition temperatures of about 44 and 32°K are found for alloys containing 75 and 50 percent erbium respectively.

There do seem to be inconsistencies between the transitions reported for the alloys by Child et al. and those found for the alloys in this study. There are also differences within the present study between the 52°K anomaly in pure erbium and the anomalies in the alloys. The transition temperatures reported by Child et al. fall between those found by different methods (i.e., extrapolating the data to zero field, or to zero moment, and also considering the MIB data) for corresponding alloys in this study. Also, in the present study, the $Lu_{25}Er_{75}$ and the $Y_{50}Er_{50}$ alloys don't exhibit the anomaly at low fields and therefore seems to be inconsistant with the zero-field neutron diffraction data. Finally, no anomaly is observed in any of the basal-plane data for the alloys while a change in slope in the basal-plane moment vs. temperature data is observed in erbium at this temperature.

Another possibility for the above anomalies is a transition similar to that which occurs in pure erbium at 28°K.

As stated above, none of the alloys are ferromagnetic in zero field. Three alloys, $Lu_{25}Er_{75}$, $Lu_{50}Er_{50}$, and $Y_{25}Er_{75}$, however, undergo a transition (as shown by the c-axis data in Figures 29, 39, and 24) to the ferromagnetic state at the highest fields attainable in this study. The saturation moment of all these alloys is only slightly less than that of pure erbium. This is to be expected since, if the material saturates at all, the moment per erbium ion should be nearly the same as in the pure metal.

In addition to the ferromagnetic saturation, all except the alloys containing 25% erbium have at least one low-moment pseudosaturation region in the c-axis data. Two alloys, $Lu_{25}Er_{75}$ and $Y_{50}Er_{50}$, have two pseudosaturation regions. This indicates the presence of two, and sometimes

three, distinct magnetic structures. Bozorth and Gambino (13) also observed two magnetic structures in a $Lu_{25}Er_{75}$ alloy at $4.2^{o}K$, which is consistant with these results. It is not clear why the appearance of the third structure appears to be so haphazard. It does not exist at all at low fields, except perhaps in the $Y_{25}Er_{75}$ alloy as indicated by the anomaly in the MIB data, nor at temperatures below about $10^{o}K$ in any field. As mentioned in an earlier section, it is this structure that gives rise to the peak at intermediate fields in the isofield data.

It is interesting to note that there seems to be something unique about a moment of approximately 35 emu/g. in all the alloys except those containing 25% erbium. In the two alloys with the "double plateau", the higher plateau levels out at about this value. In $Y_{25}Er_{75}$, the moment at the single plateau is about this value. Finally, in $Lu_{50}Er_{50}$, the decreasing field curve levels out in this neighborhood.

The basal-plane data for pure erbium illustrated in Figures 15 to 20 show there is some slight anisotropy at low temperatures. Above $40^{o}K$, the a- and b-axis data are identical. Below $40^{o}K$, no general statement with regard to all temperatures and fields can be made about the easier direction of magnetization in the basal plane. The b-axis moment is slightly larger, however, at $4.2^{o}K$ in high fields.

In the alloys, the difference between the b-axis moment and the a-axis moment is also small. Separate runs on the same sample, however, show that the anisotropy is only slightly larger than experimental error. Possibly for this reason, the amount of anisotropy from one alloy to the next seems to be somewhat erratic. At any rate, it can be said that the b-axis moment is the same or slightly larger for all alloys (about 2.5%

larger at 4.2°K in the alloys containing 75% erbium) and that the anisotropy decreases with decreasing erbium content and also with increasing temperature.

Elliott (12) has made anisotropy calculations which correctly predict the c-axis to be the easy direction of magnetization in erbium. He also correctly predicts the basal-plane anisotropy to be several times smaller than the anisotropy between the c-axis and the basal plane. The theory also predicts the a-axis moment to be slightly larger than the b-axis moment, while the experimental data show the reverse to be true. This slight discrepancy between experiment and theory does not seem to be particularly serious in light of the overall accuracy of the theory, and only minor modifications of the theory would likely be required to bring it into line with the experimental facts.

B. Suggested Further Work

From the results of this study, it is evident that three areas, at least, need further investigation. One concerns the intermediate-field peaks which occur in the $Lu_{25}Er_{75}$ and the $Y_{50}Er_{50}$ alloys. Another has to do with the apparent lack of agreement between this work and that of Child et al. (15) in the matter of the two different antiferromagnetic structures in the alloys. The third involves the possibility of being able to reach the theoretical saturation moment in pure erbium with smaller fields applied at an angle of 23° to the c-axis than are required along either the c-axis or the basal plane.

With regard to the intermediate-field peaks, two areas of further study immediately suggest themselves. First, additional alloys should be

investigated. By choosing compositions on both sides of the alloys displaying the peaks in question, the variation of the peak with composition would be better determined. Also, magnetic studies of alloys more concentrated in erbium might provide a more direct correlation between these peaks and some transition in pure erbium if, in fact, any correlation exists. In particular, it would be interesting to find out how both the 28°K and the 52°K transitions in pure erbium change with dilution. The second area of further work is in the field of neutron diffraction. By studying single crystals of these alloys in the presence of an applied magnetic field, it should be possible to determine the magnetic structures at the various plateaus and thus the origin of the anomalous peaks.

The work suggested above would probably also shed some light on the disagreement mentioned. As has already been stated, it seems strange that this study gave no evidence for two different antiferromagnetic structures in some alloys and questionable evidence in others. From their description of sample preparation, it is not clear whether Child *et al.* were careful to remove all the strain from their samples. It would be interesting to learn what effect strain would have on the different antiferromagnetic structures they observed.

Finally, the basal-plane data for pure erbium provide an estimate of the field required to observe the full saturation moment if applied at an angle of about 23° to the c-axis. The internal field would have to be large enough to give a component along the basal plane of at least 18.5 K-Oe. This corresponds to a total internal field of about 47.5 K-Oe. Flippen (49) and Foner and McNiff (50) have shown that the theoretical saturation moment is not reached in pure erbium for the c-axis either

parallel or perpendicular to fields as large as 170 K-Oe.

C. Discussion of Errors

The errors in the measured magnetic moment can be placed into two categories; one I shall call relative errors, and the other absolute errors. Relative errors include errors in crystal alignment, sample centering with respect to the pick-up coils, and general reproducibility of the apparatus. The absolute errors include errors in sample weight and, in the case of alloys, the composition of the sample.

The reproducibility of the apparatus includes errors in centering as well as the precision with which the voltage divider potentiometer (mixer) could be read (i.e., how precisely the signal could be nulled). It is estimated that the sample could be centered well enough to yield a measured magnetic moment that was correct to better than ±0.1%. The mixer could be read to about ±0.02% in most cases although this precision fell off to about ±0.5% for very small moments in the paramagnetic region above about 200°K.

Since reproducibility, centering, and mixer errors cannot be separated, they will all be lumped into the term "reproducibility". This term is included in these discussions because the reproducibility of the apparatus was not as good as the centering and mixer errors would indicate. This is commented upon below in the discussion of calibration errors.

Aside from the absolute error in the calibration itself, which is dependent on how well the saturation magnetization of nickel is known as well as the accuracy with which the standard was weighed, a major source of error is the reproducibility of the calibrations. For reasons that are

not completely understood, the short term reproducibility of the calibrations was about ±0.2%. By short term reproducibility is meant running a calibration, removing the standard from the apparatus, replacing and recentering it, and running the calibration again. The long-term reproducibility (i.e., calibrations separated by two or three weeks) was of the order of ±1%. For this reason, a calibration was made at least twice a week while data was being taken. It is estimated that this resulted in a relative calibration error of the order of ±0.4%. As already stated, the source of the reproducibility error is not known for certain. Part of this error may be associated with temperature changes in the reference and pick-up coils and in the phase shifter and mixer portions of the electronics. What is termed "electronic drift" may also be responsible for some of the error.

Most values quoted over the years for the saturation magnetization of nickel are within about ±0.5% of the value obtained by Weiss and Forrer in 1926 (51). This is also true of the value, 55.05 ±0.05 emu/g. at 288°K, reported by Danan in 1958 (32). However, the work by Danan appears to have been done carefully, and the results in this thesis are based on this value. The uncertainty given by Danan, i.e., about 0.1%, is also used here in the discussion of errors. The nickel standard used in this study had a mass of about 0.1 g. which could be weighed to about ±0.2%. Thus the total estimated calibration error, including reproducibility is $\pm[(0.4)^2 + (0.2)^2 + (0.1)^2]^{\frac{1}{2}} \simeq \pm 0.46\%$.

The error in the measured magnetic moment of any sample includes the same short-term reproducibility error as was discussed for the calibration (i.e., ±0.2%). Most samples had a mass of the order of 0.15 to 0.2 g.

which could be measured to about ±0.1%. The error in crystal alignment is estimated to be ±1° for the alloys and about ±0.5° for pure erbium where there is a factor of about 10 difference in the basal-plane and c-axis magnetization. This results in a completely negligible error in magnetic moment for the alloys where there is usually less than a factor of 2 or 3 difference in basal-plane and c-axis magnetizations. For pure erbium, a 0.5° error in alignment gives a negligible error in the c-axis moment but can result, in the worst cases, in about 0.35% error in the basal-plane moment.

Since the magnetization of any sample is given by

$$\sigma = \frac{(DR)(C)}{w}$$

the error in the magnetization is given by

$$\frac{\Delta\sigma}{\sigma} = \left[\left(\frac{\Delta DR}{DR}\right)^2 + \left(\frac{\Delta C}{C}\right)^2 + \left(\frac{\Delta w}{w}\right)^2\right]^{\frac{1}{2}}$$

where DR = dial reading of mixer
ΔDR = reproducibility error discussed above
C = calibration constant
w = weight

Thus the relative error in σ which includes only the reproducibility errors of both the calibration and the sample is about ±0.45%. The absolute error which also includes the uncertainty in the saturation magnetization of nickel as well as the weighing errors is about ±0.51%. This does not include errors in sample composition or in crystal alignment.

There are also errors in magnetic field and in temperature. These errors are difficult to incorporate into the error in σ, but they can be

quoted as separate errors. The error in the field varies from about 0.5% at low fields to about 0.1% at high fields. Error in temperature measurement is estimated to be about $\pm 0.1^{\circ}K$ up to $20^{\circ}K$ and about $\pm 0.05^{\circ}K$ at higher temperatures. However, taking into consideration the possibility of slight thermal inequilibrium between the thermocouple and sample, a more realistic estimate of error is probably $\pm 0.5^{\circ}K$.

VI. ACKNOWLEDGMENTS

The author wishes to express his sincere gratitude to Dr. F. H. Spedding for suggesting this investigation and for his continued interest and guidance throughout the author's graduate study at Iowa State University; to Dr. A. H. Daane whose guidance during the first part of the author's graduate study at Iowa State University is gratefully acknowledged; and to Dr. A. E. Miller who designed and built, with only a limited amount of help from the author, the vibrating-sample magnetometer used in this study. The author is also indebted to Dr. A. E. Miller, Dr. R. G. Jordan, and Dr. S. Legvold for many helpful discussions; to Dr. B. C. Gerstein for the use of his mutual inductance bridge; and to Mr. P. E. Palmer and Mr. J. J. Croat for their efforts in furnishing the purest metals possible for this study.

The author would also like to publicly express his gratitude to his wife, Edee, for her unlimited patience and understanding during the author's graduate study.

VII. LITERATURE CITED

1. F. H. Spedding and J. E. Powell, J. Metals 6, 1131 (1954).
2. F. H. Spedding and A. H. Daane, J. Metals 6, 504 (1954).
3. G. Urbain, P. Weiss, and F. Trombe, Compt. Rend. 200, 2132 (1935).
4. W. Klemm and H. Bommer, Z. Anorg. Allgem. Chem. 231, 138 (1937).
5. H. Bommer, Z. Anorg. Allgem. Chem. 242, 277 (1939).
6. H. E. Nigh, J. Appl. Phys. 34, 3323 (1963).
7. C. Zener, Phys. Rev. 85, 324 (1951).
8. M. A. Ruderman and C. Kittel, Phys. Rev. 96, 99 (1954).
9. T. Kasuya, Progr. Theoret. Phys. 16, 45 (1956).
10. K. Yosida, Phys. Rev. 106, 893 (1957).
11. H. Miwa and K. Yosida, Progr. Theoret. Phys. 26, 693 (1961).
12. R. J. Elliott, Phys. Rev. 124, 346 (1961).
13. R. M. Bozorth and R. J. Gambino, Phys. Rev. 147, 487 (1966).
14. R. M. Bozorth, J. Appl. Phys. 38, 1366 (1967).
15. H. R. Child, W. C. Koehler, E. O. Wollan, and J. W. Cable, Phys. Rev. 138, 1655 (1965).
16. E. O. Wollan, J. Appl. Phys. 38, 1371 (1965).
17. P. G. de Gennes, Compt. Rend. 247, 1836 (1958).
18. W. C. Koehler, J. Appl. Phys. 36, 1078 (1965).
19. S. Legvold, F. H. Spedding, F Barson, and J. F. Elliott, Rev. Mod. Phys. 25, 129 (1953).
20. R. V. Colvin, S. Legvold, and F. H. Spedding, Phys. Rev. 120, 741 (1960).
21. R. E. Skochdopole, M. Griffel, and F. H. Spedding, J. Chem. Phys. 23, 2258 (1955).
22. J. F. Elliott, S. Legvold, and F. H. Spedding, Phys. Rev. 100, 1595 (1955).

23. W. C. Koehler and E. O. Wollan, Phys. Rev. 97, 1177 (1955).

24. R. W. Green, S. Legvold, and F. H. Spedding, Phys. Rev. 122, 827 (1961).

25. J. W. Cable, E. O. Wollan, W. C. Koehler, and M. K. Wilkinson, Phys. Rev. 140, 1896 (1965).

26. S. Foner, Rev. Sci. Instrum. 30, 548 (1959).

27. W. T. Scott, The Physics of Electricity and Magnetism, New York, New York, John Wiley and Sons, Inc., c1959.

28. J. Mallinson, J. Appl. Phys. 37, 2514 (1966).

29. A. E. Miller, A Study of Some Nonstoichiometric Rare-Earth Oxides, Unpublished Ph.D. thesis, Ames, Iowa, Library, Iowa State University of Science and Technology, 1964.

30. A. E. Miller, U.S. Atomic Energy Commission Rept. IS-1717 [Iowa State University of Science and Technology, Ames. Institute for Atomic Research], [To be published ca. 1967].

31. C. Herring, R. M. Bozorth, A. E. Clark, and T. R. McGuire, J. Appl. Phys. 37, 1340 (1966).

32. H. Danan, Compt. Rend. 246, 73 (1958).

33. R. M. Bozorth, Ferromagnetism, New York, New York, D. Van Nostrand Co., Inc., 1951.

34. S. Foner and E. D. Thompson, J. Appl. Phys. 30, 229S (1959).

35a. R. L. Powell, M. D. Bunch, and R. J. Corruccini, Cryogenics 1, 139 (1961).

35b. B. C. Gerstein, Heat Capacity and Magnetic Susceptibility of Thulium Ethylsulfate, Unpublished Ph.D. thesis, Ames, Iowa, Library, Iowa State University of Science and Technology, 1960.

36. A. E. Miller and A. H. Daane, Trans. Met. Soc. AIME 230, 568 (1964).

37. C. E. Habermann and A. H. Daane, J. Chem. Phys. 41, 2818 (1964).

38. A. H. Morrish, The Physical Principles of Magnetism, New York, New York, John Wiley and Sons, Inc., 1965.

39. R. G. Jordan and E. W. Lee, Proc. Phys. Soc. [To be published ca. December, 1967].

40. D. R. Behrendt, S. Legvold, and F. H. Spedding, Phys. Rev. 109, 1544 (1958).

41. D. L. Strandburg, S. Legvold, and F. H. Spedding, Phys. Rev. 127, 2046 (1962).

42. T. J. Hendrickson, Ferromagnetic-Antiferromagnetic Phase Transitions, Unpublished Ph.D. thesis, Ames, Iowa, Library, Iowa State University of Science and Technology, 1956.

43. S. Chikazumi, Physics of Magnetism, New York, New York, John Wiley and Sons, Inc., c1964.

44. R. G. Jordan, Magnetic Properties of Terbium-Holmium Alloys, unpublished data, Ames, Iowa, Department of Physics, Iowa State University of Science and Technology, 1967.

45. E. J. Darnell, Phys. Rev. 132, 1098 (1963).

46. S. Arajs and D. S. Miller, J. Appl. Phys. 31, 325S (1960).

47. T. Nagamiya, K. Nagata, and Y. Kitano, Progr. Theoret. Phys. 27, 1253 (1962).

48. Y. Kitano and T. Nagamiya, Progr. Theoret. Phys. 31, 1 (1964).

49. R. B. Flippen, J. Appl. Phys. 35, 1047 (1964).

50. S. Foner and E. J. McNiff, Jr., J. Appl. Phys. 38, 1377 (1967).

51. P. Weiss and P. Forrer, Ann. Phys. 5, 153 (1926).